# NATURE-BASED SOLUTIONS FOR COASTAL PROTECTION:

# A MULTI-SCALE INVESTIGATION OF WAVE-VEGETATION INTERACTIONS

**Acacia Markov**

Submitted under the supervision of

Dr. Ioan Nistor

Dr. Jacob Stolle

A thesis submitted to the University of Ottawa in partial fulfillment of the requirements for the degree of

**Master of Applied Science in Civil Engineering**

---

Department of Civil Engineering
Faculty of Engineering
University of Ottawa

University of Ottawa
Ottawa, Ontario, Canada

# Abstract

Nature-based solutions (NBS) are promising strategies for protecting vulnerable coasts in the context of climate change, utilizing the coastal protection capabilities of natural ecosystems for engineering applications. The ability of coastal marsh vegetation to attenuate wave energy and prevent coastal erosion has been acknowledged for decades, however, consideration for their use in coastal protection strategies is presently limited, particularly in Canada due to a lack of engineering guidelines and limited available research considering region-specific variables. Physical modelling presents a useful tool for investigating the coastal protection function provided by marsh vegetation in a controlled, repeatable environment, which can ultimately inform the design of nature-based coastal protection strategies. To date, such studies have investigated the influence of plant biophysical parameters (stem flexibility, width, and height) and hydrodynamic conditions (wave height, wave period, and plant submergence) on wave attenuation. These studies have used either live vegetation, requiring full-scale wave testing, or surrogate vegetation, which allows simplified testing at either full- or reduced-scale. Overall, live vegetation studies have been limited in the variety of saltmarsh plants considered, with few studies considering plant species native to the Canadian coastline. Several physical modelling studies have been performed using surrogate plants, however, methods of surrogate development for flexible vegetation or reduced-scale testing are not yet well developed.

This thesis aims to address knowledge gaps pertaining to the use of marsh vegetation in coastal protection strategies, particularly through the development of experimental methods with both live and surrogate plants. A full-scale flume study with live vegetation was performed to develop fundamental knowledge of wave-vegetation interactions for *Spartina alterniflora* and *Spartina patens*, two salt marsh species native to Canada's Atlantic coast. *S. alterniflora* was observed to demonstrate a resistance strategy in response to hydrodynamic forcing, versus the avoidance strategy of *S. patens*, supporting complementary functioning of the two species if utilized together in coastal protection schemes. Observations of plant properties and stem bending from live plant tests were subsequently applied in the development of a small-scale flume study, which examined wave attenuation associated with a downscaled *S. alterniflora* meadow in the configuration of a "living dyke" structure. Wave damping induced by surrogate vegetation was observed to be minimal for the tested wave conditions ($0.073\ \text{m} < H_{m0} < 0.225\ \text{m}$, $2.0 < T_p < 3.2$ s, 1:4 scale) and beach slope (1V:20H), with wave height evolution dominated by wave shoaling and breaking. Several methods were considered for modelling the *S. alterniflora* meadow at reduced scale, and results demonstrated a sensitivity to surrogate diameter but not flexibility.

The development of robust experimental methods for investigating the performance of nature-based coastal infrastructure is essential for the establishment of appropriate design conditions. The scale series approach of this thesis supports such methodological advancements and is expected to make preliminary contributions to design guidance on coastal marsh-based NBS and provide critical direction for future studies.

# Acknowledgements

I am extremely grateful for the knowledge and opportunities the last two years have brought me; my experience as a graduate student could not have been nearly as rich without the incredibly generous (with their knowledge and time) individuals I have met throughout this journey.

To my thesis supervisors, Dr. Ioan Nistor and Dr. Jacob Stolle, I express my immense gratitude. They have provided endless support, guidance, and wisdom that has without a doubt made me a better researcher. I started my Master's with minimal experience in coastal engineering, but a love for coastal marshes, and I have learned more from them both than I could have imagined. They provided numerous opportunities to engage with the academic community, including supporting me to participate in several national and international conferences. These were invaluable experiences for which I am forever grateful. Above all, they have taught me what it means to be an exemplary supervisor, leader, and educator.

Thank you also to Andrew Cornett, Enda Murphy, Scott Baker and Damien Pham Van Bang for their significant contributions to, and guidance throughout, the experimental programs. Their support was integral to the success of the experiments, and I feel so lucky to have had the opportunity to collaborate with and learn from such highly experienced and knowledgeable individuals.

I would also like to acknowledge the Institut National de la Recherche Scientifique's (INRS) Environmental Hydraulics Laboratory (LHE) and the National Research Council's Ocean, Coastal and River Engineering Research Centre. LHE and NRC-OCRE provided the experimental facilities, equipment and training that form the basis of this thesis. Particular gratitude is expressed to Dominik Lapierre and Raky Rezgui from LHE, and David Hnatiw from NRC for their invaluable assistance in conducting the experiments.

Thank you to the undergraduate and fellow graduate students that lent their time and knowledge to this project, as well as their friendship over the last two years: Ross Henteleff, Dario Sirianni, Dana Pothier and Margo Muller. Ross and Margo contributed countless hours to the experimental programs, and I am immensely grateful.

Finally, so much gratitude is owed to my friends and family. Thank you for listening intently, for the countless motivational speeches, and for the support you provided during challenging times. Thank you to my partner, Félix, for inspiring me to stay passionate about my work. And thank you to my best friend, Becca, for talking endlessly about coastal science and academia with me when no one else will. I would not have made it to this point without you all.

# Table of Contents

# List of Figures

# List of Tables

# List of Acronyms

| | |
|---|---|
| **ADV** | Acoustic Doppler Velocimeter |
| **CFD** | Computational Fluid Dynamics |
| **COULWAVE** | Cornell University Long and Intermediate Wave Modelling |
| **EDPM** | Ethylene Propylene Diene Monomer |
| **JONSWAP** | Joint North Sea Wave Project |
| **LDPE** | Low-density Polyethylene |
| **MHW** | Mean High Water |
| **MHHW** | Mean Higher High Water |
| **MTL** | Mean Tide Level |
| **NBS** | Nature-based Solution |
| **NbCA** | Nature-based Coastal Adaptation |
| **PVC** | Polyvinyl Chloride |
| **RANS** | Reynolds-Averaged Navier Stokes |
| **RMS** | Root-mean Square |
| **SWAN** | Simulating Waves Nearshore |
| **SWASH** | Simulating Waves till Shore |
| **TS** | Test Series |
| **WP** | Wave Probe |
| **XLPO** | Cross-lined Polyolefin |
| **OD** | Outer Diameter |
| **ID** | Inner Diameter |

# List of Symbols

| | |
|---|---|
| $A$ | Wave orbital excursion (m) |
| $A_p$, $FA$ | Projected plant frontal area ($m^2$) |
| $a_1$, $a_2$, $a_3$ | Polynomial distortion coefficients from camera correction (-) |
| $B$ | Buoyancy parameter (-) |
| $b$, $b_v$ | Stem width/diameter (m) |
| $B_s$ | Significant forward bending angle (°) |
| $Ca$, $C_y$ | Cauchy number (-) |
| $C_d$ | Drag Coefficient (-) |
| $C_r$ | Reflection coefficient (%) |
| $d$, $h$ | Water depth (m) |
| $D_{50}$ | Mean grain diameter ($\mu$m) |
| $E$ | Modulus of elasticity (Pa) |
| $EI$ | Flexural rigidity ($Nm^2$) |
| $F_D$, $F_x$ | Drag force, horizontal drag force (N) |
| $Fr$ | Froude number (-) |
| $F_s$ | Significant forward bending angle (°) |
| $H_b$ | Breaking wave height (m) |
| $H_{m0}$ | Zeroth-moment wave height (Irregular waves) (m) |
| $H_s$ | Significant wave height (Irregular waves) (m) |
| $H_{1/3}$ | Average of the highest one-third of wave heights (m) |
| $I$ | 2nd moment of inertia ($m^4$) |
| **KC** | Keulegan-Carpenter number (-) |
| $L$ | Ratio of stem length to wave orbital excursion (-) |
| $l$, $h_v$ | Stem/plant length (m) |
| $l_e$ | Effective length (m) |

| | |
|---|---|
| $L_0$ | Deepwater/offshore wavelength (m) |
| $m_0$ | Zeroth moment of the wave spectrum (m) |
| $L_m$ | Model length (m) |
| $L_p$ | Prototype length (m) |
| $N_L$ | Scale ratio for geometric similitude (-) |
| $N$, $N_v$ | Number of vegetation stems/stem density (-) |
| $P^*$ | Stem/surrogate spacing to diameter ratio (-) |
| **Re** | Reynolds number (-) |
| $S$ | Slenderness number (-) |
| $S(f)$ | Spectral density function (-) |
| $T$ | Wave period (s) |
| $t$ | Time (s) |
| $T_p$ | Peak wave period (irregular waves) (s) |
| $U$ | Mean in-canopy velocity (m/s) |
| $u$ | Undisturbed fluid velocity (m/s) |
| $U_c$, $u_c$ | Characteristic velocity (m/s) |
| $U_{max}$, $U_w$ | Maximum velocity over the wave period (m/s) |
| $u_r$ | Relative plant-fluid velocity (m/s) |
| $\dot{U}$ | Characteristic streamwise fluid acceleration ($m/s^2$) |
| $x$ | Distance in cross-shore direction (m) |
| $\theta$, $\alpha$ | Beach slope (m/m) |
| $\alpha$ | Vegetation solid volume fraction, scaling factor (-) |
| $\lambda$ | Stem spacing (center to center) (m) |
| $\mu$ | Wave height attenuation coefficient (-) |
| $\nu$ | Kinematic viscosity ($m^2/s$) |
| $\lambda_1$ | Force balance ratio, buoyancy to restoring (Ghisalberti & Nepf, 2002) (-) |
| $\lambda_2$ | Force balance ratio, restoring to drag (Ghisalberti & Nepf, 2002) (-) |

| | |
|---|---|
| $\boldsymbol{\rho}$ | Fluid density (kg/m$^3$) |
| $\boldsymbol{\rho_w}$ | Density of water (kg/m$^3$) |
| $\boldsymbol{\rho_g}$ , $\boldsymbol{\rho_v}$ | Density of vegetation (kg/m$^3$) |
| $\boldsymbol{\omega}$, $\boldsymbol{\sigma}$ | Wave angular frequency (rad/s) |
| $\boldsymbol{\xi}$ | Irribarren number (-) |

# 1. Introduction

## 1.1 Background

Population densities adjacent to shorelines are significantly higher than any other areas across the globe, owing to the numerous human ecosystem services associated with these coastal zones; humans have settled near coastal areas for water access, commerce, agriculture, aquaculture, recreation and transportation (Wu et al., 2011; Temmerman et al., 2013). It is currently estimated that over one-third of the world's population resides within 100 km of the coast, and this proportion is projected to increase to one-half by 2030 (Bilkovic et al., 2017).

As a result of decades of human activities proximate to coastal areas, shorelines have been dramatically modified, primarily through hardening for coastal protection or land reclamation for agriculture (Temmerman et al., 2013; Bilkovic & Mitchell, 2017; Wollenberg et al., 2018; Smith et al., 2020). This has resulted in a significant loss of ecosystem function within the coastal zone (Barbier et al., 2011; Bilkovic & Mitchell, 2017; Wollenberg et al., 2018).

Shoreline hardening or armouring has been adopted as a means of protecting highly populated coastal zones from natural threats inherent to the area: erosion, saltwater intrusion, land subsidence, tsunamis and floods (Small & Nicholls, 2003). In general, shoreline armouring consists of the construction of traditional "hard" coastal engineering structures such as seawalls, bulkheads, breakwaters, jetties, groynes and revetments (Wu et al., 2011; Bilkovic & Mitchell, 2017; Rahman et al., 2018). These structures primarily act to reflect incident wave energy and prevent wave overtopping (USACE, 2002).

While shoreline armouring has traditionally been effective in mitigating erosion and flooding, the associated modifications to coastal zones have been detrimental. Hard shoreline infrastructure alters morphologic and hydrodynamic properties of coastal ecosystems, limiting the natural flow of sediment, and compromising the ecosystem's ability to maintain emergent conditions through depositional processes (Temmerman et al., 2013; Bilkovic et al., 2017; Rahman et al., 2019; Gracia et al., 2018). Degradation of coastal habitats has led to a loss of numerous associated ecosystem services such as greenhouse gas sequestration capacity, and nursery habitat for aquaculture systems (Wollenberg et al., 2018; McClenachan et al., 2020).

Furthermore, the impacts of climate change on coastal areas have significant implications for the continued efficacy of traditional hard shoreline infrastructure (Gracia et al., 2018). Global sea-levels are predicted to rise at a rate of 3.7 mm/year throughout the first half of the 21$^{st}$ century, according to the Fifth Assessment Report of the Intergovernmental Panel on Climate Change (IPCC) (Church et al., 2013). This constant rate of change requires coastal protection structures to be highly adaptive. On the contrary, hard coastal structures, such as those mentioned above, are designed to be static and are often difficult to modify once they are established (van Gent, 2010; Gracia et al., 2018). The cost of maintaining or rebuilding hard infrastructure is projected

to be on the order of billions by the next century if they are relied upon for the main source of coastal protection in the context of climate change (Rahman et al., 2019).

Coincidentally, the very ecosystems that are being degraded by shoreline armouring have been recognized through their capacity for ecosystem-based coastal defence (Bilkovic et al., 2016; Maza et al., 2019; Anderson & Smith, 2014; Chen & Zhao, 2012; Augustin et al., 2009; Smith et al., 2020; Lei & Nepf, 2019). Vegetated coastal ecosystems such as mangroves, salt marshes and reef systems have been proven effective at reducing incident wave heights between 31 and 72% (Rahman et al., 2019). Additionally, these environments may adapt to rising sea levels through depositional processes and are self-repairing, meaning they can provide adaptive protection in the context of climate change with minimal associated long-term costs (Shepard et al., 2011; Rahman et al., 2019; Smith et al., 2020).

Nature-based solutions (NBS) is a term often used to describe the application of natural coastal environments for coastal protection. NBS encapsulates many adaptation approaches, sometimes also referred to as ecological engineering, natural infrastructure, or ecosystem-based adaptation (Rahman et al., 2019). Rahman et al. (2019) utilizes a similar term "nature-based coastal adaptation" (NbCA) to describe NBS, defined as:

> *"any coastal adaptation approach that uses (i) ecologically available adaptation options (e.g., natural space, ecological process and species) and (ii) socio-politically available opportunities (e.g., values, policy, rules and regulations) (iii) to allow for natural adjustment to coastal climate change impacts, (iv) considering societal demand for diverse ecosystem services (e.g., provisioning, regulating, cultural and supporting) (v) minimizing engineered construction as a supporting component." (Rahman et al., 2019, pp. 2).*

Presently, the development and wide-scale application of NBS for coastal protection is hindered by a lack of clear engineering guidance. Guidance that does exist is not well established, relying largely upon "grey literature", and is predominantly case-specific (Pontee et al., 2016). Robust guidelines for the successful application of NBS should consider a base of peer-reviewed literature, incorporating findings from both field and modelling approaches (Morris et al., 2018). This thesis aims to address this critical knowledge gap, through the development of physical modelling methodologies for the investigation of coastal marsh-based NBS, particularly within a Canadian context.

## 1.2 Objectives

The overall objective of this thesis is to contribute to the formulation of engineering design guidance for the incorporation of NBS in coastal protection schemes. Physical modelling presents a useful tool for investigating the coastal protection function provided by marsh vegetation in a controlled, repeatable environment, which can ultimately inform such design guidelines. Considering this, two distinct experimental programs were conducted to improve the development of physical modelling methods for investigating wave interactions with coastal

marsh meadows, as well as to enhance knowledge of the coastal protection function of marsh species native to Canada. The dynamic behaviour of live vegetation under wave action was first investigated at prototype-scale, followed by a reduced-scale experimental program that was developed through the findings of the former. This scale series approach aims to address uncertainties associated with the modelling of coastal marsh-based NBS in laboratory settings, considering both live vegetation and vegetation surrogates. The objectives of each experimental program are broken down as follows.

1) Prototype-scale experiments with live vegetation:
   a) Characterize wave-vegetation interactions for live vegetation species native to the Canadian coastline, through examination of:
      i) Plant parameters (stem thickness, length, and flexibility, plant morphology) and
      ii) Irregular wave-induced vegetation motion utilizing submerged cameras and a video tracking algorithm.
   b) Yield practical insight for the use of live vegetation in experimental wave tests.
   c) Utilize results from experimentation with live vegetation to improve the development and use of plant surrogates.

2) Small-scale modelling with surrogate vegetation:
   a) Quantify the wave damping capacity of a simulated *Spartina alterniflora* meadow under increasingly severe wave conditions, for an engineered, vegetated dyke scenario (1V:20H beach slope, irregular waves).
   b) Investigate methods for downscaling vegetation meadows in laboratory settings, including sensitivities to the selection of model element diameter and spacing.
   c) Compare the performance of various surrogate proxies for the semi-flexible *S. alterniflora*, to inform guidelines for plant surrogate selection.

## 1.3 Scope

Two experimental studies are presented in this thesis, investigating the use of coastal marsh vegetation in engineered coastal protection strategies, particularly considering vegetation-induced wave attenuation. The large-scale experimental program was implemented in the large wave flume of the Environmental Hydraulics Laboratory (LHE), at the Institut National de la Recherche Scientifique (INRS) located in Quebec City, Canada. Small-scale experiments (1:4) were conducted in the Steel Wave Flume (SWF) at the National Research Council's Ocean, Coastal and River Engineering research centre (NRC-OCRE), located in Ottawa, Canada.

This study considers vegetated beach profiles with moderate slopes between 1V:18H and 1V:20H, comprised of sand (moveable) and concrete (fixed). Two marsh species were considered: *Spartina alterniflora* and *Spartina patens*. Large-scale experiments utilized live specimens of both species, and small-scale experiments used surrogate elements (rigid and flexible) to model *S. alterniflora*. Wave programs considered in this thesis cover a wide range of hydrodynamic conditions, with prototype-scale wave heights between $H_{m0}$ = 0.10-0.92 m and

wave periods between $T_p$ = 2.0-10.0 s. All tests were conducted with irregular waves, synthesized from JONSWAP spectra. Wave testing was conducted at several water depths to consider vegetation submergence ratios (stem length/water depth) between 0.45 and >>1 (fully emergent). Overall, the following data was collected within the scope of this thesis:

- Live and surrogate vegetation parameters, including morphology, stem width, stem height, frontal area and biomechanical properties.
- Water surface elevation, measured by either acoustic wave gauges or capacitance wire wave gauges.
- Water velocities, measured by either acoustic doppler velocimeters (ADVs) or electromagnetic current meters (EMCMs).
- Video footage of flexible plant/surrogate element motion.

The collection of the above data allowed testing of the sensitivity of wave-vegetation interactions (including wave height attenuation and flexible vegetation motion) to wave height, wave period, water depth (or relative plant submergence), and plant bio-physical parameters (inter- and intra-species differences). Due to temporal and physical constraints, this study is limited as follows:

- No formal field surveys were conducted to obtain plant parameters for *S. alterniflora* and *S. patens* under natural marsh conditions. Thus, the vegetation parameters obtained from live vegetation testing and used for surrogate testing could not be validated against field data. However, the plant parameters obtained in this study fall within the range of values available in literature (e.g., Feagin et al., 2011; Chatagnier et al., 2012; Ysebaert et al., 2011; Knutson et al., 1982).
- This study only considers the marsh species *S. alterniflora* and *S. patens*. Thus, the extension of the present findings to other coastal marsh plants native to the Canadian coastline is ultimately unknown, particularly for species with significantly differing morphological and biomechanical traits.
- This study does not consider plant damage expected to be associated with exposure to high energy waves. The upper limit of the wave protocol for the live vegetation tests, which had the potential to capture damage, was limited by the wave generation capabilities of the facility, combined with the location of the constructed slope within the flume and the water depths selected for testing. Stem damage could not be directly captured with surrogate vegetation for the higher-energy wave scenarios tested at small-scale.
- Tests with the downscaled marsh meadow were done at a 1:4 scale, selected based upon the wave generation capacity of the facility and the target wave regime. Scale effects resultant from further reduced models are thus unknown and may present challenges that were not encountered in this study.
- Erosion protection is not directly considered in this study, as a full-density salt marsh meadow was not planted for the large-scale experimental program, and a fixed bed (concrete) was used for small-scale testing, along with surrogate elements that did not

capture belowground vegetation structures. Measurements of wave run-up reduction resultant from the presence of vegetation are also outside of the scope of this thesis.

## 1.4 Publications

The following is a list of publications affiliated with the present thesis, for which the author is a primary contributor.

**Journal Publications**

1) **Markov, A.**, Stolle, J., Henteleff, R., Nistor, I., Pham Van Bang, D., Murphy, E., and Cornett, A. (2022). *Deformation of Spartina Patens and Spartina Alterniflora Stems Under Wave Action*. **(Under review, Coastal Engineering Journal, Taylor & Francis).**
2) **Markov, A.**, Muller, M., Nistor, I., Baker, S., Stolle, J., Murphy, E., and Cornett, A. (2022). *Wave Interactions with S. Alterniflora on A Living Dyke Model: New Insights to the Use of Scaled Surrogate Meadows*. **(Submitted, Journal of Waterway, Port, Coastal and Ocean Engineering, ASCE).**

**Conference Proceedings**

1) **Markov, A.,** Henteleff, R., Nistor, I., and Stolle, J. (2021). *Sediment Transport and Controls on Coastal Marshes in a Changing Climate.* Oral Presentation at Coastal Zone Canada. Virtual.
2) **Markov, A.**, Stolle, J., Henteleff, R., Nistor, I., Pham Van Bang, D., Cornett, A., and Murphy, E. (2022). *Motion Response of Live Saltmarsh Vegetation to Irregular Wave Forcing.* Oral presentation at MEOPAR Annual Scientific Meeting. Virtual.
3) **Markov, A.,** Henteleff, R., Stolle, J., Nistor, I., Murphy, E., and Cornett, A. (2022). *Characterizing Live Vegetation Response to Wave Forcing*. Proceedings from the 39th IAHR World Congress. Granada, Spain.
    - John F. Kennedy Student Paper Competition - Awarded 2$^{nd}$ prize out of 91 applicants
4) **Markov, A.,** Muller, M., Baker, S., Nistor, I., Murphy, E., Stolle, J., and Cornett, A. (2022). *New Insights on Using Scaled Marsh Plant Surrogates for Wave Attenuation.* 37$^{th}$ International Conference on Coastal Engineering. Sydney, Australia. **(Abstract accepted for oral presentation and conference proceedings)**.

## 1.5 Contributions and Novelty of the Study

This study is the first in Canada to investigate wave-vegetation interactions using live vegetation in a large-scale, outdoor wave flume. Few similar programs have been conducted in other parts of the globe, with the methods presented by such studies not entirely applicable to Canada due to region-specific restrictions on plant procurement, as well as plant husbandry methods that consider only local species and climate. This study considers two salt marsh species native to the Canadian coastline, one of which (*Spartina patens*) has never been investigated for its application in nature-based coastal protection schemes. The other species, *Spartina alterniflora,*

has received more research attention with respect to coastal protection applications, however, not in a Canadian context. This is critical, as previous studies have reported significant natural variation in the physical and biomechanical properties of *S. alterniflora*, specifically considering seasonality and geography.

The scale series approach of this thesis also enables an investigation of scale effects associated with physical modelling of NBS. Such scale effects may result from the use of surrogate proxies for live plants, or from the downscaling of vegetation meadows. This is the first study to consider several surrogate proxies for *S. alterniflora* in a high energy wave climate, where significant flexibility effects (in the form of stem motion) are expected. It is also the first study to critically assess the methods for downscaling vegetation meadows that have been previously implemented in published works.

Finally, previous investigations of wave attenuation by coastal marsh vegetation have predominantly targeted natural conditions, considering flat marsh platforms and mild hydrodynamic settings. The present study investigates wave-vegetation interactions for constructed marsh scenarios, considering gentle beach slopes representative of vegetated dyke applications, and higher energy wave regimes. As a result, this study considers the effects of wave breaking, as well as potential hydrodynamic limits on wave attenuation by marsh-based coastal protection structures.

## 1.6 Outline of the Thesis

This thesis presents two studies that were conducted to meet the objectives outlined in Section 1.2. The remaining sections of the thesis are organized as follows:

- **Section 2.0** presents a literature review to provide context to the experimental studies and outline the current state-of-the-art with regards to nature-based solutions for coastal protection. The review focuses on the use of vegetated coastal ecosystems for coastal adaptation, including mangrove forests, sea grass meadows and salt marshes. In consideration of the thesis objectives, emphasis is placed on the use of salt marsh vegetation for coastal protection and on physical modelling methods, although numerical models are briefly discussed.
- **Section 3.0** presents the two experimental wave studies performed. Experiments conducted at full-scale with live vegetation are presented first (Section 3.1), followed by the reduced-scale, surrogate vegetation study (Section 3.2), which was directly informed by the outcomes of the former. Both studies are presented as preprints of manuscripts submitted to the Coastal Engineering Journal, Taylor & Francis (under review) and the Journal of Waterway, Port, Coastal, and Ocean Engineering, ASCE (submitted). The contributions of the author (AM) to each article are as follows:
    - Section 3.1: AM contributed to the conception and design of the experimental program, conducted the data collection with support from JS and RH, and completed the data analysis with support from JS. AM wrote the main sections of the manuscript

with inputs from JS. All authors contributed to manuscript revision, and final approval.
    - Section 3.2: AM completed the design of the experimental program, conducted the data collection with support from MM, and completed the data analysis. AM wrote the main sections of the manuscript. All authors contributed to manuscript revision, and final approval.
- In **Section 4.0,** potential limitations associated with the studies presented in Section 3.0 are discussed. This section also presents practical guidelines for testing coastal marsh-based NBS in a laboratory setting, based upon lessons learned from the experimental programs. This section then identifies the advantages and limitations associated with wave testing at full-scale with live vegetation, versus small-scale testing with surrogate vegetation, and provides recommendations for the appropriate application of each method.
- **Section 5.0** summarizes the thesis, providing key conclusions from the two experimental programs. Opportunities for future research are also identified from experimental findings, as well as in consideration of the limitations mentioned in Section 4.0.

# 2. Literature Review

## 2.1 Background on Vegetated Coastal Environments

### 2.1.1 Mangrove

Mangroves are coastal forests that grow along sheltered bays, estuaries and inlets (Barbier et al., 2011). Most mangrove forests are found in the subtropical or tropical zones throughout the world (Barbier et al., 2011; Maza et al., 2019). Mangrove trees are characterized by their highly complex root systems, that provide various ecosystem services such as: nursery habitat, wave attenuation and enhanced sediment capture (Barbier et al., 2011; Atwood et al., 2017; Maza et al., 2019). The complex root structures, combined with resultant high sedimentation rates and additional factors such as anoxic, waterlogged soils, result in high carbon burial rates (Atwood et al., 2017). Mangrove ecosystems are responsible for storing 5-10.4 Pg of soil carbon globally (Atwood et al., 2017). In addition, the root structures act to stabilize sediment and retain soil, preventing shoreline erosion (Barbier et al., 2011). They can also serve as a coastal barrier, protecting upland areas or landward coastal marshes through attenuating waves and thus reducing storm surges (Barbier et al., 2011; Rasmeemasmuang & Sasaki, 2015; Mei et al., 2011). Natural mangrove forests were found to provide protection even under extreme storm events such as the 2004 Indian Ocean Tsunami, and the cyclone that struck Orissa, India in 1999 (Barbier et al., 2011). The presence of mangrove forests along the impacted shorelines resulted in a significant reduction in mortality and reduced damage to property, agriculture and fisheries (Barbier et al., 2011).

Mangrove root systems can be classified into four main groups: prop roots (*Rhizophora* type); pneumatophore roots (*Avicennia* type); knee roots (*Bruguiera* type), which are a sub-group of pneumatophore; and buttress roots (*Xylocarpus granatum* type) (Rasmeemasmuang & Sasaki, 2015). *Rhizophora* species of mangroves, in particular, have gained a lot of attention due to their highly complex structure compared to the other groups (Maza et al., 2019). As a result, *Rhizophora* type mangroves are the primary focus for physical and numerical modelling studies that consider wave attenuation through mangrove forests (Maza et al., 2019; Hoque et al., 2018). These studies will be discussed in Section 2.3.

### 2.1.2 Seagrass

Seagrasses are flowering plants that generally colonize protected, shallow coastal waters such as estuaries, embayments and coastal lagoons (Barbier et al., 2011; Koch et al., 2006). Many seagrass species colonize on soft substrates such as mud and sand (Barbier et al., 2011). The soft-substrate colonizers generally require wave-sheltered conditions (Koch et al., 2006). Disturbances due to waves or currents often lead to patchy seagrass beds or an absence of seagrass colonization altogether (Barbier et al., 2011; Koch et al., 2006). A few seagrass species, namely the *Phyllospadix* and *Posidonia* genera, are capable of colonizing hard substrate such as

cobbles or rock (Koch et al., 2006). These species are alternatively exposed to relatively high wave energies. In wave dominated environments, seagrasses are generally found in areas where waves are classified as intermediate type (depth to wavelength ratio between 1:20 and 1:2) (Manca et al., 2012). Seagrasses require approximately 11-20% surface light to survive, and thus grow only in relatively shallow waters (<90 m depth) (Koch et al., 2006). The combined root and rhizome system of seagrasses allow them to effectively capture and stabilize sediment (Koch et al., 2006; Barbier et al., 2011).

Seagrasses provide a wide range of ecosystem services, similar to those provided by mangroves, including provisions, coastal protection, erosion control, water purification, fishery enhancement, carbon sequestration and recreation (Barbier et al., 2011). The wave attenuation capacity of seagrasses has received attention for its application to coastal protection (Fonseca & Cahalan, 1992; Mendez & Losada, 2004; Sanchez-Gonzalez et al., 2011; Manca et al., 2012; Maza et al., 2013; Henry et al., 2015; Chen & Zou, 2019; Suzuki et al., 2019). The coastal protection capacity of seagrasses is maximized when the plants occupy most of the water column, often referred to as a seagrass canopy (Barbier et al., 2011; Koch et al., 2006). When most of the seagrass biomass is found near the bottom, wave attenuation capacity is reduced (Fonseca & Cahalan, 1992; Barbier et al., 2011). These seagrass environments are often called seagrass meadows (Koch et al., 2006). Fonseca & Cahalan (1992) identified the following as four seagrass species common to North America: *Halodule wrightii, S. filigorme, T. testudium,* and *Zostera marina.*

### 2.1.3 Salt marsh

Salt marshes are intertidal grasslands, often found along protected shorelines or at the edge of estuaries (Barbier et al., 2011; Wu et al., 2011). Salt marshes form upon fine sediment that has been transported by water and stabilized as vegetation establishes (Wu et al., 2011). The extent of salt marshes can range from vast complexes enclosing tidal creeks to narrow fringe marshes along the shoreline (Bilkovic & Mitchell, 2017). The extend of salt marsh development is primarily controlled by shoreline slopes, tidal range, sediment process and the hydrodynamic climate (Bilkovic & Mitchell, 2017). Salt marshes are characterized by low species diversity and a sharp zonation of plants between high and low marsh regions (Barbier et al., 2011). This zonation is based on the favourable physical environments of specific salt marsh species (Bilkovic & Mitchell, 2017). For example, *Spartina alterniflora* plants are more flood tolerant than *Spartina patens,* and thus *S. alterniflora* generally colonize the frequently inundated low marsh zone (**Fig. 2-1**) (Augustin et al., 2009; Wu et al., 2011; Bilkovic & Mitchell, 2017).

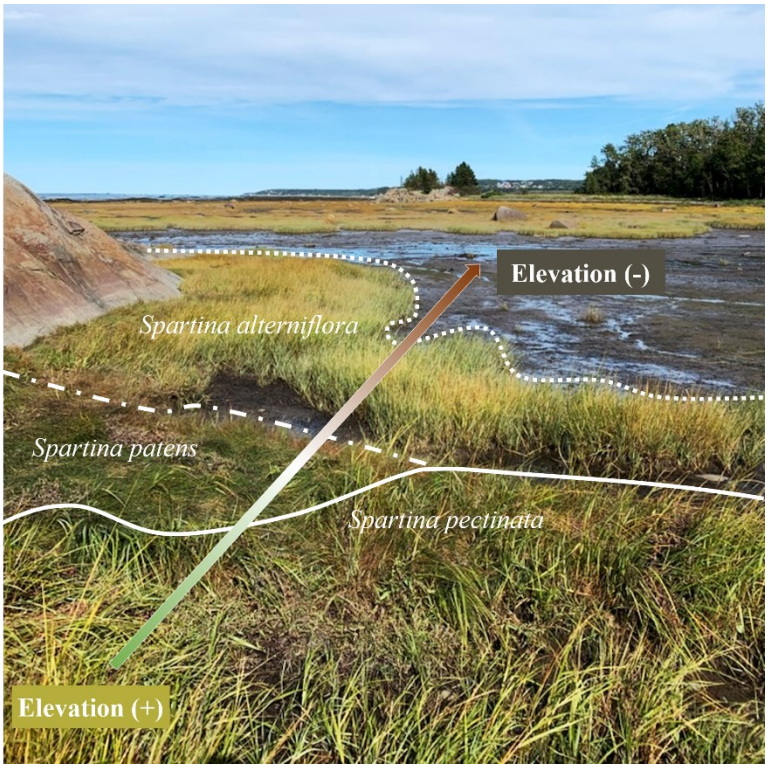


**Fig. 2-1.** Salt marsh species zonation for three *Spartina* sp. common to the Atlantic coast of Canada. Photo was taken in a natural marsh located near Trois-Pistoles, Québec.

Frequent tidal inundation and nutrient uptake through enhanced sediment deposition make these environments some of the most productive in the world (Barbier et al., 2011; Temmerman et al., 2013; Davis et al., 2015). Salt marshes provide numerous ecosystem services, similar to those mentioned for mangrove and seagrass environments (Barbier et al., 2011). Salt marshes provide nursery habitat for many species of fish and shellfish, thus supporting fisheries and biodiversity (Wu et al., 2011). The ability of salt marshes to slow flow and enhance deposition of suspended sediments also makes them effective for water purification, often benefitting nearby ecosystems such as seagrasses, which can be sensitive to nutrient pollution (Barbier et al., 2011). Similar to seagrass beds and mangrove forests, the high productivity and slow remineralization processes characteristic to salt marshes make them highly effective carbon sinks (Davis et al., 2015).

The coastal protection capacity of salt marshes is of particular interest for this paper. Salt marshes stabilize soils through their root systems and can accrete sediment to increase intertidal height (Rupprecht et al., 2017; Barbier et al., 2011). This makes salt marsh systems highly effective for erosion prevention and coastal protection, even considering rising sea levels (Shepard et al., 2011). Furthermore, salt marsh vegetation act as vertical baffling structures, reducing the velocity, height and duration of incoming waves (Barbier et al., 2011). Salt marshes can also reduce storm surge and prevent coastal flooding by providing extra water storage in comparison to unvegetated coastal areas (e.g., mudflats) (Shepard et al., 2011; Barbier et al., 2011; Wu et al., 2011).

### 2.1.4 Canadian Context

Canada has the longest marine coastline in the world, accounting for 29% of the total global coastal extent (Federal, Provincial and Territorial Governments of Canada, 2010). Canada's coastline is comprised of several coastal habitats, including extensive salt marshes and seagrass meadows (Federal, Provincial and Territorial Governments of Canada, 2010). Salt marshes are found from the southwestern coast of British Columbia, up through the Hudson Plains, and along the Atlantic Coast and the Gulf of St. Lawrence (Federal, Provincial and Territorial Governments of Canada, 2010). Eelgrass beds are an important seagrass habitat native to Canada, found extensively along the Pacific Coast, James Bay, Nova Scotia, Newfoundland and Quebec shorelines (Federal, Provincial and Territorial Governments of Canada, 2010).

The Bay of Fundy, in Nova Scotia and New Brunswick, is dominated by two main salt marsh species: smooth cordgrass (*Spartina alterniflora*) and salt marsh hay (*Spartina patens*) (Gordon et al., 1985; Wu et al., 2011). *S. patens* are also found along the west coast of Canada, whereas the distribution of *S. alterniflora* is primarily limited to Canada's east (Atlantic) coast, as shown in **Fig. 2-2** (Natural Resources Conservation Service, 2021). As mentioned previously, the flood-tolerant *S. alterniflora* dominates low marsh areas, while *S. patens* thrives in the high marsh. *S. alterniflora* is generally taller than *S. patens* but grows in less dense stands (Bilkovic & Mitchell, 2017).

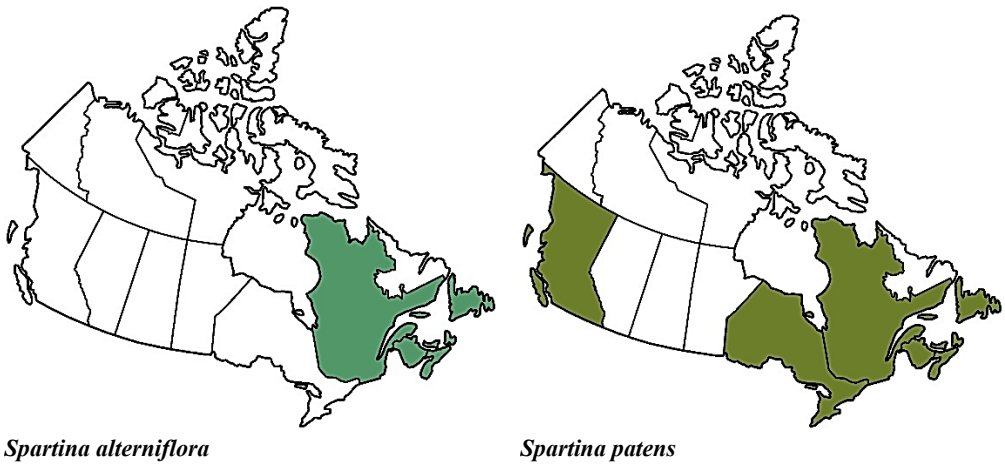


**Fig. 2-2.** North American species distribution for two popular salt marsh species. Maps adapted from USDA NRCS Plants Database (2021).

## 2.2 Coastal Protection Using Vegetation

### 2.2.1 Living Shorelines

Nature-based solutions for coastal protection can take many forms along a continuum of green to grey infrastructure (**Fig. 2-3**) (Smith et al., 2020). Techniques that fall on the softer end of the continuum (left-hand side, **Fig. 2-3**) are generally termed "Living Shorelines" and emphasize the use of vegetation in the coastal protection scheme (NOAA, 2015). In general, a "vegetation only" approach is primarily suitable for the lowest energy settings. In increasingly energetic

coastal areas, other natural features such as large woody debris, coir logs or oyster reefs may be used as marsh edging or to form stabilizing sills.

Bilkovic & Mitchell (2017) define living shorelines by two main objectives: (1) incorporate natural habitats to reduce the risk of coastal flooding and erosion, and enhance shoreline resilience (the ability to withstand disturbances while maintaining structure and function); and (2) create environments that will also yield some level of ecosystem function (e.g. habitat) in addition to coastal defense, hopefully emulating the natural systems they are designed to mimic. Bilkovic & Mitchell (2017) identify coastal wetlands, oyster reefs, dunes and sea grasses as natural habitats that could be considered for living shorelines. Commonly, marsh vegetation is used as the primary natural element for living shoreline design (Bilkovic & Mitchell, 2017).

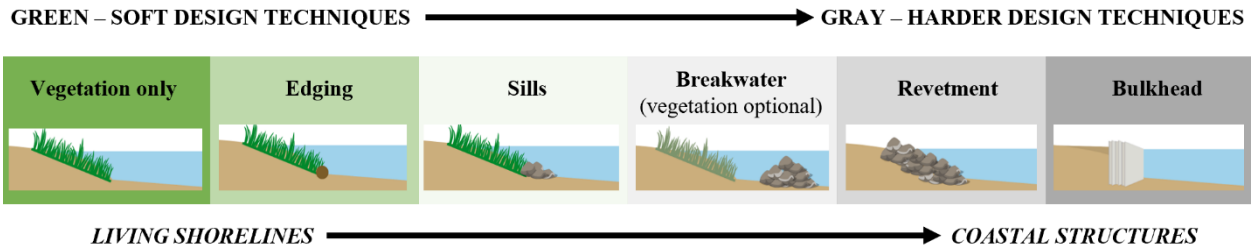


**Fig. 2-3.** Green-to-grey continuum of coastal protection strategies, adapted from NOAA (2015).

Bilkovic & Mitchell (2017) identify site selection as the most important design element for living shoreline success across both above objectives. The physical features of the site must facilitate wetland establishment, including shoreline orientation (~6h of direct sunlight during the growing season), salinity regimes, flood frequency and wave climate. Additional design elements that can dictate the ecosystem service capacity of living shorelines are the vegetation buffer width; plant species composition, configuration and density; habitat access and soil composition (Bilkovic & Mitchell, 2017).

### 2.2.2 Managed Coastal Realignment

Living shorelines are the primary engineered/built approach to using coastal ecosystems for shoreline stabilization. However, coastal wetland restoration projects also take advantage of ecosystem-based coastal defense. Projects where historically reclaimed land (generally for agriculture) is converted back into marshes or swamps for coastal defense have been called "managed coastal realignment" (Temmerman et al. 2013). Coastal realignment projects generally involve the landward relocation, opening or removal of hard coastal defense structures, allowing reinstatement of tidal influence to previously reclaimed low-lying areas (Shepard et al., 2011; Wollenberg et al., 2018). Restored tidal connections promote the creation of new intertidal habitat, and previous projects have found that these new habitats are quickly dominated by salt marsh plants (Wollenberg et al., 2018).

Managed coastal realignment projects have become increasingly popular within the United States, including the restoration of near 8,000 ha of tidal marshes in San Francisco Bay,

California, and large-scale marshland restoration in the Mississippi Delta (Temmerman et al., 2013). The marshland restoration in the Mississippi Delta was proposed as a strategy to protect against hurricane flooding in New Orleans, demonstrating that these large-scale restoration projects can potentially provide adequate protection for extreme weather events (Temmerman et al., 2013).

### 2.2.3 Design Guidance

There is a growing body of literature to support the claims that vegetated coastal environments such as mangrove forests, seagrass meadows and salt marshes are effective in reducing wave energy and preventing shoreline erosion and flooding. Thus, many jurisdictions are recommending the use of natural infrastructure for coastal defense wherever feasible, primarily in the form of living shorelines (Bilkovic et al., 2016).

In the United States, several states and a few environmental agencies have produced guidance documents for promoting the use of living shorelines as coastal defence strategies (Niedowski, 2000; NOAA, 2015; Miller et al., 2016; Hardaway et al., 2017; NYSDEC, 2017; Woods Hole Group, 2017). Several reviewed guidance reports are summarized in **Table 2-1**. Unfortunately, design documentation specific to Canada was very limited, and no extensive documents were found similar to those that exist for the United States (Ecology Action Centre, 2020). However, the Coastal Zone Canada Association has developed the Cold Regions Living Shorelines Community of Practice in order to facilitate information sharing for the effective use of living shorelines in a Canadian climate (Coastal Zone Canada Association, n.d.). This community is open to anyone who is seeking knowledge in the cold-region application of living shorelines.

Many guidance reports for the United States were focused around permitting processes, which have been identified as a significant barrier to the widespread application of living shorelines (Miller et al., 2016; Hardaway et al., 2017; NYSDEC, 2017; Smith et al., 2020). The permitting necessary for installation of a living shoreline is comparatively more extensive than conventional shoreline protection structures (Woods Hole Group, 2017; Smith et al., 2020).

None of the guideline documents directly quantified the attenuation capacity of the recommended wetland plantings. The only quantified parameters were the site hydrodynamic setting (waves, currents, ice, storm surge, wakes, tidal range) (Miller et al., 2016; NYSDEC, 2017; Woods Hole Group, 2017). In many of the reviewed documents, appropriate living shoreline protection strategies were recommended primarily based on the hydrodynamic setting. Often, a three-tier ranking system was defined for the tidal range and wave heights characteristic to a site: Low, Medium and High (Miller et al., 2016; NYSDEC, 2017; Woods Hole Group, 2017). Low energy waves were typically defined as < 2 ft in height, medium energy was defined as 2-5 ft, and high energy was defined as >5 ft (NYSDEC, 2017; Woods Hole Group, 2017). There were large discrepancies in the ranking of tidal conditions, and smaller discrepancies for wave conditions (Miller et al., 2016; NYSDEC, 2017; Woods Hole Group, 2017). These

inconsistencies indicate that there is not a consensus amongst the guidance documents in terms of which environments are appropriate for each living shoreline approach.

Tidal marsh plantings or marsh sill creation are the most relevant living shoreline strategies within the scope of this review. Most of the guidance documents considered these strategies to be applicable to low-moderate energy settings (NOAA, 2015; Miller et al., 2016; Hardaway et al., 2017; NYSDEC, 2017; Woods Hole Group, 2017).

In a few guidance documents, specific species of vegetation were recommended based on marsh zonation. *Spartina alterniflora* was predominantly mentioned as a low marsh species to be used for marsh creation, and *Spartina patens* for high marsh planting (Niedowski, 2000; Miller et al., 2016; Hardaway et al., 2017; Woods Hole Group, 2017). Other native species mentioned in the guidance documents are provided in **Table 2-1**. Note that these species recommendations may be specific to the geographic region of the guidance document. Several guidance documents did not mention any specific species for planting recommendations, limiting the usefulness of the document for engineering design purposes (NOAA, 2015; NYSDEC, 2017; Ecology Action Centre, 2020). Vegetation selection and placement has significant implications for the sustainability of a living shoreline project, as these factors control sedimentation rates and organic matter production, and thus marsh accretion rates (Bilkovic & Mitchell, 2017). Consequently, further research into species-specific recruitment, survival and efficacy for coastal protection is needed to better inform guidance documents.

Recommendations for implementation strategies were also limited. In general, recommendations from the reviewed grey literature were that marsh species should be planted between Mean Tide Level (MTL) and Mean High Water (MHW) (Hardaway et al., 2017; Woods Hole Group, 2017). Mean Tide Level is defined as the arithmetic mean of mean high and mean low water, and Mean High Water is the average of all the high-water heights (NYSDEC, 2017). Maximum marsh slopes were recommended as low as 1:10, and as high as 1:5 (Hardaway et al., 2017; Woods Hole Group, 2017). The New England Living Shorelines document recommended that slopes higher than 1:5 (up to 1:3) be supported with toe stabilization structures (Woods Hole Group, 2017). Miller et al. (2016) recommended a constructed marsh width between 30-70 ft for low-moderate energy settings. This aligns with Bilkovic *et al*. (2016), where it is stated that living shorelines often aim to mimic narrow fringing marshes, typically less than 20 m wide. Spacing and arrangement of plantings was largely not addressed in the guidance reports.

It is clear from the reviewed resources that engineering guidance for using vegetation in coastal protection schemes is limited. The resources that were reviewed provided little quantifiable evidence of the protection provided by various living shoreline approaches. Quantifying the attenuation capacity of different marsh configurations through experimental studies could be integral for making recommendations for optimal protection strategies. These studies should focus on the wave attenuation capacity of various plant species (i.e., resilience, flexibility, seasonal biomass variations, geographic extent), planting densities and arrangements, and under

varying hydrodynamic conditions. The results from physical and numerical modelling should be used to inform design guidelines, to better guide practitioners in designing living shorelines in a manner that maximizes attenuation capacity of native species, while ensuring recruitment success in the site's hydrodynamic setting. An overview of various physical and numerical modelling studies completed to-date is provided in Section 2.3.

**Table 2-1**. Summary of reviewed guidance documents for the design of living shorelines in North America.

| GUIDANCE DOCUMENT | Site Evaluation Parameters | | | Hydrodynamic Rankings (Low, Moderate, High) | Living Shoreline Strategies | Marsh vegetation mentioned | Planting location | Marsh slope | Spacing/ Arrangement |
|---|---|---|---|---|---|---|---|---|---|
| | Physical | Hydrodynamic | Ecological | | | | | | |
| **Virginia (Hardaway et al., 2017)** | • Fetch,<br>• depth offshore,<br>• shoreline morphology,<br>• shoreline orientation,<br>• nearshore morphology,<br>• erosion rates,<br>• bank condition,<br>• bank height,<br>• upland land use,<br>• proximity to infrastructure,<br>• existing shoreline structures | • Tidal range,<br>• storm frequency,<br>• wave climate,<br>• sea-level rise,<br>• boat wakes | • Presence of submerged aquatic vegetation,<br>• width and elevation of beach features,<br>• riparian buffer vegetation | n/a | • Tidal Marsh Planting and Management (small, narrow creeks),<br>• Sills with Planted Marshes,<br>• Marsh Toe Revetment/Sill,<br>• Oyster Reef Sills | *Spartina alterniflora* (low), *Spartina patens* (high, above MHW),<br><br>High marsh/riparian: *Panicum virgatum, Baccharis halimifolia, Morella spp.* | MTL to MHW | 1:10 | 1 - 2 ft apart, clusters preferred over straight rows |
| **New Jersey (Miller et al., 2016)** | • erosion history,<br>• upland slope,<br>• shoreline slope,<br>• width,<br>• nearshore slope,<br>• offshore depth,<br>• soil bearing capacity | • Sea level rise,<br>• tidal range,<br>• wind waves,<br>• currents,<br>• ice effects,<br>• storm surge | • water quality,<br>• soil type,<br>• sunlight exposure | **Waves:** <1 ft, 1-3 ft, >3 ft;<br>**Wakes:** < 1 ft, 1-3 ft, >3 ft;<br>**Currents:** <1.25 kts, 1.25-4.75 kts, >4.75 kts;<br>**Ice:** <2 in, 2-6 in, >6 in;<br>**Storm Surge:** <1 ft, 1-3 ft, >3 ft;<br>**Tidal Range:** <1.5 ft, 1.5-4 ft, > 4 ft | • Marsh Sill,<br>• Breakwater,<br>• Revetment,<br>• Living Reef,<br>• Reef Balls | *Spartina alterniflora, Spartina patens* (salinity tolerant) | n/a | 1:8 - 1:10 | n/a |
| **NOAA (NOAA, 2015)** | • Erosion rates/extent,<br>• site physical characteristics (slope, orientation, bathymetry, fetch),<br>• other structures present,<br>• nearby land & water use | • Currents,<br>• Waves,<br>• boat traffic | • Habitat present | n/a | • Vegetation only,<br>• Edging,<br>• Sills;<br>• Structural components (oyster shells, biologs, concrete reef balls, rock) | n/a | n/a | n/a | n/a |
| **New York State (Tidal Wetlands) (NYSDEC, 2017)** | • Erosion rates,<br>• existing shoreline infrastructure,<br>• shoreline slope | • Waves<br>• boat traffic,<br>• ice,<br>• surface runoff,<br>• tidal range,<br>• sea-level rise | • Habitat present,<br>• soil and sediment types | **Waves:** <2 ft, 2-5 ft, >5 ft; | • Beach nourishment,<br>• Bank stabilization (vegetation, edging or toe protection),<br>• Vegetated slope with structural protection,<br>• Low profile sill with vegetation | n/a (just "native plantings") | n/a | n/a | n/a |

| | | | | | | | | | |
|---|---|---|---|---|---|---|---|---|---|
| **New England (Woods Hole Group, 2017)** | • Elevation,<br>• intertidal slope,<br>• bathymetric slope,<br>• erosion | • Tidal range, energy state (waves, currents, surge) | • Existing environmental resources (bank, dune, beach, salt marsh, mud flat, subtidal, vegetated upland),<br>• nearby sensitive resources | **Waves:** <2 ft, 2-5 ft, >5 ft;<br>**Tidal Range:** <3 ft, 3-9 ft, >9 ft | • Dune Restoration, Beach Nourishment, Coastal Bank Protection, Natural Marsh Creation/Enhancement (with/without toe protection), Living breakwaters | *Spartina alterniflora* (low marsh), *Spartina patens* (high marsh) | Low marsh: MTL to MHW;<br><br>High marsh: MHW to MHHW | 1:6 - 1:10, 1:3 - 1:5 use toe stabilization | n/a |
| **New York State (Salt Marsh) (Niedowski, 2000)** | • Morphology<br>• inlets,<br>• slope,<br>• elevation of site features,<br>• nearshore bottom topography | • Tides, inundation duration, wave energy, water table, terrestrial runoff, precipitation frequency | • Water chemistry & physical properties (salinity, temp, pH, BOD, contaminant conc'ns),<br>• substrate properties (grain size, organic matter, pH, salinity) | n/a | • Salt marsh restoration | Low marsh: *Spartina alterniflora, Salicornia europaea;*<br><br>High marsh: *Spartina patens, Distichlis spicata, Juncus gerardii, Panicum virgatum, Limonium carolinianum, Plantago maritima, Agalinis maritima, Salicornia spp.;* | n/a | 1-3% for marsh establishment | High energy: 1.5-2 ft spacing;<br><br>Low energy: ~3.0 ft spacing (*Spartina alterniflora* specific) |
| **Nova Scotia (Ecology Action Centre, 2020)** | • Erosion,<br>• fetch,<br>• shoreline orientation,<br>• bank slope,<br>• bank height,<br>• nearshore water depth,<br>• substrate type,<br>• width/size of property,<br>• shoreline type,<br>• nearby infrastructure,<br>• neighbouring properties,<br>• outreach opportunities,<br>• research opportunities | • Wave energy, hydrology (tidal regime, freshwater drainage) | • Presence of protective vegetation,<br>• shading,<br>• wildlife habitat potential | n/a | n/a | n/a ("salt-tolerant" species) | n/a | n/a | n/a |

## 2.2.4 Co-Benefits

### 2.2.4.1 Ecological Considerations

The concept of living shorelines was initially conceived as a means of compensating for the environmental degradation imparted by conventional coastal defense structures, particularly habitat fragmentation and biodiversity loss (Bilkovic et al., 2016). Living shorelines provide significant ecological benefits over hard engineering structure through the creation or restoration of highly productive coastal ecosystems.

### 2.2.4.2 Habitat

Natural salt marshes are characterized by high rates of primary productivity (Davis et al., 2015). They also possess the ability to improve water quality, thereby enhancing aquatic habitat for fish, shellfish, mollusks and crustaceans (Horizon Advisors, 2019). Salt marshes have also been identified as essential nursery habitat, as many species of fish and shellfish spend their early stages of life in this sheltered and food-rich environment (Wu et al., 2011).

Living shorelines are designed to mimic natural coastal marshes, and thus incorporate many of the ecological processes associated with their natural counterpart (Bilkovic & Mitchell, 2017). The primary difference between the two environments is the use of a coarse sand material as wetland fill, which can potentially lead to different nutrient pathways than those associated with a natural marsh (Bilkovic & Mitchell, 2017). Additionally, the use of a stone sill or toe protection structure may restrict faunal access to the marsh surface (Bilkovic & Mitchell, 2017). Despite these differences, the habitat benefits associated with living shorelines have been demonstrated in literature (Davis et al., 2006; Gittman et al., 2016). Gittman et al. (2016) found that living shorelines with a sill structure supported higher fish species abundance and diversity in comparison to unvegetated sites proximate to a hardened shoreline reach. Additionally, Gittman et al. (2016) found that the living shoreline constructed with a sill provided better habitat than even the control marshes, due to additional refugia provided by the sill. Davis et al. (2006) found that living shorelines can assume “natural” ecological function almost immediately when considering faunal species recruitment rates. Davis et al. (2006) also proposed, based on the results of their field study, that incorporation of multiple structural habitats within a living shoreline design may enhance its ecological value (i.e. riprap, oyster shell, vegetation and woody debris). Efforts to correlate individual design elements to habitat function could better inform design practices in order to maximize the ecological benefits of living shorelines (Davis et al., 2006).

### 2.2.4.3 Carbon Sequestration

Vegetated coastal habitats are among the most efficient biosequestration systems, often termed “blue carbon” ecosystems (Macreadie et al., 2017; Cuellar-Martinez et al., 2019). The large capacity for carbon sequestration arises from the unique structure and function of these ecosystems. Vegetated coastal habitats have high rates of primary productivity and efficiently

trap suspended particles, together contributing to an elevated rate of organic matter accumulation (Lovelock et al., 2017). Low soil oxygen conditions slow the decomposition of this organic matter, preventing the remineralization of organic carbon to atmospheric carbon dioxide (Lovelock et al., 2017). Roots and rhizomes, which account for the largest organic carbon fraction in plant biomass, also work with the canopy to stabilize soils and prevent carbon mobilization via erosion (Cuellar-Martinez et al., 2019). Previous studies have proven that blue carbon ecosystems have a much higher capacity to store carbon than terrestrial forest ecosystems – losing 1 hectare of a blue carbon environment is approximately equivalent to the loss of 10-40 hectares of terrestrial forest (Davis et al., 2015; Macreadie et al., 2017).

The carbon sequestration capacity of coastal wetlands has played a significant role in driving restoration and creation projects (Davis et al., 2015). A standard for the creation and restoration of coastal wetlands was developed in 2014, in order to provide a mechanism for quantifying the emission offsets associated with wetland restoration works (Davis et al., 2015; Verified Carbon Standard, 2014). However, development of this standard mainly relied on studies of expansive wetland sites with large ratios of marsh interior to edge (Davis et al., 2015). In contrast, living shoreline projects are generally designed to mimic narrow fringing marshes (<30 m width), and have sandy platform sediments with low organic matter content (Davis et al., 2015; Bilkovic et al., 2016). Thus, these standards are likely more applicable to estimating the carbon sequestration benefits associated with large-scale managed coastal realignment projects.

While the vegetative characteristics of living shorelines, such as stem density and plant height, will rapidly mirror natural marshes, sediment biogeochemical processes are much slower to develop (Davis et al., 2015; Bilkovic & Mitchell, 2017). These delayed processes largely dictate carbon sequestration capacity. Trajectory models for soil organic matter development in constructed marshes suggest that it could take approximately 15 years to reach equivalency with natural reference marshes (Bilkovic & Mitchell, 2017).

Despite the delay in carbon sequestration capacity of a constructed living shoreline, a study by Davis et al. (2015) demonstrated that these environments still provide significant long-term rates of carbon capture. It was estimated that living shorelines could sequester 70-80 g C $m^{-2}$ $yr^{-1}$as capture rates reach long-term equilibrium (~100-yr) (Davis et al., 2015). This study was performed specifically considering *Spartina alterniflora* marshes. While this estimate is on the lower end of the average carbon burial rates for *S. alterniflora*, living shorelines are still capable of significant carbon offset benefits considering the potential extent of wetland creation through living shoreline design (Davis et al., 2015).

#### 2.2.4.4 Economic Considerations

The costs associated with maintaining conventional “hard” shoreline protection structures in the context of climate change have been significant drivers for the development of NBS for coastal defense (Gracia et al., 2018). Several studies have estimated the costs associated with the expected maintenance and reconstruction of hard coastal structures (Temmerman et al., 2013;

Hinkel et al., 2014). For example, adjustments required to adapt to the Dutch flood defense system to increasing flood risks are estimated to cost up to €1.6 billion per year by 2050 (Temmerman et al., 2013). Hinkel et al. (2014) also estimated significant global costs of continuing to protect the coast with hard structures (e.g. dikes): between US$ 12-71 billion annually by 2100.

Similar cost metrics have not yet been developed for nature-based coastal defense strategies, however, cost-benefit analyses have demonstrated the economic benefit of nature-based alternatives over the continued maintenance and reconstruction of hard structures. A cost-benefit analysis for Humber estuary, UK, determined that the restored tidal marsh will become more economically beneficial than maintaining coastal dike systems after only 25 years (Temmerman et al., 2013). Similarly, a study for the Scheldt estuary, in Belgium, estimated that it would take as low as 20 years to recover all costs associated with the restored 2,500 ha tidal marsh (Temmerman et al., 2013). Thus, it appears evident in literature that nature-based solutions, such as wetland restoration or creation, are an economically beneficial alternative to conventional coastal engineering structures.

## 2.3 State of the Art Research in Vegetation for Coastal Protection

### 2.3.1 Physical Modelling

#### 2.3.1.1 Scaling and Scale Effects

Physical modelling approaches aim to recreate natural coastal environments in a laboratory setting, in order to investigate wave-vegetation interactions in a more controlled and accessible location. There are several considerations that must be made in order to accurately mimic natural coastal environments, including selection of model vegetation, and scaling considerations. Often, due to size limitations of physical modelling facilities, experiments must be downscaled to stay within the capabilities of the facility. The degree of scaling will depend on the size of facility as well as the target hydrodynamic conditions. In order to accurately replicate prototype-scale conditions, the model must satisfy both geometric and dynamic similitude (Falkenrich, 2020; Wu et al., 2011). Geometric similitude is often easy to achieve through maintaining ratios of linear dimensions (Wu et al., 2011). The length-scale ratio required for geometric similitude is as follows:

$$N_L = \frac{L_p}{L_m} \quad \textbf{(2-1)}$$

Where $N_L$ is the scale ratio, $L_p$ is the prototype length, and $L_m$ is the model length (Falkenrich, 2020).

Dynamic similarity is achieved through balancing the scaling of all acting forces within the system (i.e. inertia, gravity and viscosity) (Wu et al., 2011; Falkenrich, 2020). It is not possible to properly scale all forces in a manner that achieves dynamic similitude, and thus predominant

forces within the modelled system must be prioritized (Wu et al., 2011). For wave modelling experiments, Froude scaling is often adopted, assuming that bottom friction is small and that Reynolds number (Re) is large enough to assume a constant drag coefficient (Wu et al. 2011; Wu & Cox; Maza et al. 2019, Hoque et al., 2018; Blackmar et al., 2014; Sanchez-Gonzalez et al., 2011; Ozeren et al., 2014). Froude scaling parameters are provided in **Table 2-2**.

**Table 2-2.** Froude scaling ratios.

| Parameter | Unit | Scale Ratio |
|---|---|---|
| Length | m | $N_L$ |
| Area | $m^2$ | $N_L^2$ |
| Volume | $m^3$ | $N_L^3$ |
| Time | S | $\sqrt{N_L}$ |
| Velocity | m/s | $\sqrt{N_L}$ |
| Acceleration | $m/s^2$ | 1 |

When modelling vegetation, flexible vegetation in particular, it is important to ensure that vegetation motion is accurately captured (Ghisalberti & Nepf, 2002; Sanchez-Gonzalez et al., 2011; Manca et al., 2012; Koftis et al., 2013; Anderson & Smith, 2014; Lei & Nepf, 2019). Flexible vegetation motion is governed by three primary forces: drag force ($F_D$), a buoyancy force ($F_B$), and a restoring force ($F_R$) (Ghisalberti & Nepf, 2002, Sanchez-Gonzalez et al., 2011). The restoring force is dependent on the rigidity of the plant stem or blade (Ghisalberti & Nepf, 2002). Dynamic similitude may be achieved through matching two independent ratios of these forces: $F_B/F_R$ and $F_R/F_D$ (Ghisalberti & Nepf, 2002). Ghisalberti & Nepf (2002) proposed the following two scale parameters for balancing the aforementioned force ratios:

$$\lambda_1 = \frac{(\rho_w - \rho_v) l^3}{E b_v^2} \quad \textbf{(2-2)}$$

$$\lambda_2 = \frac{E b_v^3}{l^3 U^2} \quad \textbf{(2-3)}$$

Where $\rho_w$ and $\rho_v$ are the densities of water and vegetation, respectively, $U$ is the mean in-canopy velocity, $E$ is the modulus of elasticity, $b_v$ is the stem/blade thickness and $l$ is the total stem/blade length (Ghisalberti & Nepf, 2002). There is uncertainty associated with selecting the value of $U$ in **Eq. 2-3,** thus Ghisalberti & Nepf (2002) recommend selecting $\lambda_1$ as the critical scaling parameter. However, it should be noted that if the vegetation deflection angle ($\alpha$) can be accurately mimicked between model and prototype, and $\lambda_{1,p} = \lambda_{1,m}$, then $\lambda_2$ will also be matched due to the assumptions made in the development of the scale parameter equations (Ghisalberti & Nepf, 2002). These scaling parameters were used for physical modelling studies by Ghisalberti & Nepf (2002) and Sanchez-Gonzalez et al. (2011), both of which focused on modelling sea grass (*Zostera marina* and *Posidonia oceanica*, respectively).

Koftis et al. (2013), also modelling sea grass, proposes that the critical scaling parameter, $\lambda_1$, developed by Ghisalberti & Nepf (2002) is not sufficient for vegetation models as it does not directly consider flow velocity, which has been shown to be a key parameter in determining

deformation of an elastic solid under flow effects. Instead, Koftis et al. (2013) recommend using the Cauchy number ($C_y$) for scaling of flexible vegetation. The Cauchy number is the ratio of dynamic pressure and the modulus of elasticity, defined by Koftis et al. (2013) as follows:

$$C_y = \frac{\rho_w U_c^2}{E} S^3 \quad \textbf{(2-4)}$$

Where $S$ is the slenderness number, defined as the ratio of the plant leaf maximum cross-sectional dimension, over the minimal cross-sectional dimension, and $U_c$ is the characteristic velocity (Koftis et al., 2013).

#### 2.3.1.2 Surrogate Vegetation

An important consideration for physical modelling of coastal vegetation is the selection of appropriate model elements. Some studies have utilized live vegetation in large-scale physical modelling studies, collected either through excavation, acquisition of nursery seedlings, or by growing the plants from seed (Poppema et al., 2019; Moller et al., 2014; Rupprecht et al., 2017; Fonseca & Calahan, 1992; Tschirky et al., 2000). Lara et al. (2016) provides a thorough overview of the requirements for physical modelling with live vegetation, including experimental design considerations, and growing versus collecting methods.

Growing or excavating live vegetation is not always feasible for physical modelling, especially when experiments cannot be conducted at prototype-scale. In these cases, a surrogate vegetation element must be developed. Various materials have been used to represent sea grass, salt marsh and mangrove species in a physical modelling setting (see **Table 2-3**). Some of these vegetation surrogates were developed at prototype-scale to avoid errors associated with downscaling and Froude similitude assumptions (Lima et al., 2006; Augustin et al., 2009; Manca et al., 2012; Koftis et al., 2013; Anderson & Smith, 2014; Ozeren et al., 2014; Zeller et al., 2014). A few studies utilized vegetation surrogates at small-scale, namely Maza et al. (2019), Vettori & Nikora (2020), Hoque et al. (2018), Blackmar et al., (2014), Lovas & Torum (2000), and Sanchez-Gonzalez et al. (2011), requiring additional scaling of the selected surrogate elements.

Important considerations for selecting surrogate elements that can accurately mimic natural vegetation include: flexibility of the target vegetation, biophysical vegetation parameters, and plant mechanical characteristics (Johnson et al., 2014). Some species of vegetation may be successfully mimicked using rigid elements such as aluminum rods (mangroves) or wooden dowels (salt marsh), despite demonstrating some degree of flexibility in reality (Maza et al., 2019; Augustin et al., 2009; Hoque et al., 2018; Wu, et al., 2011; van Veelen et al., 2020). A combined field-numerical study by Jadhav et al. (2013) demonstrated that *Spartina alterniflora* can be reasonably modeled as a rigid cylinder. Similarly, Augustin et al. (2009) modelled *Spartina alterniflora* using both rigid and flexible elements and found that the two models produced similar attenuation effects for the tested flow conditions. Thus, the appropriate selection of rigid versus flexible elements may depend on the experimental hydrodynamic conditions.

Often elements are selected to mimic the geometric parameters of the target vegetation, including stem/blade length, width, diameter and planting density (Maza et al., 2019; Anderson & Smith, 2014; Augustin et al., 2009; Ozeren et al., 2014). For small-scale physical models with surrogate vegetation, mimic diameters should only downscaled if a reasonable Reynolds number can be maintained, as this will strongly influence the drag coefficient (Blackmar et al., 2014).

Anderson & Smith (2014) identified posture and motion as the two most important parameters when selecting surrogate vegetation. Thus, in the study by Anderson & Smith (2014), materials were selected considering density and modulus of elasticity in order for the surrogate to accurately mimic the wave-induced swaying motion of *Spartina alterniflora*, while also maintaining an upright position in shallow waters. Mimics were similarly selected for experiments performed by Augustin et al. (2009), Koftis et al. (2013), Lima et al. (2006), and Manca et al. (2012).

Similar to the scale ratios proposed by Ghisalberti & Nepf (2002), Zeller et al. (2014) selected mimic materials to match field sea grass conditions based on three non-dimensional parameters that compare buoyancy, rigidity and inertial forces. The three parameters are as follows:

$$\lambda_B = \left(\frac{\rho_g}{\rho_w} - 1\right)\frac{b_v g}{U_{\max}^2} \quad \textbf{(2-5)}$$

$$\lambda_I = \frac{b_v \dot{U}}{U_{max}^2} \quad \textbf{(2-6)}$$

$$\lambda_R = \frac{E b_v^3}{\rho_w l^3 U_{max}^2} \quad \textbf{(2-7)}$$

Where $\rho_g$ and $\rho_w$ are the density of the blade and water, respectively, $g$ is gravitational acceleration, $U_{max}$ is the maximum phase-averaged free-stream velocity over the wave period, and $\dot{U}$ is the characteristic streamwise fluid acceleration (Zeller et al., 2014).

One significant limitation of modelling real vegetation using surrogate elements is that there is significant seasonal and geographical variation in plant biophysical and biomechanical parameters within-species (Neumeier, 2005; Schulze et al. 2019, Schoutens et al. 2020). Thus, it may be necessary to identify the target region and season for replication. An additional limitation associated with the use of surrogate vegetation is the difficulty of modelling vertical variation in plant characteristics (Wu et al., 2011; Tempest et al., 2015; Vettori & Nikora, 2020). A study by Wu et al. (2011) demonstrated that the vertical density and biomass distribution of live plants has an impact on their wave attenuation capacity, particularly with respect to relative water depth, which was not captured through the surrogate vegetation as it was uniform across its length. Furthermore, selected surrogate elements may be an oversimplification of live vegetation elements, ignoring macro-features that contribute to flow structure and therefore attenuation capacity. This was demonstrated by Vettori & Nikora (2020), who modelled *Saccharina latissimi* seagrass using a single long, rounded rectangular element (LDPE). The oversimplification of the live seaweed structure, which has a wider blade with bullations and ruffles, yielded biased low

drag coefficients for the surrogate elements in comparison to the live vegetation (Vettori & Nikora, 2020). This study highlights the importance of incorporating macro-features of live vegetation into model elements for certain species.

#### 2.3.1.3 Testing Parameters

The main factors found to influence the wave attenuation capacity of vegetation fields are: (1) wave height, (2) wave period, (3) relative depth, (4) stem spatial density and (5) plant flexibility (Maza et al., 2019; Augustin et al., 2009; Anderson & Smith, 2014; Blackmar et al., 2014; Ozeren et al., 2014; Lei & Nepf, 2019; Rupprecht et al., 2017; Paul et al., 2016; van Veelen et al., 2020). The influence of the aforementioned test variables on wave attenuation has been investigated through several decades of physical modelling studies, at both prototype- and small-scale. These studies also varied in the material used for modelling vegetation (i.e. surrogate versus live plants). A summary of all physical modelling studies reviewed herein is provided in **Table 2-3**. The relative influence of each testing variable on the wave attenuation capacity of coastal vegetation, as demonstrated through the reviewed physical modelling studies, is discussed in the following sections.

##### *Wave Conditions (height and period)*

Maza et al. (2019) investigated the influence of wave height and period on the wave attenuation capacity of mangrove forests, using PVC and aluminum rods to model a scaled (1:6) *Rhizophora* forest. Damping coefficients determined for various water depths, wave heights and wave periods indicated that, in general, higher damping coefficients are associated with higher wave heights and shorter wave lengths (i.e. smaller wave periods). In addition, higher correlations were found between the damping coefficient and wave height than with wave steepness, indicating that wave height has greater control than wave period in terms of attenuation capacity (Maza et al., 2019). The influence of wave period on wave attenuation capacity appears to be variable throughout performed physical modelling studies and may depend on vegetation parameters or the relative influence of other testing variables (Anderson & Smith, 2014; Maza et al., 2019).

Anderson & Smith (2014) investigated the wave attenuation capacity of *Spartina alterniflora* using semi-flexible cross-linked polyolefin (XLPO) tubing. Surrogate vegetation was tested with various irregular wave configurations, through varying submergence ratio (or relative depth), wave height and wave period. Stem density was also varied between wave tests. Wave conditions (height and period) were not found to have as strong of an influence on attenuation as the other tested parameters (submergence and stem density). In contrast to the study by Maza et al. (2019), the influence of wave period on wave attenuation was inconclusive, with different trends occurring for emergent (i.e. stem height > water depth) versus submerged conditions (Anderson & Smith, 2014; Maza et al., 2019). More specifically, emergent conditions yielded a small positive correlation between wave period and attenuation, while submerged conditions yielded a negative correlation (Anderson & Smith, 2014).

Many physical modelling studies investigating the wave attenuation capacity of salt marsh or sea grass canopies were performed for relatively low energy conditions (wave heights < 20 cm) (**Table 2-3**). Contrastingly, Rupprecht et al. (2017) investigated the potential for a rapid decline in the wave attenuation capacity of vegetation under extreme hydrodynamic conditions as a result of stem breakage or permanent deformation (bending/folding). Live vegetation was used in this prototype-scale study: two common salt marsh species with differing biophysical parameters (*Puccinellia maritima* and *Elymus athericus*). The results confirmed that as wave heights increase beyond a threshold (measured through orbital velocities in this study), biomass loss (stem breakage) or stem folding caused a rapid decrease in flow obstruction, thereby reducing flow attenuation (Rupprecht et al., 2017). This threshold was found to be different for the two tested marsh species. Rupprecht et al. (2017) also investigated the impact of increasing wave energy on plant motion, which further influenced attenuation capacity due to changes in relative velocities between the vegetation and the waves. Elucidation of this hydrodynamic threshold contradicts studies that stated wave attenuation capacity generally increases with increasing wave height (Maza et al., 2019). This threshold concept is further confirmed through the large-scale physical modelling study performed by Moller et al. (2014), who determined that assuming the empirical relations proposed for wave attenuation as a function of wave height from previous studies yielded an overestimation of wave dissipation when considering storm conditions (large wave heights).

### *Relative Depth*

Maza et al., (2019) also investigated the effects of varying water depth on the damping capacity of model *Rhizophora* forests. Water depth dictates the frontal area of the mangrove that is exposed to flow, which was found to influence damping coefficients (Maza et al., 2019). Damping coefficients were greatest for smallest water depths, as the frontal area was the largest for these testing scenarios. The results from Maza et al. (2019) were consistent with the findings of a previous physical study performed by Hoque et al. (2018), who also investigated wave damping through scaled *Rhizophora* forests.

Augustin et al. (2009) investigated the effect of water depth on the wave attenuation capacity of *Spartina alterniflora,* utilizing prototype-scale model vegetation. The effect of water depth was assessed using the concept of submergence ratio, defined as the ratio of plant stem height or blade length to water depth (Augustin et al., 2009). Thus, as the submergence ratio increases, the vegetation occupies a larger percentage of the water column. Augustin et al. (2009) found submergence ratio to have a significant influence on wave height decay, specifically that emergent conditions yielded a higher amount of wave attenuation, thus corresponding to larger effective bulk drag coefficients ($C_{d,submerged}$ = 0.01-0.08; $C_{d,emergent}$ = 0.05-0.15). Augustin et al. (2009) also determined that submergence ratio may dictate the relative influence of other testing variables on wave attenuation, specifically stem density and wave period. Stem density was found to have more of an impact on wave attenuation under emergent conditions, and the influence of wave period on drag forces decreased as the vegetation became more submerged

(Augustin et al., 2009). Furthermore, Augustin et al. (2009) linked submergence ratio to the strength of the relationship between $C_d$ and Reynolds number versus $C_d$ and the Keulegan-Carpenter number (KC). Under emergent conditions, drag coefficients were found to have a stronger link to the Reynolds number, versus a greater dependence on KC under submerged conditions (Augustin et al., 2009).

Anderson & Smith (2014) had similar findings for the influence of water depth relative to plant height with respect to model salt marsh vegetation. Anderson & Smith (2014) evaluated wave attenuation under emergent and near-emergent conditions, and found drag coefficients for emergent conditions to be much larger.

Conversely, Ozeren et al. (2014) found that $C_d$ does not significantly depend on submergence ratio for rigid model elements in the emergent and near-emergent conditions tested in their study. The study by Ozeren et al. (2014) utilized a much higher stem density than Anderson and Smith (2014) or Augustin et al. (2009), which may indicate that the relative influence of stem density might outweigh submergence ratio at high densities. Ozeren et al. (2014) did, however, find submergence ratio to have an impact on drag coefficients for live models, emphasizing the significance of vertical variation in vegetation properties that was not captured through the surrogate elements.

Fonseca & Cahalan (1992) observed a loss of wave reduction effects induced by sea grass (live plants) as waves approached deepwater conditions (water depth > wavelength/2). More specifically, their physical modelling tests indicated that waves may pass over a sea grass canopy with little to no effects if the sea grass is submerged by >25 cm. Manca et al. (2012) and Koftis et al. (2013) also investigated the effect of submergence on wave attenuation by sea grass meadows using surrogate elements (PVC). Both studies found that wave damping increased with increasing submergence ratio (Manca et al., 2012; Koftis et al., 2013).

Wu & Cox (2016) investigated the impacts of water depth on flow attenuation through stands of homogeneous versus heterogeneous salt marsh vegetation. Wu & Cox (2016) utilized zip ties to model *Schoenoplectus pungens* at small-scale (1:4). A homogeneous stand was assessed with all model elements having the same length. A heterogeneous stand was also tested where stems of various heights were installed throughout the flume. Wu & Cox (2016) found a notable difference in attenuation capacity between the two cases, with uniform stands exemplifying a greater attenuation capacity due to vegetation occupying the entire water column. The difference in damping factors between uniform and heterogenous vegetation increased dramatically with increasing water depth. The results from Wu & Cox (2016) indicated that the vertical biomass distribution within a field of salt marsh vegetation may be the most important factor in dictating attenuation or drag coefficients, more significant than wave nonlinearity or plant flexibility. This is an important consideration for accurate modelling of the attenuation capacity of natural salt marshes, which exhibit significant variability throughout a stand (Schulze et al., 2019).

The influence of relative water depth or submergence ratio on the wave attenuation capacity of coastal vegetation is also important when considering flexible versus rigid vegetation, as the effective height of flexible vegetation may be reduced as a result of bending or swaying. The influence of vegetation flexibility will be discussed further in a later section.

### *Stem Density/Arrangement*

Several physical modelling studies have tested the influence of stem density (number of plants per unit area) and arrangement on wave attenuation (Augustin et al., 2009; Ozeren et al., 2014; Lei & Nepf, 2019; Blackmar et al. 2014). The results of each study have been somewhat conflicting, however this could be due to minimal overlap with respect to the test vegetation and stem densities. Augustin et al. (2009) tested the influence of stem density through installing a heterogeneous field of model vegetation, with the front of the field planted at a higher density (194 stems/$m^2$) than the back (97 stems/$m^2$). Augustin et al. (2009) found the lower stem density yielded higher drag coefficients than high density, potentially due to sheltering between the individual plant stems.

Contrastingly, Manca et al. (2012), Blackmar et al. (2014), Ozeren et al. (2014) and Lei & Nepf (2019) each found that higher stem densities resulted in higher wave attenuation rates. Additionally, Lei & Nepf (2019) tested different stem densities with both staggered and random arrangements and found that plant configuration did not play a significant role in wave damping. The stem densities tested in Manca et al. (2012), Blackmar et al. (2014), Ozeren et al. (2014) and Lei and Nepf (2019) were much higher than those tested in Augustin et al. (2009), which may account for their differing conclusions with respect to stem density influence on wave attenuation.

### *Stem Rigidity/Flexibility*

Vegetation flexibility has been found to have a significant impact on wave attenuation, particularly when hydrodynamic conditions are high enough that wave-induced vegetation motion occurs (Rupprecht et al., 2017). Vegetation motion changes the relative velocity between the fluid and vegetation, consequently impacting drag forces and wave attenuation (van Veelen et al., 2020).

The response of coastal vegetation to hydrodynamic forcing is inextricably tied to plant rigidity and is often categorized into either an “avoidance” response or a “resistance” strategy (Schoutens et al. 2020). Plants that exhibit an avoidance strategy have developed morphological adaptations to minimize the drag forces imparted by incoming waves (shape reconfiguration, compact size or simple architecture) (Rupprecht et al., 2017; Vuik et al., 2018; Schoutens et al., 2020). Alternatively, some plants exhibit stronger anchoring or enhanced rigidity in order to resist drag (“resistance” strategy) (Rupprecht et al., 2017; Vuik et al., 2018; Schoutens et al., 2020). The strategy adopted by certain vegetation has an influence on its response to hydrodynamic forces, with “resistance” vegetation often bending or breaking at lower hydrodynamic conditions than “avoidance” plants (Rupprecht et al., 2017, Vuik et al., 2018).

The degree of vegetation motion is also significantly influenced by plant rigidity. Rupprecht et al. (2017) identified two mechanisms of wave-induced vegetation motion: swaying motion and whip-like motion. To investigate the onset of the two types of motion, Rupprecht et al. (2017) performed a full-scale physical modelling study using two species of live vegetation with differing flexural rigidities. Results from the experiment indicated that *Puccinellia* exhibited a lower potential for wave dissipation than the more rigid vegetation of the *Elymus* canopy, however *Puccinellia* experienced significantly lower physical damage. Contributing to the lower wave attenuation capacity was the earlier onset of "whip-like" motion in the *Puccinellia* canopy. Whip-like motion is characterized by an extended, wider-angled forward bend, followed by a rapid, small-angled backward bend (Rupprecht et al., 2017). Whip-like movement can cause a flattening of the vegetation canopy for an extended portion of the wave cycle, resulting in a reduction in vegetative resistance to flow (Rupprecht et al., 2017). The study by Rupprecht et al. (2017) highlights an important trade-off in the wave attenuation capacity of flexible versus rigid vegetation. While flexible vegetation may provide reduced attenuation capacities, it is more resilient under extreme hydrodynamic conditions. The importance of this trade-off, and its potential application for design, has been discussed in several other studies as well (Bouma, et al., 2005; Paul et al., 2016; Schoutens et al., 2020).

Paul et al. (2016) performed a physical modelling study using vegetation mimics where only biomass and stiffness were altered to identify the relative influence of each parameter on wave attenuation. Results indicated that vegetation stiffness was the driving parameter, as it dictated the bending angle for stems/blades which directly influenced the effective leaf length. A reduction in the effective leaf length was correlated to reduced attenuation, in alignment with the studies that found that decreasing submergence ratio or frontal area yielded lower attenuation rates (Augustin et al., 2009; Wu & Cox, 2016; Fonseca & Cahalan, 1992; Anderson & Smith, 2014; Maza et al., 2019). Results from physical modelling by Ozeren et al. (2014) also demonstrated that flexible vegetation generally yields lower wave attenuation values than rigid vegetation.

Van Veelen et al. (2020) modelled salt marsh vegetation using both flexible and rigid surrogates (silicon rods and bamboo dowels, respectively). Considering the tested wave conditions, van Veelen et al. (2020) found that the drag coefficient of flexible vegetation was up to 70% lower than rigid vegetation mimics. Furthermore, van Veelen et al. (2020) determined that the drag coefficient for flexible vegetation had consistent correlations with Reynolds number, relative wave height, Froude number and Keulegan-Carpenter number. This indicates that the attenuation capacity of flexible vegetation is primarily dictated by hydrodynamic conditions (van Veelen et al., 2020). Conversely, rigid vegetation was more strongly correlated to the Reynolds and Keulegan-Carpenter numbers, which both depend on stem diameter. This indicates that attenuation by rigid vegetation is dictated by vegetation physical properties and not flow conditions (van Veelen et al., 2020).

### *Standing Biomass*

Considering the combined influences of stem density and flexibility, Bouma et al. (2010) investigated the wave attenuation of live *Puccinellia maritima* and *Spartina anglica,* two marsh species with significantly different biomechanical properties. Bouma et al. (2010) found wave attenuation for the more flexible *P. maritima* to be comparable to the more rigid *S. anglica*, when considered on the basis of standing biomass. This contrasts with previous findings that indicate that flexible species cannot provide the same level of wave attenuation as more rigid species. Maza et al. (2022) investigated this further, comparing the wave attenuation of live *Spartina maritima*, *Salicornia europaea*, *Juncus maritimus* and *Halimione portulacoides*, species with differing morphologies and biomechanical properties. Through their flume study, Maza et al. (2022) demonstrates a strong relationship between wave damping and standing biomass, particularly when considering a "hydraulic standing biomass" term, that additionally takes into account relative stem submergence, water depth, and incident hydrodynamic conditions.

### *Heterogeneity*

The influences of heterogeneity in vegetation fields have been investigated through physical modelling studies by Blackmar et al. (2014) and Wu & Cox (2006). Both studies represented heterogeneity primarily through changes in stem height. As mentioned previously, Wu & Cox (2006) found that heterogeneity can cause a reduction in wave attenuation capacity as not all stems occupy the same proportion of the water column. The study by Blackmar et al. (2014) investigated the potential use of linear combinations of drag coefficients from homogenous stands for predicting the wave attenuation capacity of heterogeneous stands. The predictions from this linear combination method yielded results that were fairly consistent with the physical modelling results for the heterogeneous vegetation stand (Blackmar et al., 2014). The results from Blackmar et al. (2014) are consistent with results from a field investigation by Augustin et al. (2009), who similarly found that friction factors from homogeneous vegetation fields can be applied in a patchwork manner to determine the overall wave attenuation across a heterogeneous stand.

### *Flume Friction Effects*

The physical modelling study performed by Maza et al. (2019) found that neglecting the contributions of wall and bottom friction to wave attenuation can lead to an overestimation of vegetation-induced damping. Thus, it was recommended that all physical modelling studies considering wave attenuation through vegetation be tested with and without vegetation, in order to remove flume friction effects and obtain accurate estimates of vegetation attenuation capacity (Maza et al., 2019).

**Table 2-3.** Summary of physical modelling studies for flow/wave attenuation through coastal vegetation. All values are presented in prototype-scale.

| Study | Target Species | Environment | Model Material | Scaling | Testing Variables | Observed Variables | Wave Conditions | Wave Type | Re | KC | Stem Density |
|---|---|---|---|---|---|---|---|---|---|---|---|
| ***Maza,* et al. *(2019)*** | *Rhizopohora forest* | Mangrove | PVC (trunk), aluminum rods (roots) | 1:6 (Froude similarity) | • water level,<br>• wave height,<br>• wave period | • wave attenuation,<br>• forces exerted on model mangroves | Peak period: 2.94-6.47 s<br><br>Wave height: 0.24-0.90 m | Regular (Stokes II, Stokes III & Cnoidal); Random (JONSWAP) | 5000 < Re < 55000 | n/a | n/a |
| ***Anderson & Smith (2014)*** | *Spartina alterniflora* | Salt marsh | XLPO tubing | 1:1 | • stem density,<br>• submergence,<br>• wave height,<br>• peak period | • wave attenuation | Peak period: 1.25-2.25 s<br><br>Wave height: 5.0-19.2 cm | Irregular (TMA shallow-water), single and double-peaked cases. | 533 < Re < 2296 | 26 < KC < 112 | 200-400 stems/$m^2$ |
| ***Augustin* et al. *(2009)*** | *Spartina alterniflora* | Salt marsh | Cylindrical wooden dowels (rigid), polyethylene foam tubing (flexible) | 1:1 | • peak period,<br>• relative water depth,<br>• stem density,<br>• stem rigidity | • wave attenuation | Peak period: 1.5-2.0 s<br><br>Wave height: 8.5 cm | Irregular (TMA shallow-water) | 3300 < Re < 8500 (approx.) | 40 < KC < 105 (approx.) | 97 - 194 stems/$m^2$ |
| ***Rupprecht* et al. *(2017)*** | *Puccinellia maritima, Elymus athericus* | Salt marsh | Live plants | 1:1 | • stem flexibility,<br>• stem density,<br>• stem height | • stem breakage,<br>• plant motion,<br>• wave orbital velocity | Period: 1.5-6.2 s<br><br>Wave height: 0.1-0.9 m | Regular, non-breaking | n/a | n/a | *Elymus:* 1225+/-575 stems/$m^2$<br>*Puccinellia:* n/a (too many to count) |
| ***Paul* et al. *(2016)*** | *n/a* | Sea grass/ salt marsh | Plastic strips (Lexaan plates) | n/a | • flexural rigidity,<br>• stem density,<br>• stem frontal area | • drag force | Peak period: 1.4-5.1 s<br><br>Wave height: 0.1-0.9 m | Irregular (JONSWAP); Regular | n/a | n/a | n/a |
| ***Poppema* et al. *(2019)*** | *Spartina anglica* | Salt marsh | Live plants | 1:1 | • water depth,<br>• wave height,<br>• accretion/ erosion treatment depth,<br>• seedling age | • critical disturbance depth,<br>• bed level change,<br>• seedling survival | Period: ~15 s<br><br>Wave height: 3-9 cm | Single wave | n/a | n/a | n/a |
| ***Moller* et al. *(2014)*** | *Puccinellia maritima, Elymus athericus, Atriplex prostrata* | Salt marsh | Live plants | 1:1 | • wave height | • wave dissipation,<br>• soil surface response,<br>• vegetation motion (video) | Peak period: 1.5-6.2 s<br><br>Wave height: 0.1-0.9 m | Irregular (JONSWAP); Regular | n/a | n/a | *Elymus:* 1225+/-575 stems/$m^2$<br>*Puccinellia:* n/a<br>*Atriplex:* n/a |
| ***Ghisalberti & Nepf (2002)*** | *Zostera marina* | Sea grass | Wooden dowels (stem), LDPE film (blades) | n/a | • flow depth<br>• flow rate | • velocity profiles/spectra | n/a | n/a (unidirectional flow) | 1100 < Re < 9400 | n/a | ~315 stems/$m^2$ (randomly placed) |
| ***Ozeren* et al. *(2014)*** | *Spartina alterniflora, Juncus roemerianus* | Salt marsh | EPDM foam-rubber cords, live plants | 1:1 | • stem height,<br>• stem density,<br>• model vs. real vegetation | • wave attenuation,<br>• bulk drag coefficient | Peak period: 0.7-2.0 s<br><br>Wave height: 3-15 cm | Regular; Irregular (JONSWAP) | 200 < Re < 4500 (approx.) | 2 < KC < 80 (approx.) | Model: 156-623 stems/$m^2$<br>*S. alterniflora:* 405-545 stems/$m^2$<br>*J. roemerianus:* 2857 stems/$m^2$ |
| ***Vettori & Nikora (2020)*** | *Saccharina latissima* | Sea grass | LDPE sheeting | 1:5 (geometric), 1:1 (mass density), 25:1 (elastic modulus) | • Surrogate vs. live vegetation performance,<br>• flow velocity | • drag force,<br>• reconfiguration | n/a | n/a (unidirectional flow) | n/a | n/a | single blade |

| | | | | | | | | | | | |
|---|---|---|---|---|---|---|---|---|---|---|---|
| ***Wu & Cox (2016)*** | *Schoeno-plectus pungens* | Salt marsh | Plastic strips (zip ties) | 1:4 (Froude similarity) | • wave period,<br>• wave height,<br>• vertical variation in stem density (heterogeneous stem height),<br>• stem density | • wave attenuation,<br>• drag coefficient | Peak period: 0.8-2.8 s<br><br>Wave height: 6-14 cm | Random (JONSWAP) | 590 < Re < 810 | 19 < KC < 45 | 1,618-3,236 stems/$m^2$ |
| ***Hoque* et al. *(2018)*** | *Rhizophora sp.* | Mangrove | Rigid cylinders | 1:25 (Froude similarity) | • water depth,<br>• forest width | • reflection coefficient,<br>• transmission coefficient,<br>• dissipation coefficient, | Peak period: 3.5-12.5 s<br><br>Wave height: 1-5 m | Regular; Irregular (JONSWAP) | n/a | n/a | 0.06 tree/$m^2$ |
| ***Lei & Nepf (2019)*** | *Thalassia testudinum, Zostera marina, Posidonia oceanica* | Sea grass | LDPE film (blades), cylindrical wood (stems) | n/a | • blade length,<br>• blade thickness,<br>• hydrodynamic conditions,<br>• meadow density | • wave decay coefficient | Period: 1.0-2.0 s<br><br>Wave amplitude: 0.8-5 cm | Regular | n/a | n/a | 280-1370 stems/$m^2$ |
| ***Blackmar* et al. *(2014)*** | *Schoeno-plectus pungens* | Salt marsh | Flexible artificial vegetation, material not specified | 1:4 (Froude similarity)* | • stem density,<br>• plant height,<br>• heterogeneous combination stands | • wave attenuation | Peak period: 1.2-1.6 s<br><br>Wave height: 0.072-0.12 m | Random (JONSWAP) | 200 < Re < 1700 | n/a | 556-5,000 stems/$m^2$ |
| ***Zeller* et al. *(2014)*** | *Thalassia testudinum* | Sea grass | LDPE strip (blade), wooden dowel peg (stem) | 1:1 | • wave height,<br>• wave period,<br>• blade length,<br>• blade thickness | • Drag coefficient | Period: 2.80-5.19 s<br><br>Wave amplitude: 2.75 - 15.2 cm | Regular | n/a | n/a | single blade |
| ***Fonseca & Cahalan (1992)*** | *Halodule wrightii, Syringodium filiforme, T. testudinum, Zostera marina* | Sea grass | Live plants | 1:1 | • water depth,<br>• shoot density,<br>• wave parameters (period & wavelength | • wave energy reduction (wave attenuation) | Period: 0.4-0.7 s<br><br>Wave height: 1.8-4.9 cm | Unknown | n/a | n/a | *H. wrightii:* 1900-2870 stems/$m^2$<br>*S. filiforma:* 230-1350 stems/$m^2$<br>*T. testudinum:* 850-1500 stems/$m^2$<br>*Z. marina:* 750-1000 stems/$m^2$ |
| ***Koftis* et al. *(2013)*** | *Posidonia oceanica* | Sea grass | PVC | 1:1 | • submergence ratio,<br>• stem density,<br>• wave height,<br>• wave period | • wave attenuation,<br>• wave orbital velocities | Peak period: 2.0-4.5 s<br><br>Wave height: 0.28-0.40 m | Irregular (JONSWAP) | 1000 < Re < 3500 | 20 < KC < 100 | 360-180 stems/$m^2$ |
| ***Lima* et al. *(2006)*** | *Brachiaria subquadrip-ara* | Salt marsh | Braided nylon rope | 1:1 | • wave height,<br>• wave period,<br>• stem density | • wave attenuation,<br>• velocity | Period: 1.00-1.50 s<br><br>Wave height: 0.05-0.15 m | Regular | n/a | n/a | 400-1600 stems/$m^2$ |
| ***Lovas & Torum (2000)*** | *Laminaria hyperborea* | Sea grass (kelp) | Molded plastic | 1:10 | • flume bottom composition,<br>• wave period,<br>• wave height,<br>• kelp field location. | • wave attenuation | Peak period: 7.9-14.2 s<br><br>Wave height: 0.8 – 1.7 m | Irregular (JONSWAP) | n/a | n/a | 12 stems/$m^2$ |

**plant diameter not scaled to maintain prototype conditions for $Re_{veg}$*

| | | | | | | | | | | | |
|---|---|---|---|---|---|---|---|---|---|---|---|
| ***Manca* et al. *(2012)*** | *Posidonia oceanica* | Sea grass | PVC foam strips | 1:1 | • water depth,<br>• wave period,<br>• wave height,<br>• stem density,<br>• submergence | • wave attenuation | Peak period: 1.97-4.27 s<br><br>Wave height: 0.21-0.34 m | Regular; Irregular (JONSWAP) | 32,000 < Re < 530,000 | n/a | 180-360 stems/$m^2$ |
| ***Mei* et al. *(2011)*** | *n/a* | Mangrove | Perspex cylinders | n/a | • wave type | • free surface elevation (wave attenuation) | Peak period: 0.8-3.0 s<br><br>Wave height: 0.005-0.0272 m | Periodic waves, transient wave packets, solitary waves | 200 < Re < 2500 | n/a | n/a |
| ***Sanchez-Gonzalez* et al. *(2011)*** | *Posidonia oceanica* | Sea grass | Polyethylene and poly-propylene | 1:10 (Froude similarity) | • peak period,<br>• wave height,<br>• water depth | • free surface elevation (wave attenuation) | Peak period: 4-8 s<br><br>Wave height: 0.3-1.3 m | Regular; Random (JONSWAP) | 100 < Re < 1600 | 15 < KC < 425 | 280,000 blades/$m^2$ |
| ***Tschirky* et al. *(2000)*** | *Scirpus validus* | Freshwater marsh | Live plants | 1:1 | • wave height,<br>• peak period,<br>• plant density,<br>• planting extent,<br>• water depth | • wave transmission | Peak period: 1.25-2.25 s<br><br>Wave height: 5.0-21 cm | Irregular | n/a | n/a | 25-150 stems/$m^2$ |
| ***Wu* et al. *(2011)*** | *Spartina alterniflora, Juncus roemerianus* | Salt marsh | Live plants, birch dowels (rigid), EPDM foam rubber (flexible) | 1:1 | • vegetation type,<br>• stem density, | • wave attenuation | Peak period: 0.6-2.0 s<br><br>Wave height: 0.010-0.163 m | Regular; Irregular (JONSWAP) | 20 < Re < 4200 (approx.) | 3 < KC < 350 (approx.) | 156-2857 stems/$m^2$ |
| ***van Veelen* et al. *(2020)*** | *n/a* | Salt marsh | Bamboo dowels (rigid), silicon sealants (flexible) | 1:1 | • plant rigidity,<br>• wave height,<br>• wave period,<br>• submergence ratio | • wave particle velocity,<br>• wave attenuation | Period: 1.4-2.0 s<br><br>Wave height: 0.08-0.2 m | Regular | 779 < Re < 1658 | 53 < KC < 133 | 1111 stems/$m^2$ |
| ***Yin et al. (2019)*** | *n/a* | Salt mash | Rigid cylinders | 1:4 | • slope ratio<br>• wave steepness<br>• x-shore location of vegetation relative to slope toe | • wave runup attenuation | Period: 3.0-6.0 s<br><br>Wave height: 0.24-0.48 m | Regular | n/a | n/a | 462 stems/$m^2$ |
| ***Keimer et al. (2021)*** | *n/a* | Salt marsh | PVC rods | 1:10 | • submergence ratio<br>• relative vegetation field length<br>• wave steepness<br>• stem density | • wave reflection<br>• wave attenuation<br>• wave setup<br>• wave runup | Peak period: 3.2-15.8 s<br><br>Wave height: 0.8-2.0 m | Irregular | n/a | n/a | 200-400 stems/$m^2$ |
| ***Wang et al. (2022)*** | *Spartina alterniflora* | Salt marsh | Polyethylene flexible cylinders | 1:1 | • submergence ratio<br>• stem density<br>• wave height<br>• wavelength | • wave attenuation | Period: 1.0-1.5 s<br><br>Wave height: 0.08-0.14 m | Regular | 1500 < Re < 8000 | 15 < KC < 75 | 133-444 stems/$m^2$ |
| ***Baker et al. (2022)*** | *Spartina alterniflora* | Salt marsh | Birch dowels, flexible Tygon polymer tubing | 1:20 | • vegetation field length<br>• stem density<br>• stem height<br>• stem flexibility<br>• water depth<br>• wave height<br>• wave period | • wave attenuation<br>• dyke overtopping<br>• dyke structural damage | Peak period: 3-15 s<br>Wave height: 1.0-2.0 m | Irregular | 5026 < Re < 23121 | 241 < KC < 5359 | 150-550 stems/$m^2$ |

| | | | | | | | | | | | |
|---|---|---|---|---|---|---|---|---|---|---|---|
| ***Bouma et al. (2010)*** | *Puccinellia maritima, Spartina anglica* | Salt marsh | Live plants | 1:1 | • stem density<br>• standing biomass<br>• wave height | • wave attenuation<br>• drag force | Period: 1 s<br><br>Wave height: < 0.07 m | Regular | n/a | n/a | n/a |
| ***Maza et al. (2022)*** | *Spartina maritima, Salicornia europaea, Juncus maritimus, Halimione portulacoides* | Salt marsh | Live plants | 1:1 | • standing biomass<br>• submergence ratio<br>• water depth<br>• wave height<br>• relative meadow length | • wave attenuation | Peak wave period: 1.8-4.8 s<br><br>Wave height: 0.05–0.15 m | Irregular | n/a | n/a | 310.3 – 1858.0 $g/m^2$ (standing biomass) |

### 2.3.2 Numerical Modelling

Development of numerical modelling approaches for capturing wave-vegetation interactions and wave attenuation over vegetation fields has been ongoing since the 1980s. Dalrymple et al. (1984) proposed the pioneering method for modelling wave diffraction through vegetation, considering salt marsh vegetation as rigid cylinders. This theoretical model followed linear wave theory, and attributed wave attenuation to the drag force exerted by vegetation stems (Suzuki et al., 2019; Dalrymple et al., 1984). This drag force ($F_D$) was expressed by the Morison equation (**Eq. 2-8**), originally formulated for force estimation on cylindrical piles:

$$F_D = \frac{1}{2} C_D \rho A u^2 \quad \textbf{(2-8)}$$

where $C_D$ is the coefficient of drag, $\rho$ is the fluid density, $A$ is the projected area of the encountered object perpendicular to flow (for plant stems, $A = b_v N_v$, where $N_v$ is the stem array density), and $u$ is the undisturbed fluid velocity relative to the object (Morison et al., 1953). The model by Dalrymple et al. (1984) assumed a constant bulk drag coefficient with depth, and a locally flat bottom.

The theoretical model developed by Dalrymple et al. (1984) has since been extended by Mendez & Losada (2004) to shallow water, random waves and wave breaking conditions. Several other models have been developed since the extended energy conservation model proposed by Mendez & Losada (2004), utilizing various control equations to model flow through vegetation fields: wave action balance, spectral action balance, Boussinesq-type equations (linear and non-linear), shallow water equations (linear and non-linear), Reynolds-Averaged Navier Stokes (RANS) equations, extended mild slope equations, and various combinations of these (Suzuki et al., 2019). Most models consider vegetation as either rigid cylinders or cantilever beams with drag forces determined using Morison-type equations (Vuik et al., 2018; Reis et al., 2020; Suzuki et al., 2019; Suzuki et al., 2011; Chen & Zou, 2019; Cao et al., 2015; Yang et al., 2018; Maza et al., 2013; Wu et al., 2011). These models consider vegetation flexibility and wave-induced motion indirectly through calibration of the bulk drag coefficient ($C_d$), usually from experimental trials or empirical formulas (Vuik et al., 2018; Suzuki et al., 2011; Chen & Zou, 2019; Cao et al., 2015; Yang et al., 2018; Maza et al., 2013).

More recently, models have been developed that directly consider vegetation flexibility and motion through modelling vegetation as flexible elements or using elastic rod theory with a finite element solver (Chen & Zou, 2019; Lima et al., 2006). This allows direct determination of relative velocity and effective stem length within the model, which can reduce pressure on the selection or accurate calibration of the bulk drag coefficient. These models are also effective for incorporating vertical variation in vegetation properties, which have been found to have significant impacts on wave damping when considering varying water depth (Chen & Zou, 2019; Wu & Cox, 2016).

Summaries of all numerical modelling studies considered for this review are provided in **Table 2-4**. Modelling approaches are generally divided amongst two temporal resolutions: phase-

resolving and phase-averaging (Suzuki et al., 2019). Phase-averaging models directly compute wave spectral variations in space and time, utilizing a time-averaged wave energy equation to yield statistical wave parameters such as characteristic wave height, period and spectral shape. (Wu et al., 2011). Phase-averaging models often use the wave energy or spectral action balance equations, and may be 1D, depth-averaged 2D, vertical 2D or 3D (Wu et al., 2011). Phase-resolving models usually utilize shallow water, Navier-Stokes, or Boussinesq equations, to compute dynamic wave deformation processes (Wu et al., 2011). Phase-resolving models can yield detailed wave phase information, required for accurate representation of physical processes such as diffraction (Wu et al., 2011; Cao et al., 2015). However, phase-resolving models often require more computational effort (Wu et al., Suzuki et al., 2019). In general, phase-averaging models have the lowest computational costs, followed by phase-resolving models that use shallow water or Boussinesq equations, and then phase-resolving RANS models, requiring the highest computational efforts (Suzuki et al., 2019).

**Table 2-4.** Summary of numerical modelling approaches for vegetation-wave interactions.

| Study | Control Equation | Vegetation Schematization | Temporal Resolution | Incident Wave Condition | Vegetation Motion Considered | Dimens-ions | Modelling Software | Advantages | Limitations |
|---|---|---|---|---|---|---|---|---|---|
| ***Chen & Zhao (2012)*** | Wave action balance + spectral action balance, Energy Conservation | Bottom friction | Phase-resolving | Irregular | No | 1D | n/a | Not limited to narrow-banded random wave fields (improvement over Rayleigh distribution approach) | Needs more robust validation to understand the spectral distribution of energy dissipation. |
| ***Augustin* et al. *(2009)*** | Boussinesq | Bottom friction | Phase-resolving | Regular/ irregular | No | 2D | COULWAVE | Capable of modelling emergent and near-emergent conditions. | Results only applicable to rigid/flexible plants that exhibit minimal swaying motion. |
| ***Vuik* et al. *(2018)*** | Wave energy balance (linear wave theory + static mechanics) | Circular and triangular cantilever beams | Phase-averaging | Regular/ irregular | Yes (right- angle bending) | 1D | n/a | Predicts critical orbital velocity for stem breakage, which impacts relative attenuation capacity of a vegetation field under storm conditions. | Stem leaning angle strongly influences model results, accurate estimates of this angle require understanding of the relationship between wave properties, flexural rigidity and stem leaning. Still uncertainty with drag coefficient for broken short stems. |
| ***Mendez & Losada (2004)*** | Energy flux conservation equation | Rigid/flexible cylinders | Phase-averaging | Irregular (breaking and non-breaking) | No | 2D | n/a | Able to reproduce RMS wave height transformation observed in experimental data. Applicable for regular & random waves. Extended Dalrymple et al. (1984) to shallow water & mild sloping bottom. | Plant flexibility and motion is not directly modelled, only incorporated through selection of the drag coefficient and using relative velocity estimates. |
| ***Reis* et al. *(2020)*** | Nonlinear shallow water equations | Rigid cylinders | Phase-resolving | Irregular | No | 2D | SWASH | Capable of modelling with multiple layers - improved model performance for kelp seaweed. | Vegetation motion that would cause changes in vegetation height/area, and thus Cd, is neglected. |
| ***Suzuki* et al. *(2011)*** | Spectral action balance | Rigid cylinders | Phase-averaging | Irregular (breaking and non-breaking) | No | 2D | SWAN | Considers effect of horizontal variation in vegetation and of wave diffraction around vegetation patches. | Sensitive to peak period (can only handle narrow-banded random waves), requires calibration of bulk drag coefficient. |
| ***Suzuki* et al. *(2019)*** | Nonlinear shallow water equations | Rigid cylinders (vertical & horizontal) | Phase-resolving | Regular/ irregular | No | 2D | SWASH | Includes horizontal vegetation cylinders & considers porosity effects (more accurate for modelling mangroves), multi-layer calculation - advantage over depth-integrated models. | Vegetation flexibility not considered. |
| ***Chen & Zou (2019)*** | RANS | Elastic rod theory (finite element) | Phase-resolving | Regular | Yes (flexible vegetation with large deflections) | 3D | OpenFOAM | Robust in incorporating spatial variations of geometric and mechanical properties of vegetation. | Vegetation geometry is not resolved, only total tip displacement. |
| ***Cao* et al. *(2015)*** | Extended mild slope (EMSE) | Rigid cylinders | Phase-resolving | Irregular | No | 2D | n/a | Phase-resolving better represents physical processes | Does not consider non-linear deformation that may occur in |

| | | | | | | | | | |
|---|---|---|---|---|---|---|---|---|---|
| | | | | | | | | such as diffraction, potentially better than SWAN which is phase-averaged. | shallow water/high frequency waves, however, could potentially account for swaying due to phase-resolving nature. |
| ***Yang* et al. *(2018)*** | Boussinesq (non-linear) | Rigid cylinders | Phase-resolving | Regular | No | 2D | COULWAVE | Able to demonstrate wave attenuation sensitivity to water depth, vegetation configuration, wave height and wave period. | Simplification of vegetation as rigid sticks does not account for natural vegetation complexity (branches, flexibility, etc.). |
| ***Dalrymple* et al. *(1984)*** | Energy flux conservation equation | Rigid cylinders | Phase-averaging | Regular | No | 2D | n/a | First procedure proposed for wave damping through a vegetation field | Does not incorporate wave breaking, wave irregularity or wave-current interactions. Does not directly consider flexible vegetation or vegetation motion. |
| ***Maza* et al. *(2013)*** | RANS | Cantilever beams | Phase-averaging | Regular | Yes. Includes equation for plant motion (swaying), linear deformation only. | 2D | n/a | Allows modelling of submerged and emergent vegetation. Turbulence is considered. Drag force on plant is estimated more precisely with the model as it considers plant motion (relative velocity). | Mostly applicable for small deformations. Does not consider non-linear deformations. |
| ***De Oude* *(2010)*** | Spectral action balance | Rigid cylinders | Phase-averaging | Irregular | No | 2D | SWAN | Able to quantify wave attenuation due to vegetation when Cd is accurately calibrated. | Experimental factors that showed impact to wave attenuation (floating leaves, plant interactions) not captured in the model. Only suitable for wave periods > 2s. High dependency on Cd calibration. |
| ***Lima* et al. *(2006)*** | Momentum equations | Flexible elements (string of nodes) | Phase-averaging | Regular | Yes | 2D | n/a | Allows modelling of flexible elements, captures stem displacement. | Does not consider interaction between flexible stems. |
| ***Mei* et al. *(2011)*** | Shallow water equations | Rigid cylinders | Phase-averaging | Regular | No | 2D | n/a | Provided fair comparison with physical modelling experiments. | Does not consider deformation of submerged plants. |
| ***Wu* et al. *(2011)*** | Shallow water equations, Boussinesq, Navier-Stokes, Wave action balance | Rigid/flexible cylinders | Phase-resolving | Regular, Irregular | Yes | 1D, 2D | n/a | All 4 tested models provided good agreement with experimental observations. | Depth-averaged models require modified drag coefficient equations. |

#### 2.3.2.1 Empirical Formulas

Most of the numerical modelling approaches developed thus far rely on an accurate calibration of the bulk drag coefficient for the vegetation field within the model. In particular, models that consider vegetation as rigid elements (i.e. that neglect impact of vegetation flexibility), or that neglect vegetation motion (bending or swaying), must instead incorporate these impacts into the bulk drag coefficient. This has been done through changing the approach velocity in the Morison type equation to consider relative velocity (between flow and stem motion), through utilizing an empirical formula developed through physical modelling, or through treating $C_d$ as a calibration parameter for the numerical model (Mendez & Losada, 2004; de Oude, 2010; Maza et al., 2013; Cao et al., 2015).

Both physical and numerical modelling studies have found that the bulk drag coefficient for vegetation is related to the Reynolds number (Re) and the Keulegan-Carpenter number (KC) (Kobayashi et al., 1993; Augustin et al., 2009; Maza et al., 2013; Henry et al., 2015). The Reynolds number is a function of the approach velocity, diameter of the cylinder (or stem), and the kinematic viscosity, while the Keulegan-Carpenter number considers the ratio between the fluid particle excursion amplitude and the characteristic dimension of the plant (Tempest et al., 2015; Henry et al., 2015). Equations for each parameter are provided below (**Eq. 2-9** and **2-10).**

$$Re = \frac{U_w b_v}{v} \tag{2-9}$$

$$KC = \frac{U_w T}{b_v} \tag{2-10}$$

Where $U_w$ is the maximum horizontal velocity within the wave cycle, $b_v$ is the mean plant width normal to flow, $v$ is the fluid kinematic viscosity, and $T$ is the wave period (may be replaced with peak period, $T_p$, for random waves) (Henry et al., 2015).

Kobayashi et al. (1993) and Mendez et al. (1999) developed the following empirical relationship for $C_d$ as a function of Re:

$$C_D = \alpha + \left(\frac{\gamma}{Re}\right)^{\beta} \tag{2-11}$$

with values for the coefficients $\alpha$, $\gamma$ and $\beta$ provided from experimental data. Since then, new coefficients have been proposed for the consideration of plant motion or for species-specific experimental results (Maza et al., 2013; Koftis et al., 2013). Additionally, the use of a modified Reynolds number that incorporates submergence ratio has also been proposed for a more accurate determination of $C_D$ in emergent conditions (Anderson & Smith, 2014).

In some cases, the bulk drag coefficient has shown a better fit with the Keulegan-Carpenter number (Augustin et al., 2009; Mendez & Losada, 2004; Wu et al., 2011; Ozeren et al., 2014; Zeller et al., 2014; Van Veelen et al. 2020). A generic formulation for the bulk drag coefficient as a function of KC was proposed by Kobayashi et al. (1993) using fitting coefficients *a, b*, *c*:

$$C_D = \left(\frac{a}{KC}\right)^b + c \quad \textbf{(2-12)}$$

Mendez & Losada (2004) found the best empirical relation for $C_D$ to be a function of a modified Keulegan-Carpenter parameter that considers relative plant height due to bending. Similarly, Zeller et al. (2014) found the horizontal excursion of the blade tip (blade-bending excursion, $L_{BBE}$) to be a more appropriate length scale within the KC equation for vegetation, providing more accurate predictions of $C_D$ for flexible vegetation.

In general, results from physical and numerical modelling indicate that the bulk drag coefficient has a stronger relationship with KC when considering submerged conditions or when deformations due to vegetation flexibility cannot be ignored (Augustin et al. 2009; Mendez & Losada, 2004). A more extensive review of empirical bulk drag formulations for wave forces on coastal vegetation can be found in Henry et al. (2015).

## 2.4 Discussion

Traditionally, coastlines have been protected from wave hazards through the use of hard engineering structures (Wu et al., 2011; Temmerman et al., 2013). These structures, such as seawalls and bulkheads, are employed to reflect incident wave energy and prevent wave overtopping, thereby protecting backshore infrastructure and properties from damage (Bilkovic & Mitchell, 2017). Global climate change has increased pressures on coastal protection structures, due to associated rising sea levels and increasing severity and frequency of coastal storms (Church et al., 2013; Temmerman et al., 2013). The static nature of traditional "hard" coastal protection structures makes them poorly suited to long-term protection of coastal areas in the context of climate change, requiring significant investments to maintain an adequate level of protection (for maintenance and reconstruction) (Temmerman et al., 2013). In addition, literature supports that these hard structures are a detriment to natural coastal areas, reducing ecosystem service capacity and compromising the natural ability of these areas to adapt to rising sea levels (Temmerman et al., 2013; Bilkovic et al., 2017; Gracia et al., 2018; Rahman et al., 2019). These two compounding hinderances have spurred innovation in the field of coastal engineering, as practitioners search for more viable solutions for global coastal protection in the context of a changing climate.

Vegetated coastal ecosystems, such as mangroves, seagrasses and salt marshes, host a suite of ecosystem services, including water quality benefits, ecological habitat, support for aquaculture, recreation, carbon sequestration and coastal protection (Barbier et al., 2011). The capacity of these ecosystems to stabilize sediments and attenuate waves, thereby providing protection against coastal erosion, has spurred the development of a new field in coastal engineering termed "Nature-based Solutions" (NBS) (Maza et al., 2019; Rahman et al., 2019; Smith et al., 2020; van Veelen et al., 2020). NBS in coastal engineering capitalize on the coastal protection capacity of natural coastal features such as the previously mentioned vegetated coastal ecosystems. Furthermore, NBS provide adaptive coastal protection, as these natural features are able to self-

repair and dynamically maintain their elevation above sea level through sediment transport processes (Shepard et al., 2011; Rahman et al., 2019).

Salt marsh environments are presently the dominant coastal ecosystem utilized for NBS in coastal engineering, primarily in the form of living shorelines or managed coastal realignment projects (Shepard et al., 2011; Temmerman et al., 2013; Bilkovic & Mitchell, 2017). Living shorelines are built techniques that primarily utilize natural elements (usually marsh vegetation) to control erosion and maintain coastal processes, while simultaneously restoring or conserving habitat (Bilkovic & Mitchell, 2017). Managed coastal realignment projects involve the alteration or removal of existing hard coastal protection structures in order to reinstate tidal connections to previously reclaimed coastal wetlands (Shepard et al., 2011; Temmerman et al., 2013; Wollenberg et al., 2018). While living shorelines are designed to mimic fringing coastal marshes, often less than 30 m wide, managed coastal realignment projects can involve the restoration of vast expanses of salt marsh habitat (Temmerman et al., 2013; Davis et al., 2015).

Living shorelines are the leading recommended design strategy for incorporating NBS into coastal protection schemes (Davis et al., 2015). Various living shorelines guidance documents have been published across North America, predominantly in the United States, in the form of "grey" literature (Niedowski, 2000; NOAA, 2015; Miller et al., 2016; Hardaway et al., 2017; NYSDEC, 2017; Woods Hole Group, 2017). These documents provide guidance on appropriate site selection for living shorelines, however, provide very little guidance for the shoreline design methodology. There was limited to no guidance regarding recommended plantings, recommended planting structure (homogeneous vs heterogeneous, arrangement, stem density), or marsh width, and no means of quantifying the level of protection provided (i.e., attenuation capacity or reduction in wave overtopping) (**Table 2-1**). It is likely that this information is not included in existing guidance documents due to a lack of supporting literature. In order to develop clear engineering guidelines for the design of NBS, physical and numerical modelling studies must be performed to gain a secure understanding of the wave attenuation capacity of coastal vegetation, considering varying hydrodynamic conditions, plant characteristics and design configurations.

A discussion of the existing physical and numerical works is provided below with identification of existing gaps in scientific knowledge. Emphasis is placed on physical modelling research needs in this section, in consideration of the thesis objectives. It is expected that addressing these knowledge gaps will directly support the development of engineering guidance for the design of NBS.

### 2.4.1 Physical Modelling

Several experimental works have been completed investigating wave-vegetation interactions, in support of gaining knowledge of the coastal protection capacity of natural coastal ecosystems. This work has focused on measuring wave attenuation through three primary types of coastal vegetation: mangroves, seagrasses and salt marsh plants. Both live vegetation and surrogate

elements have been used for these physical modelling studies. Live vegetation studies have been performed predominantly for salt marsh species, while only one live plant study for seagrasses and none for mangroves were reviewed herein (**Table 2-3**). The dominant target species for mangrove experimental studies has been *Rhizophora* (Hoque et al., 2018; Maza et al., 2019). *Spartina alterniflora* appeared to be the dominant target species among physical modelling studies of salt marshes (Augustin et al., 2009; Wu et al., 2011; Anderson & Smith, 2014; Ozeren et al., 2014), however *Juncus roemarianus* and *Schoenoplectus pungens* also appeared in several studies (Wu et al., 2011; Blackmar et al., 2014; Ozeren et al., 2014; Wu & Cox, 2016). The range of target species for numerical modelling of seagrasses was wider, however was dominated by *Posidonia oceanica*, *Zostera marina*, and *Thalassia testudinum* (Fonseca & Chalan, 1992; Ghisalberti & Nepf, 2002; Sanchez-Gonzalez et al., 2011; Manca et al., 2012; Koftis et al., 2013; Zeller et al., 2014; Lei & Neof, 2019).

Various materials were used for experimental studies that modelled vegetation with surrogate elements. Wooden dowels and aluminum rods were the dominant material used for rigid vegetation (i.e. mangrove roots or rigid salt marsh vegetation) and various forms of plastic sheeting or strips were used to model flexible vegetation (e.g. XLPO, EDPM, LDPE, silicon, nylon rope) (see **Table 2-3**). When modelling flexible vegetation, emphasis was placed on selecting surrogate material that would maintain live plant posture under still-water conditions and mimic plant motion under wave action (Ghisalberti & Nepf, 2002; Anderson & Smith, 2014). To achieve this, mimics and real vegetation were compared across three non-dimensional parameters that considered buoyancy forces, element rigidity and inertial forces (Ghisalberti & Nepf, 2002; Sanchez-Gonzalez et al., 2011). These parameters incorporate geometric properties of the vegetation (blade thickness and length), as well as the material density and flexibility (Youngs' modulus of elasticity) (Ghisalberti & Nepf, 2002).

Physical modelling of wave-vegetation interactions has been completed for breaking and non-breaking irregular and regular waves. A wide range of wave conditions have been tested, with prototype-scale wave heights ranging from 1.8 cm – 5 m (Fonseca & Cahalan, 1992; Hoque et al., 2018). Most experimental studies that investigated salt marsh vegetation utilized a fairly low hydrodynamic settings (<20 cm) (Lima et al., 2006; Augustin et al., 2009; Wu et al., 2011; Anderson & Smith, 2014; Ozeren et al., 2014; Wu & Cox, 2016; Poppema et al., 2019; van Veelen et al., 2020). Few high energy flume experiments were reviewed for salt marsh environments, indicating that there is a knowledge gap with regards to the response of salt marsh environments to storm conditions (Moller et al., 2014; Paul et al., 2016; Rupprecht et al., 2017). This area should receive further attention in future physical modelling studies.

Experimental works completed for wave-vegetation interactions thus far have indicated that wave conditions (wave height and wave period), relative water depth, stem density/arrangement, plant flexibility and standing biomass are all controlling factors for wave attenuation (Maza et al., 2019; Augustin et al., 2009; Anderson & Smith, 2014; Blackmar et al., 2014; Ozeren et al., 2014; Lei & Nepf, 2019; Rupprecht et al., 2017; Paul et al., 2016; van Veelen et al., 2020; Maza

et al., 2022). The relative impact of each of these factors varies interdependently. For example, results from the study by Anderson & Smith (2014) indicate that the relative influence of wave period may depend on water depth or submergence ratio. In general, results from previous experimental works have had conflicting results regarding the influence of wave period, and thus this area could receive further attention in future physical modelling studies (Anderson & Smith, 2014; Maza et al., 2019). Results from the reviewed experimental works also indicate that there may be a threshold of impact for some of the above-mentioned controlling parameters, such as stem density. At low stem densities, increasing the density may decrease attenuation capacity due to sheltering effects (Augustin et al., 2009). However, at higher planting densities these sheltering effects are overcome and the increased biomass acts to increase drag forces and enhance wave attenuation (Manca et al., 2012; Blackmar et al., 2014; Ozeren et al., 2014; Lei & Nepf, 2019). Further experimental work could be done to elucidate this threshold.

The relative control of each testing parameter is also influenced by vegetation characteristics, most significantly by plant flexibility. The attenuation capacity of flexible vegetation, that generally exhibits an "avoidance" strategy to hydrodynamic forcing, has been shown to be controlled by hydrodynamic conditions, such as wave height, wave period and water depth (Schoutens et al., 2020; van Veelen et al., 2020). Conversely, the attenuation capacity of rigid vegetation ("resistance" strategy) has a stronger tie to the plant's physical properties (i.e. stem diameter), as indicated through correlations with the Reynolds and Keulegan-Carpenter numbers (Schoutens et al., 2020; van Veelen et al., 2020). Overall, results from physical modelling studies indicate that flexible vegetation attenuates less wave energy yet has a higher hydrodynamic threshold for damage (Ozeren et al., 2014; Paul et al., 2016; Rupprecht et al., 2017; Schoutens et al., 2020; van Veelen et al., 2020). Thus, it has been recommended in literature that design of NBS using salt marsh vegetation should capitalize on this attenuation-resilience trade-off by using heterogeneous vegetation stands in coastal protection strategies (Schoutens et al., 2020). The performance and resilience of such strategies has not been adequately considered in experimental studies, presenting an investigative opportunity for future physical models of NBS.

Experimental studies have demonstrated that flexible vegetation generally provides a lower wave attenuation capacity due to stem deformation (swaying, bending or flattening), and a resultant reduction in frontal area (Paul et al., 2016; Rupprecht et al., 2017). Rupprecht et al. (2017) demonstrated that the wave attenuation capacity of flexible vegetation is not constant, as wave-induced vegetation motion changes under increasing hydrodynamic forcing. The type and degree of motion has a significant influence on wave attenuation capacity, with attenuation decreasing as plants transition from upright, to swaying, to whip-like motion, and then to either a flattened or dominantly bent/broken canopy (Rupprecht et al., 2017). Rupprecht et al. (2017) investigated the orbital velocity thresholds corresponding to the onset of these different phases of motion for *Puccinellia maritima* and *Elymus athericus*. The experimental work of Rupprecht et al. (2017) should be extended to other target salt marsh species, as the orbital velocity thresholds were found to be dependent on species-specific plant characteristics.

Predominantly, physical modelling studies have utilized vegetation mimics. Within these mimic studies, several experiments were conducted at small-scale (Lovas & Torum, 2000; Sanchez-Gonzalez et al., 2011; Blackmar et al., 2014; Wu & Cox, 2016; Hoque et al., 2018; Maza et al., 2019; Vettori & Nikora, 2020). Few studies have quantified the impacts of utilizing scaled or surrogate vegetation elements. Wu et al. (2011) and Vettori & Nikora (2020) both determined that surrogate vegetation does not accurately capture the vertical variation in plant characteristics present in live vegetation (i.e., vertical biomass distribution, vertical variation in density, or plant macro-features). This vertical variation can potentially impact the wave attenuation capacity of vegetation under varying water depths (Wu et al., 2011; Tempest et al., 2015). Thus, the development of more complex surrogate elements that can accurately capture the structure of live vegetation may be required for future experimental studies. Additionally, there have been minimal efforts to quantify the scaling errors introduced when modelling NBS at small-scale. Manca et al. (2012) observed that wave-vegetation interactions follow different trends at low energy flow regimes (low wave Reynolds number, $Re_w$). This may introduce challenges for scaled flume experiments, as small-scale tests may be unable to generate large enough Reynolds numbers to yield the vegetation response expected under prototype-scale conditions (Manca et al., 2012). It is evident that a greater understanding of the errors and limitations associated with small-scale modelling of NBS is needed. Efforts should be made in future physical modelling studies to quantify scaling impacts through comparison of small- and prototype-scale experiments.

Several of the reviewed physical modelling studies put forth empirical relationships for the bulk drag coefficient of vegetation based on experimental results. These relationships are predominantly based on Re or KC, or modified versions of the two parameters (Henry et al., 2015). Clear species-specific empirical relations have not been developed, nor is it clear which relation is most applicable or most accurate under certain hydrodynamic settings or vegetation characteristics. Based on the reviewed studies, it seems that the relative strength of the relationship of $C_d$ with Re or KC is dependent on the submergence ratio and plant flexibility, with stronger relationships to KC found under submerged conditions and when plants exhibited significant deformation under wave action (Augustin et al., 2009; Mendez & Losada, 2004). A clear development of $C_d$ vs KC and Re relationships for certain species under different hydrodynamic conditions would be valuable for better estimating attenuation capacity of natural or built marshes, as well as aiding in accurate calibration of numerical models.

#### 2.4.1.1 Physical Modelling Research Needs

Based on the reviewed body of physical modelling literature, the following areas have been identified as critical knowledge gaps that should be addressed in future research.

1) **Seasonal variation**
    - Develop knowledge of species-specific attenuation capacities, particularly considering within-species seasonal variation in biomass and plant characteristics (physical and mechanical).

2) **Attenuation-resilience trade-off**
   - Test the performance of homogeneous versus heterogeneous vegetation stands under increasing hydrodynamic settings. This is needed to address the proposition that nature-based coastal protection schemes should capitalize on the avoidance versus resistance strategy of different coastal marsh species (attenuation-resilience trade-off).
3) **Scale and mimic effects**
   - Compare small- and large-scale models to quantify scaling effects, addressing any uncertainties associated with modelling NBS at a small-scale and thus allowing practitioner to better interpret the results of small-scale testing for the design of NBS.
   - Design mimic structures to capture the vertical variation in plant characteristics observed for live vegetation, including macro-features that may impact wave attenuation.
4) **Storm conditions**
   - Perform more full-scale studies under storm conditions, to support the limited body of knowledge regarding salt marsh response to extreme hydrodynamic forcing. Within these tests, species-specific thresholds could be observed for the onset of:
     a. Swaying motion
     b. Whip-like motion
     c. Permanent deformation/breakage
5) **Wave period**
   - Test a wider range of hydrodynamic conditions to determine the impact of wave period on attenuation capacity, with the aim to address presently conflicting results from previous experimental works.
6) **Stem density/arrangement**
   - Perform further testing on stem density/arrangement within the conditions that have been previously tested for comparison. The following questions remain to be answered:
     a. When are sheltering impacts significant? Only at low stem densities?
     b. When is arrangement significant? Only at low stem densities?

### 2.4.2 Numerical Modelling

Various methods in numerical modelling have been employed to capture wave attenuation over fields of vegetation. These methods have utilized various control equations, including wave action balance, spectral action balance, energy flux conservation equations, shallow water equations, Boussinesq equations, RANS equations and extended mild slope equations, among others (see **Table 2-4**). These models can be divided into either phase-averaging or phase-resolving, each providing different capabilities in terms of the physical processes captured and their computational efficiency. For example, phase-resolving models have been shown to more accurately capture processes such as diffraction, which are important for considering wave action through vegetation, however, have higher associated computational costs (Cao et al., 2015; Henry et al., 2015).

A numerical study by Cao et al. (2015) found that diffraction plays a significant role in wave propagation through vegetation, which is better captured through phase-resolving models. Additionally, phase information provided by the phase-resolving models can be used to directly incorporate predictions of plant motion into the modelling approach (Cao et al., 2015). From this, it appears the capabilities of phase-resolving models may be better suited for the modelling of NBS. Apart from Cao et al. (2015), few studies have been completed to compare the performance of existing numerical methods with respect to wave action through vegetation.

Vegetation has been incorporated into numerical models as a bottom friction term or as a drag term due to the presence of rigid cylinders (Morison-type equations), cantilever beams, or flexible elements (**Table 2-4**). Few studies utilized flexible elements, and instead incorporated the effects of vegetation flexibility in the calibration of the bottom friction term or the bulk drag coefficient (Mendez & Losada, 2004; de Oude, 2010; Maza et al., 2013; Cao et al., 2015). This calibration often relied on experimental data or empirical drag formulations. Thus, numerical methods for considering wave attenuation through vegetation could benefit from direct incorporation of vegetation flexibility and motion into the model.

# 3. Physical Modelling of NBS for Coastal Protection

## 3.1 Deformation of *Spartina patens* and *Spartina alterniflora* stems under wave action

*Preprint of an article submitted to the Coastal Engineering Journal, Taylor & Francis (under review).*

### 3.1.1 Introduction

Globally, coastal flood and erosion risk is increasing in the context of climate change, including the effects of sea level rise (IPCC 2022; Muis et al. 2020; Vitousek et al. 2017). Conventionally, "hard" engineering structures such as seawalls and breakwaters have been used to protect developed shorelines (Temmerman et al. 2013; Wu et al. 2011). However, the static nature of these structures means they are limited in their capacity for adaptation under changing hydrodynamic conditions, and thus less resilient in a changing climate (Gracia et al. 2017; Temmerman et al. 2013). Additionally, hard coastal infrastructure is known to produce potential adverse environmental effects, including loss of intertidal habitat, sediment supply disturbances, and accelerated erosion of the structure periphery (Gracia et al. 2018; Bilkovic et al. 2017; Temmerman et al. 2013). The limitations associated with hard infrastructure have thus encouraged more multi-disciplinary approaches to coastal erosion and flood risk management. Nature-based solutions (NBS) are one such approach, providing promising strategies for protecting vulnerable coasts in the context of climate change through utilizing the natural ability of ecosystems to self-repair and dynamically respond to changing external stressors (Piercy et al. 2021; Spalding et al. 2014). The coastal protection capabilities of natural environments such as reefs, sea grass meadows, salt marshes, mangrove forests and gravel beaches have been acknowledged for decades (Manca et al. 2012; Komar 2007; Fonseca & Cahalan 1992), however their consideration for use in engineered coastal protection strategies is presently limited, particularly in Canada where there have been few studies performed to address the distinct regional climates and native fauna (Rahman et al. 2019; Tschirky et al. 2000).

Coastal marsh vegetation delivers numerous positive ecosystem services related to coastal flood and erosion risk management in low- and medium-energy wave climates, with performance under high-energy wave climates still under investigation (Rupprecht et al. 2017; Moller et al. 2014). The coastal protection capacity of marsh vegetation is strongly tied to flow-stem interactions, including wave attenuation associated with vegetation-induced flow resistance and erosion protection resulting from reduced bed shear stresses within vegetated canopies and stabilization by plant roots (Wang et al. 2021). Physical and numerical modeling efforts have endeavored to quantify the coastal protection capacity of various coastal marsh species to inform nature-based design practices. Previous physical modeling studies have investigated the relative influence of various plant biophysical parameters (stem flexibility, stem width and height) and

hydrodynamics (wave height, wave period period) on coastal protection function, particularly wave attenuation (Anderson & Smith 2014; Augustin et al. 2009; Paul et al. 2016; Moller et al. 2014; Ozeren et al. 2014; Wu & Cox 2016; Blackmar et al. 2014; Lima et al. 2006; Tschirky et al. 2000; van Veelen et al. 2020; Mendez & Losada 2004). Most of these studies yielded an estimate of the canopy bulk drag coefficient ($C_{D,canopy}$) to characterize wave energy dissipation and parameterize wave attenuation at canopy scales in numerical models (Augustin et al. 2009; Anderson & Smith 2014; Ozeren et al. 2014; van Veelen et al. 2020; Wang et al. 2021; Moller et al. 2014; Wu & Cox 2016).

To date, few experimental studies have been conducted with live vegetation due to plant husbandry challenges in laboratory settings and significant facility requirements. Alternatively, the majority have used surrogate elements of various materials and complexities to represent live vegetation. Augustin et al. (2009) investigated the effect of water depth on the wave attenuation capacity of *Spartina alterniflora* utilizing prototype-scale model vegetation. This study utilized both rigid and flexible elements to represent *S. alterniflora*: cylindrical wooden dowels and polyethylene foam tubing, respectively (Augustin et al. 2009). Wu et al. (2011) and Ozeren et al. (2014) compared the performance of live plants to vegetation surrogates using rigid birch dowels, flexible EDPM foam-rubber cords and live *S. alterniflora* and *Juncus roemarianus* plants, and found that the surrogate elements did not accurately capture the vertical variation in vegetation properties present in live vegetation. Anderson & Smith (2014) investigated the wave attenuation capacity of *Spartina alterniflora* using semi-flexible cross-linked polyolefin (XLPO) tubing. Surrogate vegetation was tested with various irregular wave configurations, through varying submergence ratio (or relative depth – stem length divided by water depth, *l/d*), wave height, wave period and stem densities (Anderson & Smith 2014). Wu & Cox (2016) investigated the impacts of water depth on irregular wave attenuation through homogeneous versus heterogeneous stands of salt marsh vegetation, utilizing zip ties to model *Schoenoplectus pungens* at small-scale (1:4). Other flexible or semi-flexible elements that have been used include braided nylon rope, used by Lima et al. (2006) to represent *Brachiaria subquadripara*, strips of plastic Lexaan plates and silicon sealants (Paul et al. 2016; van Veelen et al. 2020).

To address the limited number of live vegetation studies, Lara et al. (2016) and Maza et al. (2015) conducted a full-scale experimental program with live *Puccinellia maritima* and *Spartina anglica* plants. Their study yielded an assessment of the comparative wave damping capacity of *P. maritima* and *S. anglica*, as well as guidelines for physical modeling with live vegetation, providing recommendations for plant sourcing and plant husbandry (Lara et al. 2016; Maza et al. 2015). Overall, experimental wave studies using live coastal marsh vegetation have been limited to few salt marsh species, including *P. maritima* (Rupprecht et al. 2017; Lara et al. 2016; Maza et al. 2015; Moller et al. 2014), *S. anglica* (Paul & Kerpen 2021; Poppema et al. 2019), *Elymus athericus* (Paul & Kerpen 2021; Rupprecht et al. 2017; Moller et al. 2014), *Atriplex prostrata* (Moller et al. 2014), *Spartina alterniflora* and *Juncus roemarianus* (Wu et al. 2011).

Vegetation flexibility has been found to have a significant impact on wave attenuation, particularly when hydrodynamic conditions are high enough that wave-induced vegetation motion occurs (Luhar & Nepf 2016; Rupprecht et al. 2017; Lei & Nepf 2019). Mullarney & Henderson (2010) investigated the influence of vegetation flexibility on wave attenuation, deriving an analytical model for wave-induced single-stem motion that was validated against field observations of *Schoenoplectus americanus* stems. The model developed in their study yielded that moderately flexible salt marsh species stems, such as *S. americanus*, provide approximately 30% of the wave damping capacity of equivalent rigid stems (Mullarney & Henderson 2010). van Veelen et al. (2020) further investigated the influence of vegetation flexibility on wave attenuation through a combined physical and numerical study. The study by van Veelen et al. (2020) found that the drag coefficient associated with flexible vegetation correlated equally well with parameters that incorporated stem diameter and hydrodynamics (stem Reynolds number, Re, **Eq. 3-1**; Keulegan-Carpenter number, KC, **Eq. 3-2**) and with parameters that only incorporated hydrodynamics (Froude number, Fr, **Eq. 3-3**; relative wave height, wave height/water depth). Conversely, it was found that the drag coefficient of geometrically equivalent rigid vegetation was only strongly correlated to parameters that incorporated the stem diameter (Re and KC) (van Veelen et al. 2020). This indicates that attenuation by rigid vegetation is dictated by both stem properties and hydrodynamic conditions (as captured by Re), whereas the attenuation by flexible vegetation is more dominantly controlled by hydrodynamic conditions (van Veelen et al. 2020; Bradley & Houser 2009).

$$Re = \frac{U_c b_v}{\nu} \quad \textbf{(3-1)}$$

$$KC = \frac{U_c T}{b_v} \quad \textbf{(3-2)}$$

$$F_r = \frac{U_c}{\sqrt{gd}} \quad \textbf{(3-3)}$$

In which $U_c$ is the characteristic velocity acting on the plant stem (m/s), $b_v$ = plant stem width (m), $\nu$ = kinematic viscosity of water ($m^2s^{-1}$), $g$ = gravitational constant (9.81 $ms^{-2}$), $d$ = water depth (m) and $T$ = wave period (s). The definition of characteristic velocity varies across studies in literature. For the present study, the characteristic velocity is defined as the incident maximum horizontal orbital velocity (in the direction of wave propagation), measured 10 cm above the flume bed and adjacent to the plant stem.

This dependence of flexible vegetation drag on hydrodynamic conditions is in-part due to induced vegetation motion. Vegetation motion alters the relative velocity between the fluid and vegetation $u_r$, consequently impacting wave energy dissipation (van Veelen et al. 2020; Bradley & Houser 2009). The relative stem-fluid velocity should be used to estimate drag forces induced by flexible stems (**Eq. 3-4**):

$$F_x = \frac{1}{2}\rho C_D A_p u_r |u_r| \quad \textbf{(3-4)}$$

In which $F_x$ = horizontal drag force (N), $\rho$ = water density (kgm$^{-3}$), $C_D$ = depth-averaged stem drag coefficient, and $A$ = frontal area of the plant (m$^2$) (Zhang & Nepf 2021; Mendez & Losada 2004). Two primary mechanisms of wave-induced vegetation motion have been identified in literature: swaying motion and whip-like motion (Ghisalberti & Nepf 2002; Losada et al. 2016; Rupprecht et al. 2017). Swaying motion is characterized by symmetry in the forward (the direction of wave travel) and backward bending angles, whereas whip-like motion is characterized by an extended, wider-angled forward bend, followed by a rapid, small-angled backward bend (Bradley & Houser 2009; Paul et al. 2012; Rupprecht et al. 2017). Whip-like movement can cause a flattening of the vegetation canopy for an extended portion of the wave cycle - resembling that of vegetation under unidirectional current flow, with wide angles of stem bending towards the direction of wave travel - resulting in a reduction in vegetative resistance to flow (Rupprecht et al. 2017; Gosselin 2019). The asymmetry of motion in whip-like states can produce different effects to the relative plant-fluid velocity ($u_r$) than swaying motion states due to prolonged stem bending in the direction of wave action and potential phase shifts in plant-fluid motion cycles, with unique consequences for drag forces on flexible stems (Eq. 4) under increasing hydrodynamic conditions (Rupprecht et al., 2017).

Rupprecht et al. (2017) investigated wave-induced live vegetation reconfiguration using live *Elymus athericus* and *Puccinellia maritima*, two salt marsh species of significantly different flexural rigidities, under increasing hydrodynamic conditions (regular, non-breaking waves). Rupprecht et al. (2017) correlated the onset of motion, and transition between motion states (swaying to whip-like), to the wave Cauchy number (*Ca*) - the ratio of drag forces to restoring forces due to material stiffness (**Eq. 3-5**) - and to the ratio of stem length to wave orbital excursion (*L*, **Eq. 3-6**):

$$Ca = \frac{\rho b_v U_c^2 l^3}{EI} \quad \textbf{(3-5)}$$

$$L = \frac{l}{A}, A = \frac{U_c}{\omega} \quad \textbf{(3-6)}$$

In which $EI$ = stem flexural rigidity (Nm$^2$), defined by the product of $E$ = elastic modulus (Nm$^{-2}$) and $I$ = 2$^{nd}$ moment of inertia (m$^4$), $l$ = stem length (m), $A$ = wave orbital excursion (m), and $\omega$ = wave angular frequency ($\omega$=2$\pi$/$T$, rads$^{-1}$) (Rupprecht et al. 2017; Luhar & Nepf 2016). These dimensionless variables have been identified as the most important parameters governing vegetation motion (Luhar & Nepf 2016). For highly flexible aquatic vegetation, the buoyancy parameter (*B*), which considers restoring forces due to buoyancy, is also significant for stem reconfiguration (Rupprecht et al. 2017; Luhar & Nepf 2016). However, *B* can be neglected in the case of salt marsh plants, which exhibit relatively high stiffness versus other flexible aquatic vegetation such as seagrasses (Rupprecht et al. 2017, Luhar & Nepf 2016). For large values of *Ca*, significant deformation of flexible elements is expected, and the relative velocity ($u_r$) becomes very different from the fluid velocity, *U*. Rupprecht et al. (2017) also recorded stem bending angles in and counter to the direction of wave travel to assess transitions between

motion states and thresholds of irreversible deformation (i.e., stem folding). These thresholds are important for understanding the evolution of wave attenuation associated with live vegetation under increasing hydrodynamic conditions and are tied to species-specific responses to hydrodynamic forcing. Rigid species take a resistance approach, exhibiting minimal deformation under wave action and consequently higher propensity for stem breakage if forces increase beyond critical thresholds, whereas, highly flexible plants utilize an avoidance approach, moving passively with fluid flow through reconfiguration, minimizing risk of damage (Rupprecht et al., 2017; Vuik et al., 2018; Schoutens et al., 2020).

There are uncertainties surrounding the reliability and accuracy of data pertaining to wave-vegetation interactions captured by studies using vegetation surrogates, which exhibit morphological and biomechanical simplifications in comparison to their live counterparts and thus may not accurately mimic live vegetation flexibility or motion (Vettori & Nikora 2020; Zhang & Nepf 2021; Blackmar et al. 2014; Tempest et al. 2015; Ozeren et al. 2014). Based on the findings of Rupprecht et al. (2017) and van Veelen et al. (2020), among others, it is evident that characterization of wave-induced vegetation motion is integral for understanding and quantifying the wave attenuation capacity of coastal marsh vegetation. Few experimental studies have been conducted to date that investigate the dynamic response of live vegetation to wave forcing at prototype scale, limiting the development, optimization, and ultimately practical application of coastal nature-based solutions incorporating vegetation. The studies that have previously been performed with live vegetation have considered only a limited number of coastal marsh species, and often use intrusive methods of plant sourcing (i.e., excavation) (Paul & Kerpen 2021; Rupprecht et al. 2017; Moller et al. 2014) that may be damaging to the source environment or not feasible in regions with strict environmental regulations. To address this, prototype-scale experiments were conducted with live vegetation in the large wave canal at the Institut National de la Recherche Scientifique (INRS) in Quebec, Canada. Two saltmarsh species native to the Canadian coastline were selected: smooth cordgrass (*Spartina alterniflora*) and saltmarsh hay (*Spartina patens*). These are the dominant coastal marsh species within the Bay of Fundy, in Nova Scotia and New Brunswick (Gordon et al. 1985; Wu et al. 2011). *S. patens* are also found on the west (Pacific) coast of Canada, whereas the native distribution of *S. alterniflora* in Canada is primarily limited to the east (Atlantic) coast (Natural Resources Conservation Service 2021). This experimental program allowed for novel collection of plant biophysical parameters for both species, particularly *S. patens* which, to the authors' knowledge, has never been studied in this context.

The objectives of the experimental program were to investigate irregular wave-induced motion of the two selected plant species (*S. patens* and *S. alterniflora*), using the stem bending angle to characterize motion type and quantify stem deformation. Various wave heights, wave periods and water depths were considered to investigate the influence of hydrodynamic conditions and relative stem submergence on flexible vegetation motion. *S. patens* and *S. alterniflora* have distinct morphologies and stiffness characteristics, allowing for investigation of the role of plant

biophysical parameters in determining stem deformation and motion. Presently, few comprehensive wave-vegetation motion studies for *S. alterniflora* have been performed (Zhang & Nepf 2021) and, to the authors' knowledge, none have been performed for *S. patens*. An additional novel aspect of this study was the use of live vegetation in an outdoor flume facility for an extended period, yielding practical insight to support plant husbandry practices in controlled experimental settings.

## 3.1.2 Experimental Program

### 3.1.2.1 Flume Setup

Experiments were conducted in the Large Wave Canal of the Laboratoire Hydraulique Environnemental (LHE) at the Institut National de la Recherche Scientifique (INRS) located in Quebec City, Canada (**Fig. 3-1**). The wave flume measures 120 m long by 5 m wide and 5 m deep, and utilizes a piston-type wave generator with a 4 m stroke.

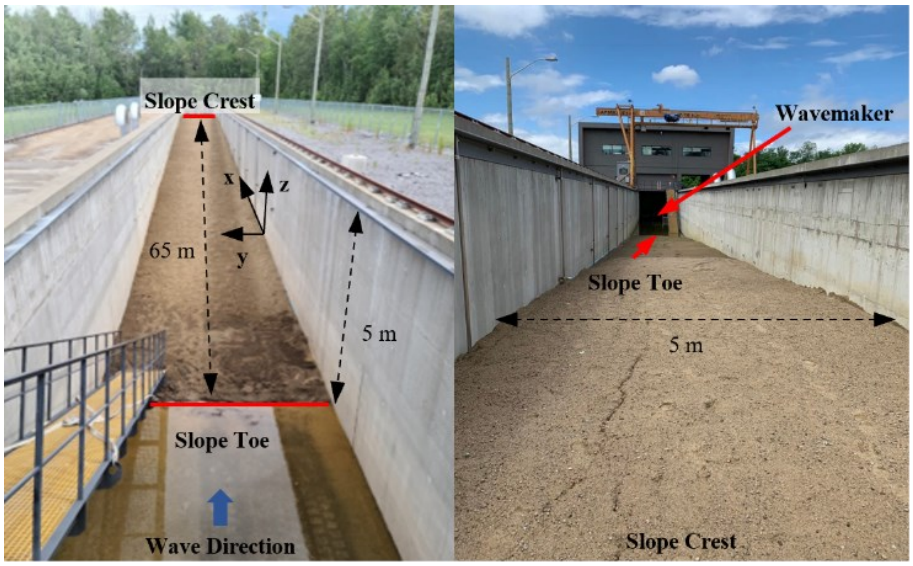


**Fig. 3-1.** View away from (left) and towards (right) the wavemaker in the large wave canal, LHE (Institut National de la Recherche Scientifique, Quebec).

A 1:18 (vertical: horizontal) sand slope (median grain diameter, $D_{50}$ = 285.9 μm) was installed in the canal, with its toe located at a distance of 27 m from the wave paddle. To avoid significant influences of bed morphology changes during experimentation, the slope was first subjected to 16-hours of moderate wave action (JONSWAP spectrum; zero-moment wave height, $H_{m0}$ = 0.5 m; peak wave period, $T_p$ = 3.5 s; water depth, $d$ = 2.5 m). Slope morphology changes during subsequent tests with smaller waves and vegetation were negligible and did not influence observed wave-vegetation interactions. The cross-shore profiles of the sand slope before and after the 16-hour exposure to $H_{m0}$ = 0.5 m waves are compared in **Fig. 3-2**; some sorting of sediments in the cross-shore direction were observed, but no large morphological changes occurred.

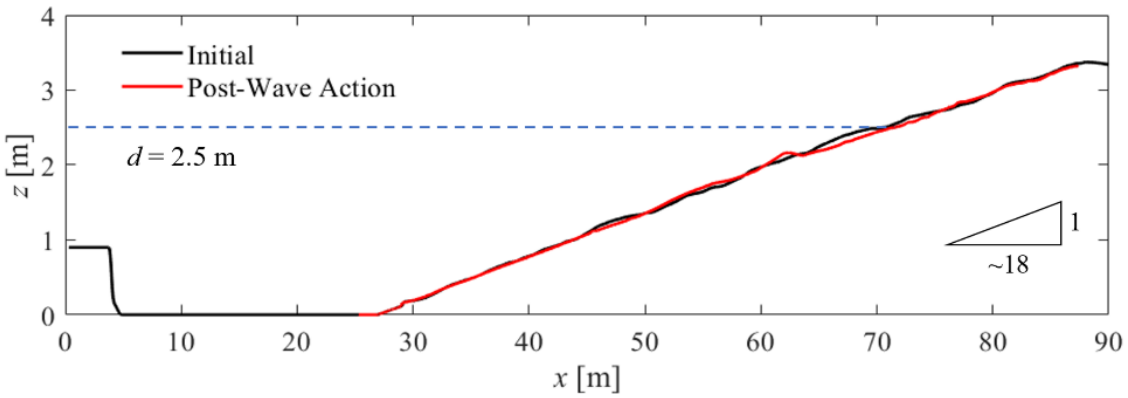


**Fig. 3-2.** Constructed sandy slope (1:18), before (black) and after (red) 16-hours of moderate wave action (JONSWAP, $H_{m0}$ = 0.5 m, $T_p$ = 3.5 s, $d$ = 2.5 m). Still water level is indicated by the blue dotted line.

#### 3.1.2.2 Plant husbandry and installation

Plants were sourced from a natural marsh located in Trois-Pistoles, Quebec, Canada, either as juvenile plants or as seeds that were subsequently grown in a local greenhouse. Plants were installed in rows with each row containing two plots (**Fig. 3-3**). Their spatial organization was selected such that there would be very little interaction between plots, allowing independent observations of wave-vegetation interactions for individual plots.

Live plants were transplanted directly into the sandy slope. The first row was placed 15.3 m from the slope toe (42.2 m from the wave paddle) at an elevation of 0.96 m above the flume bottom. Five rows of each *S. alterniflora* and *S. patens* were installed, with *S. alterniflora* populating the lower elevation section. Within each row, two plots of vegetation were installed 1 m apart laterally: (1) an individual stem, and (2) an adjacent cluster of 8 stems. Stems planted in the cluster had a 15-cm spacing, and a 3-2-3 staggered row arrangement as shown in **Fig. 3-3**. Rows were spaced 3 m apart in the cross-shore direction, so that the elevation range for each species spanned ~0.7 m. The planting configuration was primarily selected to gain knowledge about plant husbandry practices for live vegetation in laboratory settings (i.e., observe root growth, new shoot growth, stem interactions and root system development), and optimize video capture of individual plants for facilitating stem bending analysis.

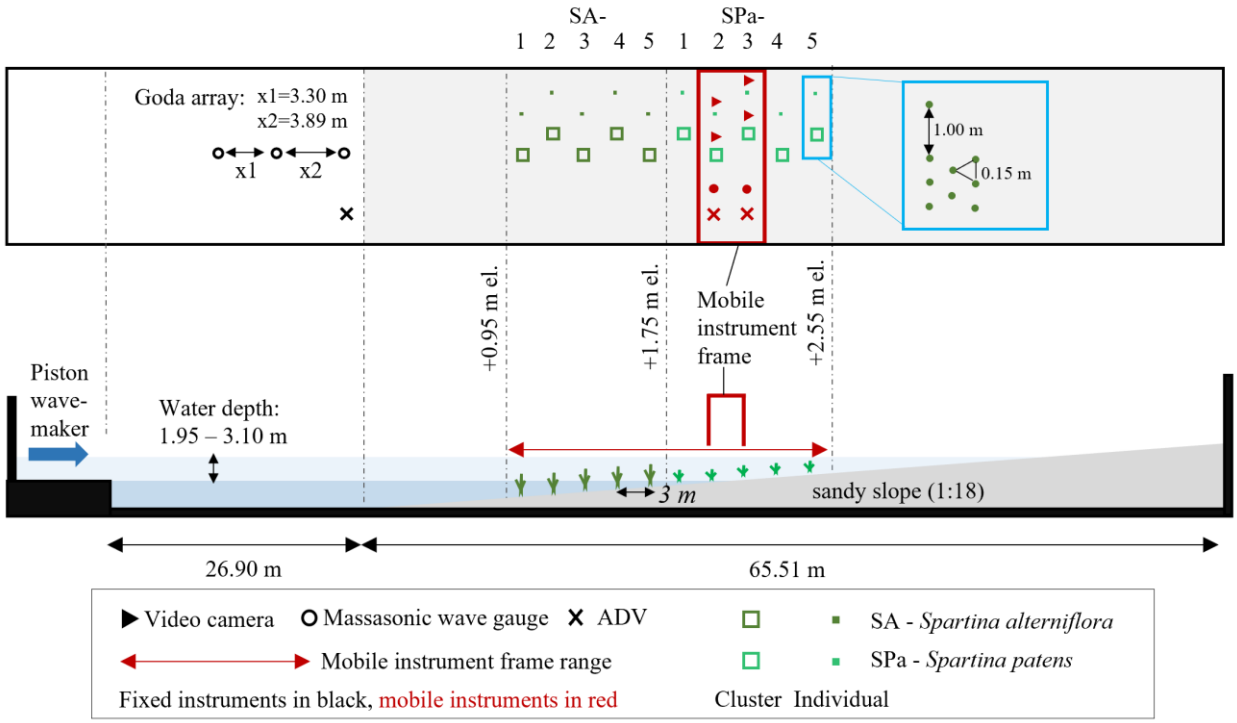


**Fig. 3-3.** Instrumentation and vegetation set-up in the large wave canal at LHE, INRS. Instruments installed on the frame (indicated by red symbols, within the red box) were moved along the flume length, within the range indicated by the red arrow. Detailed planting configurations are shown within the blue box, with 1 m lateral spacing between individual and cluster plots, and 0.15 m spacing between plants within the cluster plots.

All plants were transplanted into the wave canal between July 6-8, 2021. For each individual plant, a hole was dug approximately 20 cm deep, approximately three quarters filled with potting soil (Microrhizae ProMix BX General Purpose, commercially available) and topped with approximately 1 teaspoon of fertilizer (Botanika Green annual & perennial flowers fertilizer). Individual plants were planted in the potting soil, with an approximate planting depth of 10 cm, and then the remainder of the hole was filled in with sand and compacted manually (body weight). Each plot was watered immediately after planting. A similar planting methodology was used for the cluster plots, except the initial hole was dug wider to accommodate 8 plants at 15-cm spacing (~0.5 m diameter hole). Plants were left to grow in the flume for 3 weeks before testing began on July 28, 2021. During this period, plants were watered every 2-3 days. *S. patens* plants were hand-watered, whereas *S. alterniflora* plants were fully inundated by raising the water level in the flume for 6-8 hours. Soil was sufficiently compacted around each plant plot such that there were no observed impacts to soil levels following significant rainfall events. **Table 3-1** compares the plant husbandry methods used in this study with those used in previous experimental programs with live vegetation. The guidelines for physical modeling with live vegetation by Lara et al. (2016) were considered in the development of the experimental program and plant care techniques.

**Table 3-1.** Summary of plant husbandry methodologies for physical modeling with live vegetation.

| Study | Test Species | Source | Geography | Watering method | Fertilizer | Storage/ Growth Setting |
|---|---|---|---|---|---|---|
| **Poppema et al. (2019)** | • *Spartina anglica* | From seed (growing) | Western Scheldt Estuary, the Netherlands | Tidal mesocosms (semi-diurnal, 2-hour inundation, 23 ppt salinity) | No | Indoor |
| **Moller et al. (2014)** | • *Elymus athericus,*<br>• *Puccinellia maritima,*<br>• *Atriplex prostrata* | Excavated marsh blocks (collecting) | German Wadden Sea | Drained every 2 days for 12-hours of open-air gas exchange | No | Outdoor |
| **Wu et al. (2011)** | • *Spartina alterniflora,*<br>• *Juncus roemarianus* | Outdoor nursery (growing) | Louisiana | Fully inundated for 30 days | No | Indoor |
| **Maza et al. (2015), Lara et al. (2016)** | • *Spartina anglica,*<br>• *Puccinellia maritima* | From seed (growing) and collecting | Scheldt Estuary, the Netherlands | Primarily watered with freshwater, occasionally saltwater | Yes | Outdoor |
| **Silinski et al. (2015)** | • *Scirpus maritimus* | From seed (growing) and collecting | Scheldt Estuary, the Netherlands | n/a | No | Outdoor |
| **Paul & Kerpen (2021)** | • *Spartina anglica,*<br>• *Elymus athericus* | Sod (collecting) | The Netherlands | Watered and occasionally inundated with freshwater | No | Outdoor |

#### 3.1.2.3 Instrumentation

A mobile frame was constructed such that instruments could be deployed simultaneously along two plant rows during each test, monitoring four plant plots per wave test. The frame was designed to support two acoustic Doppler velocimeters (ADVs) and two acoustic wave gauges, one of each in line with each row of plants to provide reference incident velocities and wave height measurements, assuming uniform hydrodynamic conditions across the y-dimension of the flume (perpendicular to wave action). Adjustable mounts were installed on the frame in line with each of the four plant plots for deployment of GoPro HERO8 cameras. The mobile frame setup is shown in **Fig. 3-4**, which also shows the instrument positioning relative to the plants. The frame was moved along the length of the flume to capture data from multiple plant rows under repeated wave conditions. At each new location, the ADVs were adjusted to maintain a position 10-cm above the slope surface. ADVs were not positioned directly adjacent to the vegetation plots to avoid interference with the stem-incident flow conditions and impedance to stem deformation.

In addition to the mobile instrumentation, three fixed acoustic wave gauges were deployed between the wavemaker and the slope toe. These wave gauges formed a Goda-type array ($x_1$ = 3.30 m, $x_2$ = 3.89 m) for estimation of wave reflection during testing (Lin & Huang 2004). Wave gages obtained water surface elevation at a sampling rate of 50 Hz, and ADVs obtained velocity in the $x$, $y$ and $z$-direction also at a rate of 50 Hz. GoPro cameras obtained video footage in rectangular mode (to minimize impacts of fisheye distortion) at a rate of 30 frames per second (fps). The experimental setup (instrumentation and plant arrangement) in the Large Wave Canal is shown in **Fig. 3-3.**

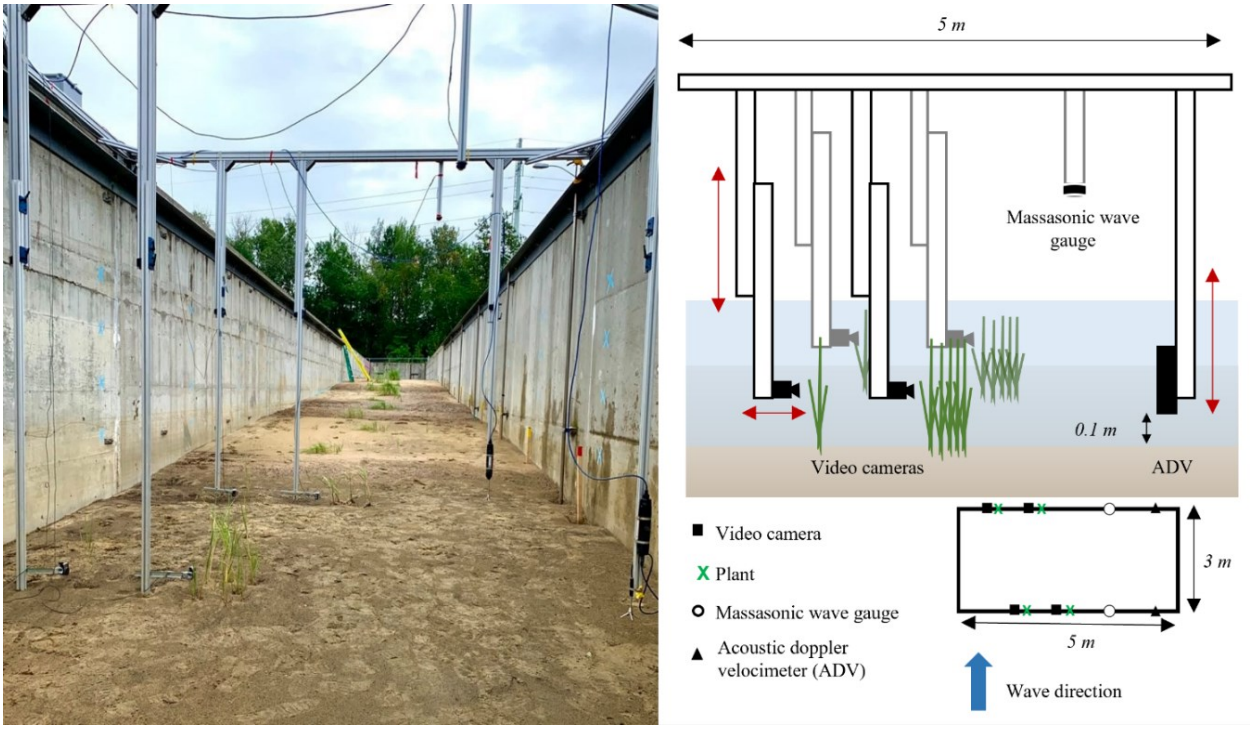


**Fig. 3-4.** Mobile instrumentation frame: photo from within the canal [left] and schematic of frame setup [right]; not drawn to scale. The individual plant plots are closest to the flume wall, with plant clusters closer to the flume center. Instrumentation deployed on the frame consisted of GoPro HERO8s (4), acoustic wave gauges (2) and Acoustic Doppler Velocimeters (2).

#### 3.1.2.4 Wave and Water Level Conditions

A series of experiments were conducted to investigate wave-induced vegetation motion under irregular wave action. Mild wave conditions, with incident offshore wave heights ranging from 0.1 m < $H_{m0}$ < 0.2 m at two different peak wave periods ($T_p$ = 2.5 s and 10 s) were used to capture the comparative response of vegetation to small, short period seas and longer period swells. All wave conditions were synthesized from JONSWAP spectra (peak enhancement factor, $\gamma$ = 3.3; number of wave components, *nc* = 100). The active wave absorption function was used for all experiments considering the water depth at the face of the wavemaker. Three water depths ($d$ =1.95 m, 2.55 m, 3.10 m, measured at the wavemaker) were selected to represent a range of submergence ratios for each plant species (*S. alterniflora*: 0.60 < $l/d$ < 2.52, *S. patens*: 0.58 < $l/d$ < 2.04). The wave and water level conditions use for testing resulted in Re and KC numbers in the range 132-1239 and 35-1925, respectively, which are consistent with ranges observed in the field for coastal marshes containing *Spartina* species (Roland & Douglass, 2005; van Veelen et al., 2020). At each water depth, the motion of several rows of plants was captured. This required incrementally moving the instrumentation frame along the slope profile as it was only equipped to record two rows at a time. The hydrodynamic conditions and plant motion at each station were recorded for five minutes before moving the frame to the next station.

#### 3.1.2.5 Video Analysis of Stem Deformation

A frame-by-frame analysis of the GoPro camera video footage was performed using Matlab, with two main steps: (1) frame pre-processing (contrast enhancement) and (2) manual stem bending angle tracking. Prior to analysis, potential lens distortion was quantified using *estimateFisheyeParameters* (MATLAB 2021). Polynomial distortion coefficients were negligible for all cameras (average $a_2$=1.3x10-4, $a_3$=-5.2x10-7, $a_4$=3.78x10-10); thus, no correction was applied to minimize the already high computational requirements for video processing. For video observations of clustered plant plots, a single stem from the cluster was selected for stem deformation tracking.

*(1) Contrast enhancement*

Video frames were pre-processed to enhance contrast and improve plant structure visibility despite the underwater setting. This was done through conversion of the image from RGB to LAB colour spaces (*rgb2lab*) and applying a contrast-limited adaptive histogram equalization function (*adapthisteq*) along the Red/Green and Blue/Yellow axes in Matlab (MATLAB 2021). The corrected image was then converted back to RGB format before continuing with bending analysis.

*(2) Stem bending angle tracking*

Manual stem tracking consisted of frame-by-frame image analysis performed in Matlab. The videos of stem motion were resampled at a frame rate between 1 and 3 Hz, selected to optimize computation time and tracking accuracy, while considering the magnitude and period of motion. For the first frame, the stem base was selected, and for every proceeding resampled frame the distal end of the stem was selected. In instances where the stem base moved throughout the video, translational corrections were applied to the selected distal stem locations. The selected coordinate pairs were then converted to angles (degrees) and adjusted for initial plant posture. Finally, a linear interpolation function was applied to compute a continuous time series of bending angle. Due to the significant time requirements associated with the video analysis described herein, bending angle tracking was completed for approximately 20 waves per wave condition. Automated stem tracking was attempted to amend analysis requirements; however, the tested methods were unsuccessful due to stem interactions and crossover. A description of the attempted automated stem tracking analysis is provided in Section 3.1.4.4.

### 3.1.3 Results

#### 3.1.3.1 Plant Husbandry

The live plants used for experimentation remained in the outdoor wave canal for 6 weeks (July 6-August 17, 2021), during which temperatures in the region (Quebec City, Canada) ranged from 9.3°C to 31.5°C, with a mean temperature of 20°C and total precipitation of 133.2 mm (Government of Canada 2021). Plots of daily precipitation and temperature data for the entire duration are provided in **Fig. 3-5**.

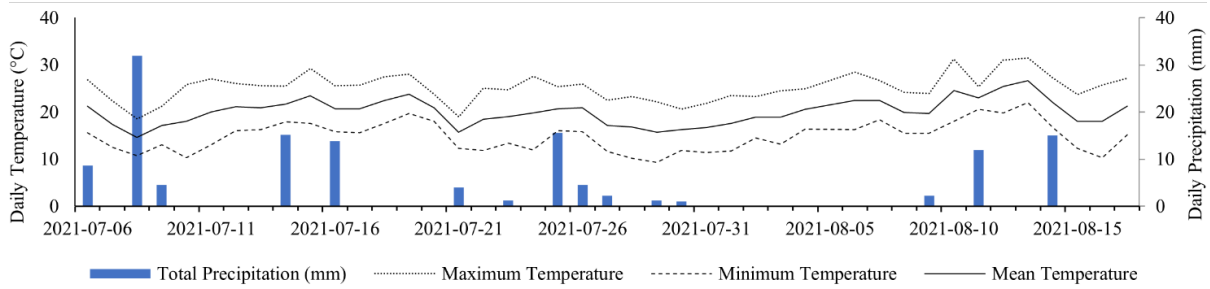


**Fig. 3-5.** Temperature fluctuations and total precipitation during period of outdoor experimentation with live vegetation. Data was obtained from the Government of Canada Historical Climate Data portal (Government of Canada 2021).

Minimal plant loss was observed during this period, demonstrating success of the implemented plant installation and maintenance techniques. New growth was identified at several plots, particularly for the *S. alterniflora*, after as few as 19 days (**Fig. 3-6**). Following experimentation, selected plant plots were harvested from the flume, maintaining intact root structures. Significant root growth was observed for both *S. patens* and *S. alterniflora* amongst the harvested plants (**Fig. 3-6**), with root interactions between individual plants particularly prominent between the *S. patens* clusters. This further demonstrates the potential value of outdoor experimental programs with live vegetation, particularly for investigating the erosion control benefits of vegetation, which depend on soil-root interactions and thus cannot be tested accurately with vegetation surrogates.

**Fig. 3-6.** Successful establishment of transplanted vegetation, demonstrated through the growth of new shoots adjacent to planted *Spartina alterniflora* stems [top, circled], and development of significant root structures [bottom left – *S. patens*; bottom right – *S. alterniflora*]; 1 m ruler used for scale. The dotted lines delineate aboveground biomass from belowground biomass (roots). Average root length post-experimentation was 28 +/- 9.9 cm for *S. patens* (n = 24), and 19 +/- 5.5 cm for *S. alterniflora* (n = 22).

### 3.1.3.2 Plant Bio-Physical Parameters

*Stem Length, Width, and Morphology*

*S. alterniflora* plants were characterized by a single semi-rigid stem, with several thinner, flexible blades. The blades were arranged uniformly around the stem, at the same approximate angle from the vertical (~ +/- 15°). Average stem length for the sampled *S. alterniflora* plants was 62 +/- 18 cm (n=18), with an average stem width of 4.47 +/- 0.89 mm (n=18), measured 10 cm from the stem base (point of stem-soil intersection). *S. patens* plants were characterized by a collection of several flexible, narrow stems, with long flat blades extending orthogonally from the main stems. Average stem length for the sampled *S. patens* plants was 55 +/- 10 cm (n=24), with an average stem width of 1.36 +/- 0.29 mm (n=21). Stem lengths were taken as the full stretched length from blade tip to the base of the stem (aboveground matter only – i.e., above the dotted line, **Fig. 3-6**), using the longest stem in the case of the multi-stemmed *S. patens* plants. Stem tapering of both species was also measured and is plotted in **Fig. 3-7**. Stem tapering measurements were terminated at a length of 50 cm from the stem base for both species, as stem widths were < 0.1 mm at this point and above. Statistically, the *S. patens* stems were narrower than the *S. alterniflora* stems (t-test; $p < 0.05$). *S. alterniflora* also demonstrated stronger stem tapering than *S. patens*, as shown in **Fig. 3-7**.

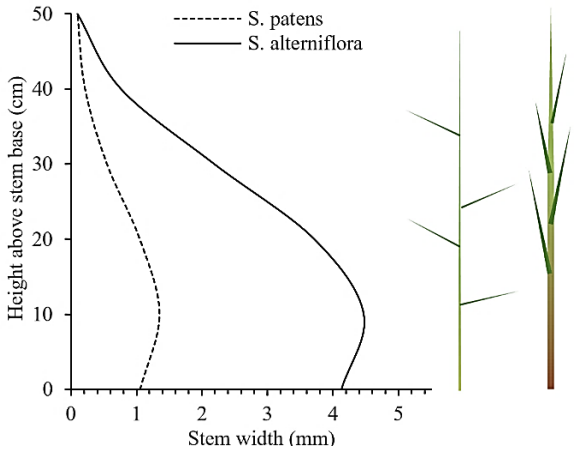


**Fig. 3-7.** Variation in stem width with increasing height above the stem base (stem tapering) for *S. patens* (left) and *S. alterniflora* (right). Reported values are averages of the measured widths at each height, considering 18 samples of *S. alterniflora* and 20 samples of *S. patens*. The stem base can be taken as analogous with the sediment surface. Stem tapering measurements were terminated at a height of 50 cm above the stem base for both species, as stem widths were < 0.1 mm at this point and above.

All of the above-mentioned plant parameters were measured immediately following wave testing. There were no appreciable changes in stem width for either species between the time of planting and the final post-testing measurements. However, stem lengths increased, on average, approximately 26% for *S. patens* and 27% for *S. alterniflora* over the six-week growth and testing period, to the final average values reported in **Table 3-2**. Inter-species differences in root structure were also observed for the cluster plots upon harvesting the plants after testing. The roots of *S. alterniflora* generally grew vertically (**Fig. 3-6**), and there was minimal interaction

between the roots of individual plants. The roots of *S. alterniflora* extended through the potting soil and into the underlying sand media. Conversely, the roots of *S. patens* developed horizontally, with significant root interaction between individual plants. The roots of *S. patens* did not grow below the potting soil, but instead extended laterally beyond the radius of the soil and into the adjacent sand.

**Table 3-2.** Summary of biophysical parameters of *S. patens* and *S. alterniflora* used for experimentation. Differences in plant parameters were statistically significant for stem width, flexural rigidity and normalized frontal area (t-test; $p < 0.05$).

| **Parameter** | | ***S. patens*** | ***S. alterniflora*** |
|---|---|---|---|
| Stem width, *b* (mm) | | 1.36 +/- 0.29 (n=21) | 4.47 +/- 0.89 (n=18) |
| Stem length, *l* (cm) | | 55 +/- 10 (n=24) | 62 +/- 18 (n=16) |
| Frontal area, FA ($cm^2$ ) | *Cluster:* | 976.5 +/- 265.6 (n=5) | 899.9 +/- 175.3 (n=5) |
| | *Individual:* | 157.2 +/- 69.2 (n=5) | 138.9 +/- 28.3 (n=5) |
| Normalized FA ($cm^2$/cm) | *Cluster:* | 24.3 +/- 7.5 (n=5) | 12.6 +/- 1.7 (n=5) |
| | *Individual:* | 6.0 +/- 2.3 (n=5) | 2.2 +/- 0.5 (n=5) |
| Young's modulus (MPa) | | 1140 +/- 460 (n=21) | 230 +/- 40 (n=18) |
| Flexural rigidity, EI ($Nm^2$) | | 0.0015 +/- 0.0002 (n=21) | 0.051 +/- 0.015 (n=18) |

### *Frontal Area and Biomass Distribution*

Average frontal area and vertical biomass distributions were quantified for each plant plot using the binary image analysis technique of Neumeier et al. (2005). A colour image of each individual plant and plant cluster was captured using a whiteboard and a tilted mirror to minimize background interference. The Matlab *ColorThresholder* application was used to convert the RGB image to a binary image with the background removed (MATLAB 2021). A scale was applied based on control points of known distance on the whiteboard background, allowing conversion of pixel count to units of frontal area. Values of frontal area, as well as normalized frontal area (divided by the maximum plant height) are provided in **Table 3-2**. Vertical biomass distribution and percent lateral obstruction were also quantified for each plant plot (**Fig. 3-8**), following the methods of Neumeier et al. (2005).

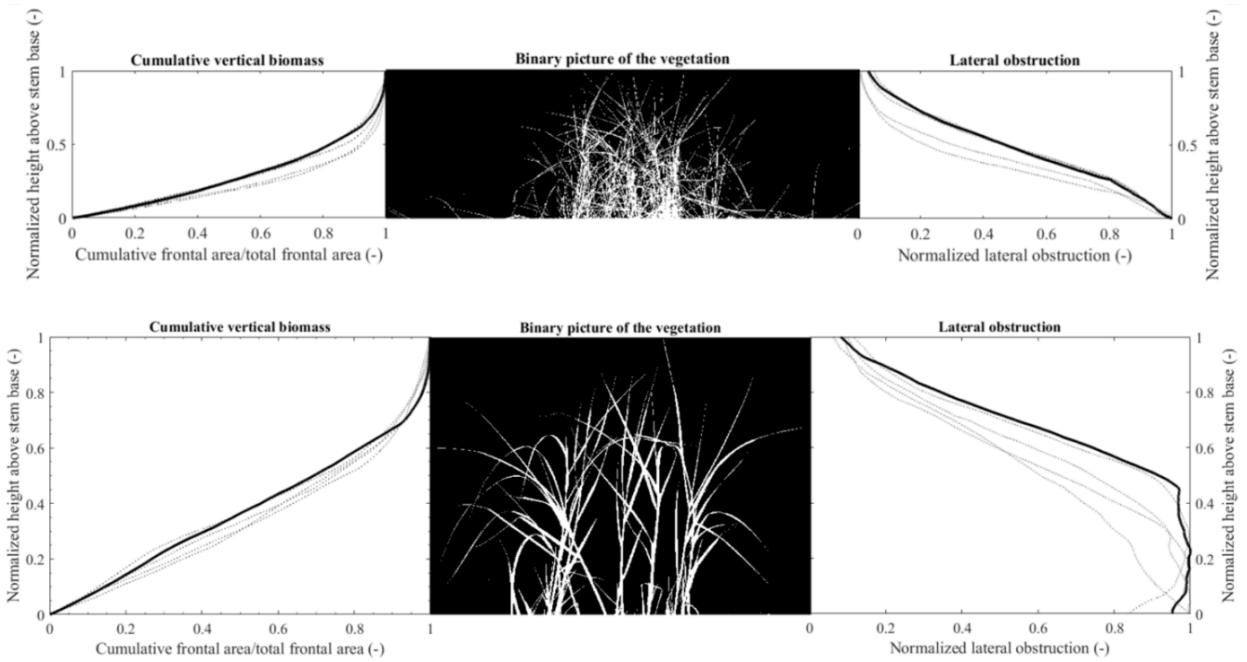


**Fig. 3-8.** Vertical variation in vegetation biomass for *S. patens* [top] and *S. alterniflora* [bottom]. Solid lines show the distributions for the displayed binary images, dashed lines provide the distribution of the other plots of the same species. Values on the y-axis (height above stem base) have been normalized by the height of each individual plant. Lateral obstruction was also normalized by the maximum percent obstruction for each plant plot.

### *Biomechanical Testing*

Elastic modulus (*E*) and flexural rigidity (*EI*) were estimated for each of the species using the field method described in Feagin et al. (2011). Stems of *S. patens* and *S. alterniflora* were subjected to a three-point bending test immediately upon harvesting. Sections 20 cm in length were cut starting from the base of the stem (one test section per stem) and laid across a beam loading apparatus consisting of two 10 cm wooden dowels spaced 10 cm apart. The stems were loaded at their midpoint with a string-supported plastic cup of known weight and volume, with incremental additions of water. GoPro cameras were mounted in front of the beam loading apparatus, and an image of stem deflection was captured following each addition of water. Image post-processing to quantify maximum deflection per incremental load required georectification to the local coordinate system (using control points stationed behind the beam loading apparatus), and conversion to a binary image based on colour thresholding. Maximum deflection for each captured image was selected as the mid-point of the binary image pixels with values of 1 (i.e., stem pixels), at the intersection point of the applied load. Results from the three-point bending test yielded estimates of elastic modulus for the harvested samples of *S. patens* and *S. alterniflora*: $E_{pat}$ = 1140 +/- 460 MPa and $E_{alt}$ 230 +/- 40 MPa. Flexural rigidity was also estimated for each species through the product of elastic modulus and the 2nd moment of inertia ($I = (\pi/4)b_v^4$). The average diameter of the 20 cm stem segment subjected to bending was taken as $b_v$ in the determination of *I*, based upon three evenly spaced measurements across the sample span (at 0 cm, 10 cm and 20 cm). *S. alterniflora* exhibited a significantly higher flexural rigidity (0.0730 +/- 0.03 $Nm^2$) than *S. patens* (0.0015 +/- 0.0002 $Nm^2$) (t-test; $p < 0.05$). Existing studies

of the biomechanical properties of *S. alterniflora* report elastic moduli differing across an order of magnitude, with *E* estimated as 1410+/- 710 MPa by Feagin et al. (2011) and 159.8 MPa by Chatagnier (2012). Estimates of elastic modulus for *S. alterniflora* in the present study fall within the range of Feagin et al. (2011) and Chatagnier (2012). Chatagnier (2012) also performed biomechanical testing on *S. patens* samples, yielding $E$ = 2950 MPa and $EI$ = 0.0028 $Nm^2$, on the same order of magnitude as the estimates for *S. patens* samples tested herein. **Table 3-2** provides a summary of the measured and calculated plant biophysical parameters, including biomechanical properties, for the sampled *S. patens* and *S. alterniflora* plants used in this study.

#### 3.1.3.3 Hydrodynamic Conditions

The zero-upcrossing method was used to obtain summary statistics for all wave gauges deployed in the Large Wave Canal during testing. Fifty-four wave tests were completed in total (6 different wave conditions at 3 water depths, and 3 replicates of each to account for movement of the instrument frame), however, the video quality for 26 of these tests was insufficient for performing bending angle analysis. A summary of the incident offshore hydrodynamic conditions (as measured by the Goda array, **Fig. 3-3**) for the tests that allowed bending angle analysis (28 total) is provided in **Table 3-3.** Significant wave heights ($H_{s,o}$) were determined through time domain analysis (zero-upcrossing) of the water surface oscillations recorded by the offshore wave gauges, where $H_{s,o}$ was calculated as the average of the highest one-third of the recorded waves. Insufficient video quality was a result of poor underwater visibility in turbid waters, from algae growth and/or sediment re-suspension. This led to a loss of several replicate tests, as reflected by the respective column in **Table 3-3.** Values of the Iribarren parameter ($\xi$), calculated using **Eq. 3-7**, are also provided in **Table 3-3** along with classification of wave breaker type. As the tests were conducted with irregular waves, calculations of $\xi$ and subsequent breaker classifications correspond to expected wave breaking associated with the significant wave height $H_{s,o}$.

$$\xi = \frac{\tan\alpha}{\sqrt{\frac{H_o}{L_0}}}, L_0 = \frac{9.81T_{s,o}^2}{2\pi}\tanh\frac{2\pi d}{L_0} \quad \textbf{(3-7)}$$

In which $\tan\alpha$ = beach slope (1/18), $H_0$ = offshore wave height (m) and $L_0$ = offshore wavelength (m). The offshore significant wave heights ($H_{s,o}$), calculated as described in the paragraph above, were used for $H_0$, and the corresponding wave periods ($T_{s,o}$), along with offshore water depths ($d$), were used in the estimation of $L_0$.

**Table 3-3.** Summary statistics for incident waves, measured offshore of the vegetated slope. Only tests where subsequent bending angle analysis was performed are included. For tests with replicates, the reported parameters are average values. Significant wave height is defined as the average of the largest one-third of the recorded waves, and the reported values present an average of the three offshore wave gauges.

| Water depth, $d$ (m) | Offshore significant wave height, $H_{s,o}$ (m) | Offshore significant wave period, $T_{s,o}$ (s) | Iribarren number, $\xi$ (-) | Breaker type | Number of waves | Number of replicates | Plant species captured |
|---|---|---|---|---|---|---|---|
| 1.95 | 0.075 | 2.37 | 0.57 | Plunging | 133 | 3 | *S. alterniflora, S. patens* |
| | 0.060 | 10.87 | 1.55 | Plunging | 28 | 1 | *S. alterniflora* |
| | 0.114 | 2.35 | 0.46 | Spilling | 138 | 2 | *S. alterniflora* |
| | 0.144 | 2.42 | 0.42 | Spilling | 125 | 2 | *S. alterniflora* |
| 2.55 | 0.080 | 2.35 | 0.57 | Plunging | 128 | 3 | *S. alterniflora, S. patens* |
| | 0.060 | 9.77 | 1.57 | Plunging | 29 | 2 | *S. alterniflora, S. patens* |
| | 0.118 | 2.43 | 0.48 | Spilling | 131 | 3 | *S. alterniflora, S. patens* |
| | 0.088 | 9.58 | 1.29 | Plunging | 31 | 1 | *S. alterniflora* |
| | 0.164 | 2.38 | 0.40 | Spilling | 124 | 3 | *S. alterniflora, S. patens* |
| | 0.125 | 9.99 | 1.10 | Plunging | 32 | 1 | *S. alterniflora,* |
| 3.10 | 0.079 | 2.41 | 0.59 | Plunging | 122 | 1 | *S. patens* |
| | 0.062 | 9.72 | 1.62 | Plunging | 33 | 1 | *S. patens* |
| | 0.122 | 2.42 | 0.47 | Spilling | 124 | 1 | *S. patens* |
| | 0.078 | 10.50 | 1.51 | Plunging | 29 | 1 | *S. patens* |
| | 0.164 | 2.44 | 0.41 | Spilling | 132 | 1 | *S. patens* |
| | 0.108 | 10.08 | 1.25 | Plunging | 30 | 1 | *S. patens* |

#### 3.1.3.4 Plant Motion Response to Wave Forcing

Eighty-seven videos of plant motion were analyzed, each capturing stem bending oscillations over a cycle of approximately 20 waves. This corresponded to 40 videos of *S. alterniflora* and 47 videos of *S. patens*. **Fig. 3-9** provides a sample of the output data from manual stem tracking for both *S. patens* and *S. alterniflora*, with the results overlaid on water surface oscillations recorded by adjacent wave gauges in **Fig. 3-9 C) and D)**. All videos of plant motion analyzed for bending data were of vegetation plots located outside of the surf zone. Thus, potential currents generated by wave breaking are not expected to contribute to vegetation motion.

Significant wave heights ($H_{s,i}$) and their associated periods ($T_{s,i}$) were extracted from the water surface elevation time series measured by the wave gauges directly in-line with the tracked plants (mobile frame wave gauges, **Fig. 3-3**) using the zero-upcrossing method. This method was also applied to the bending angle data to allow comparisons between stem deformation and hydrodynamic summary statistics, extracting the significant bending angle (average of the highest one-third angles) in the forward and backward directions ($F_s$, $B_s$, respectively). Error associated with manual stem bending angle tracking was quantified through duplicate analysis of a random sample of six videos, for which estimates of $F_s$ and $B_s$ were compared pairwise. An approximate error of +/- 0.80 degrees in bending angle estimates was determined from the mean difference between replicate data pairs at the 95% confidence level.

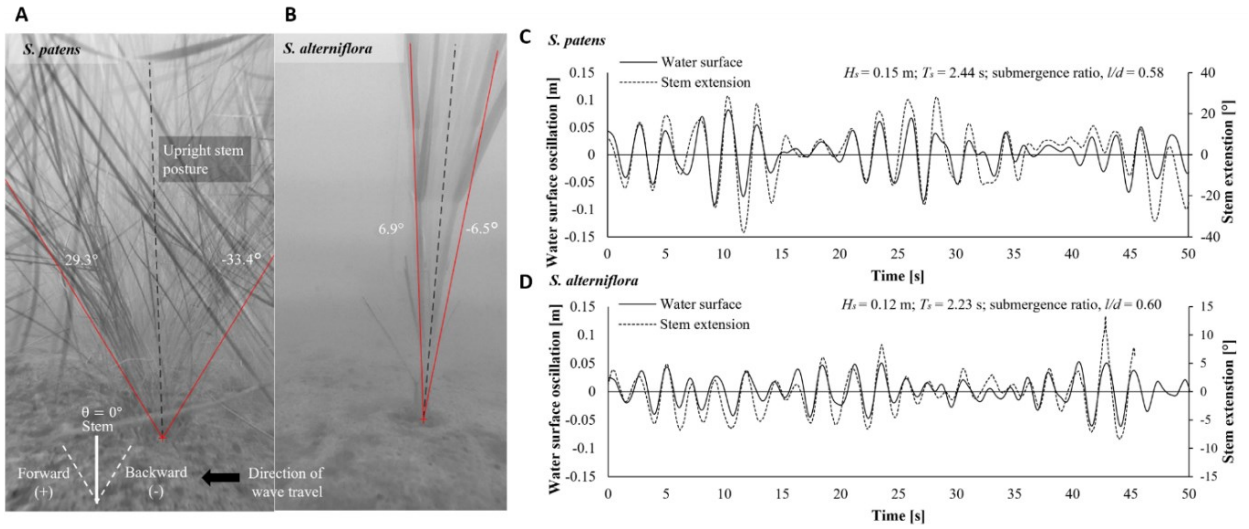


**Fig. 3-9.** Wave-induced vegetation motion for *S. alterniflora* and *S. patens* under similar hydrodynamic conditions: 0.12 m < $H_s$ < 0.15 m, 2.23 s < $T_s$ < 2.44 s, 0.58 < $l/d$ < 0.60 (as measured at the plant location). A) Visual representation of stem tracking for with overlaid image frames for one wave cycle for *S. patens* and B) *S. alterniflora*. C) Comparison of stem bending timeseries (manual tracking) with water surface oscillations as recorded by wave gauges at the plant location for *S. patens*, and D) *S. alterniflora*.

Stem deformation results were compared between adjacent individual and clustered plant plots observed under the same wave test conditions. There were 34 instances (pairs) where bending angle analysis could be performed on adjacent individual and clustered plant plots (68 video records total). Summary bending angle statistics ($F_s$ and $B_s$) were compared between the individual and clustered plants for each of these instances yielding two difference datasets: $F_s$(individual) – $F_s$(cluster) = $F_s$(difference), and $|B_s|$(individual) – $|B_s|$(cluster) = $B_s$(difference), for each *S. alterniflora* and *S. patens*. $F_s$(difference) and $B_s$(difference) datasets were subjected to pairwise t-tests for both *S. alterniflora* individual vs. cluster and *S. patens* individual vs. cluster (four statistical tests total). Results from statistical comparison indicated that there was a significant difference ($p < 0.05$) between the forward bending response of *S. patens* stems planted individually versus within a cluster, with the individual stems exhibiting higher degrees of forward bending. There was also a statistically significant difference between the backward bending response of *S. alterniflora* for clustered versus individual stems, with the clustered stems exhibiting a higher degree of bending in the backward direction. Boxplots that display the differences between $F_s$ and $B_s$ estimates for stems within adjacent individual and clustered plant plots are provided in **Fig. 3-10.** Note that the absolute values of $B_s$(individual) and $B_s$(cluster) were used to calculate the difference dataset, $B_s$(difference), such that a positive difference in both **Fig. 3-10 A)** and **Fig. 3-10 B)** indicates that stem bending was more significant for the individual stem than for the stem within the cluster.

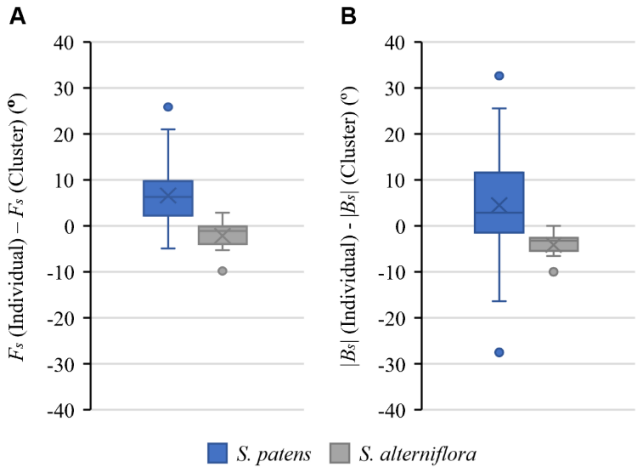


**Fig. 3-10.** Boxplots demonstrating the differences in bending angle response between tracked stems planted individually (i.e., in isolation) and those planted within a cluster of eight stems for *S. patens* (23 paired data sets) and *S. alterniflora* (11 paired datasets). A) Differences in significant forward bending angles ($F_s$) between paired tests, where differences were calculated as $F_s$ (Individual) – $F_s$ (Cluster). A positive difference indicates that the forward bending of individual plants was greater than the cluster. B) Differences in significant backward bending angles ($B_s$) between paired tests, where differences were calculated as $|B_s|$ (Individual) – $|B_s|$ (Cluster). As absolute values were used, a positive difference also indicates that the magnitude of backward bending for individual plants was greater than the cluster. The X on each boxplot indicates the mean of the dataset.

**Table 3-4.** Results from stem bending analysis of *S. patens* and *S. alterniflora.* The significant wave heights and periods reported in this table were measured by wave gauges positioned in variable cross-shore locations on the slope, in line with the target plant stems.

| Plant species | Stem incident $H_{s,i}$ (m) | Stem incident $T_{s,i}$ (s) | $F_s$ (°) | $-B_s$ (°) | $U_c$ (m/s) | $U_{max}$ (m/s) | $l/d$ (-) | Re | KC | $Ca$ | $L$ |
|---|---|---|---|---|---|---|---|---|---|---|---|
| *S. patens* | 0.10-0.28 | 2.2-10.0 | 11-63 | 14-76 | 0.10-0.27 | 0.12-0.37 | 0.58-2.04 | 132-367 | 171-1925 | 1.4-11.0 | 1.3-14.9 |
| *S. alterniflora* | 0.08-0.19 | 2.0-10.4 | 4-32 | 4-32 | 0.08-0.22 | 0.11-0.28 | 0.60-2.52 | 339-1239 | 35-482 | 0.02-1.1 | 1.8-25.2 |

Stem deformation results were also compared with the non-dimensional parameters Re, KC, *Ca* and *L*. Peak forward horizontal velocities (in the direction of wave travel) were extracted from the velocity records measured by the ADVs positioned adjacent to the plant plots (z = 10 cm above the bed). The average of the highest one-third of these peak velocities (over the 20-wave cycle for which bending analysis was performed) was taken as the characteristic velocity ($U_c = U_{1/3}$) in the calculations of all non-dimensional parameters (Re, KC, *Ca* and *L*). The wave period $T_{s,i}$ was used for estimations of KC and *L*. The maximum peak forward velocity ($U_{max}$) for each wave test was also obtained from the velocity records but was not used for further calculations. The range of test conditions for which bending analysis was conducted for each species is provided in **Table 3-4**, along with a summary of the resulting range of stem bending results. **Figure 11** summarizes the results for stem bending angle tracking for all tests, demonstrating the relationship between stem deformation and incident hydrodynamic conditions (in the form of $H_{s,i}$, $1/L$ and $CaL$). Stem bending was not plotted against the Froude number, as it is less relevant for characterization of flexible plant motion. For the experiments presented here, Fr = $O(10^{-1} - 10^{-2})$.

**Fig. 3-11** summarizes the results for stem bending angle tracking for all tests. Submergence ratio was not found to have a significant influence on stem bending within the ranges investigated (*S. alterniflora:* $0.60 < l/d < 2.52$, *S. patens*: $0.58 < l/d < 2.04$) and considering the data sample size. Emergent and submerged tests are distinguished in **Fig. 3-11 A)**, which compares stem bending with significant incident wave height ($H_{s,i}$), but are combined thereafter. The results of stem bending analysis were also plotted against $Ca$ and $L$, the primary non-dimensional parameters that govern flexible stem motion (**Fig. 3-11 B), C), and D)**). Results from linear regression for the relationships plotted in **Fig. 3-11** are provided in **Table 3-5**.

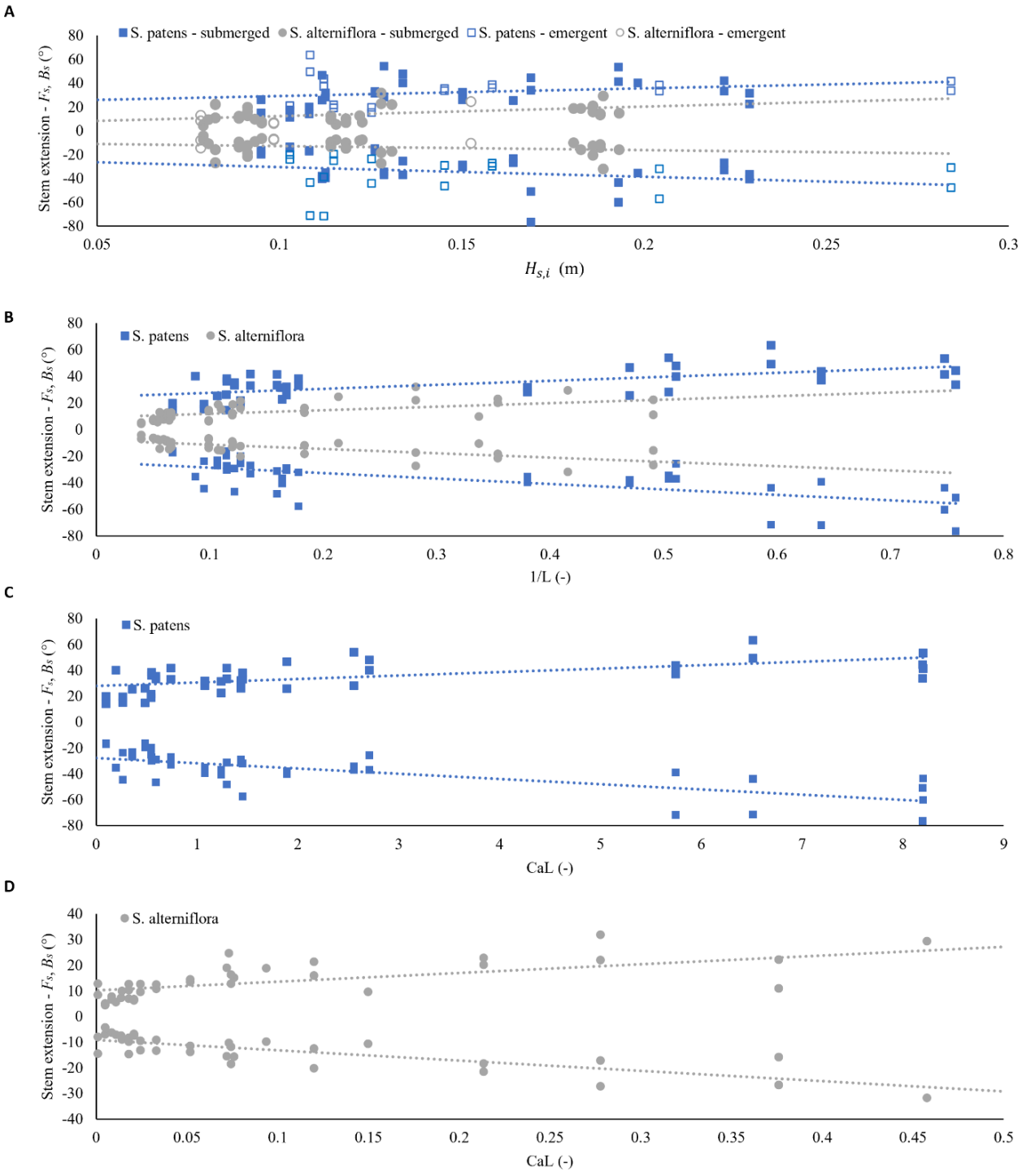


**Fig. 3-11.** Stem bending angles in the forward ($F_s$) and backward ($B_s$) directions as a function of A) Significant stem incident wave height for *Spartina alterniflora* and *Spartina patens* ($H_{s,i}$), B) 1/*L* for *S. patens* and *S. alterniflora*, C) *CaL* for S. patens and D) *CaL* for *S. alterniflora*. Bending angles are reported with an uncertainty of +/- 0.80 degrees associated with manual stem tracking analysis (95% confidence level).

**Table 3-5.** Linear regression results for the relationships between stem bending and the various non-dimensional parameters shown in Fig. 3-11.

| Figure | Plant Species | Forward | Backward |
|---|---|---|---|
| **3-11 A) -** $F_s$, $B_s$ vs. $H_{s,i}$ | *S. patens* | $y = (43.56 \pm 68.01)X + (25.9 \pm 10.6)$, $R^2 = 0.04$ | $y = (-58.78 \pm 88.27)X - (25.7 \pm 13.7)$, $R^2 = 0.04$ |
| | *S. alterniflora* | $y = 20.63 \pm 49.24)X + (11.6 \pm 5.7)$, $R^2 = 0.02$ | $y = (6.05 \pm 47.47)X - (14.1 \pm 5.5)$, $R^2 = 0.00$ |
| **3-11 B) -** $F_s$, $B_s$ vs. $1/L$ | *S. patens* | $y = (30.06 \pm 12.18)X + (24.8 \pm 4.7)$, $R^2 = 0.39$ | $y = (-41.11 \pm 15.00)X - (24.4 \pm 5.7)$, $R^2 = 0.44$ |
| | *S. alterniflora* | $y = (26.54 \pm 12.45)X + (9.3 \pm 2.8)$, $R^2 = 0.33$ | $y = (-32.32 \pm 9.92)X - (8.0 \pm 2.2)$, $R^2 = 0.53$ |
| **3-11 C) -** $F_s$, $B_s$ vs. $CaL$ | *S. patens* | $y = (2.67 \pm 1.13)X + (27.9 \pm 3.8)$, $R^2 = 0.37$ | $y = (-4.06 \pm 1.27)X - (27.7 \pm 4.3)$, $R^2 = 0.52$ |
| **3-11 D) -** $F_s$, $B_s$ vs. $CaL$ | *S. alterniflora* | $y = (33.98 \pm 12.75)X + (9.8 \pm 2.1)$, $R^2 = 0.47$ | $y = (-40.12 \pm 9.42)X - (9.1 \pm 1.6)$, $R^2 = 0.63$ |

## 3.1.4 Discussion

In this study, two live saltmarsh species (*S. alterniflora and S. patens*) were planted in a large-scale outdoor flume and after three weeks of establishment, exposed to a wide range of irregular wave conditions throughout three weeks of testing. Measures of plant health throughout and after testing indicate that the plant husbandry techniques used herein were successful, providing significant support for future large-scale experiments with live vegetation. Stem dynamics were recorded using submerged cameras for comparison of plant motion response between species and under varying hydrodynamic conditions. A discussion of the experimental findings is provided as follows.

### 3.1.4.1 Plant Physical Properties and Stem Deformation

There is significant natural variation in the biophysical properties of salt marsh plants, with different species exhibiting contrasting plant morphologies, stem widths, stem lengths, and elastic moduli (Zhang & Nepf 2021; Zhu et al. 2020; Rupprecht et al. 2017; Puijalon et al. 2011). This diversity can contribute to distinct dynamic responses to wave forcing, with species adopting what has been classified as either “avoidance” or “resistance” strategies to withstand hydrodynamic forces (Schoutens et al. 2020; Vuik et al. 2018; Puijalon et al. 2011). Morphological adaptations that typically favor resistance to hydrodynamic stress include larger frontal areas (more leaves, wider and longer stems), and greater rigidity (Schoutens et al. 2020; Puijalon et al. 2011). By contrast, avoidance species are characteristically more flexible with smaller frontal areas (shorter, thinner stems), and higher capacities to reconfigure (Schoutens et al. 2020; Puijalon et al. 2011). Hydrodynamic drag forces exerted on avoidance species are typically much lower. Consequently, they do not attenuate waves as effectively as resistance species, which experience higher drag forces and hence yield greater wave energy dissipation (Schoutens et al. 2020). However, resistant species are more susceptible to damage under increasingly severe hydrodynamic conditions (Rupprecht et al. 2017; Vuik et al. 2018). This was demonstrated by Rupprecht et al. (2017), where the more rigid *Elymus athericus* species exhibited irreversible stem deformation (folding or breakage) at lower orbital velocities than *Puccinellia maritima,* resulting in a rapid decline in flow resistance. At similar orbital velocities, extreme bending of the more flexible (“avoidance”) *P. maritima* canopy was observed, but not breakage, thus the plants still provided some wave energy dissipation as well as erosion protection in the form of shielding (Rupprecht et al. 2017). It has since been proposed in

Schoutens et al. (2020) that there are benefits to combining both types of species in coastal protection strategies, as the resistance species provide greater protection below their threshold for breakage, and avoidance species may provide prolonged protection with a greater chance of survival. In their study, Schoutens et al. (2020) demonstrated this through the complementary functioning of two *Scirpus* species: the presence of a band of *Scirpus tabernaemontani* ("avoidance" traits) placed at the marsh edge could dissipate enough wave energy to create a favorable environment for *Scirpus maritimus,* a plant with a greater frontal area that experiences higher drag forces ("resistance" traits).

Based on the measured plant parameters reported herein, *Spartina patens* presents traits typical of an "avoidance" strategy species with thinner, more flexible stems and leaves, whereas *S. alterniflora* exhibits more of a "resistance" strategy. This is further supported by the present observations of stem deformation under wave action. *Spartina patens* appeared to move more passively with the waves, exhibiting a larger total arc of stem tip excursion ($25^\circ < F_s - B_s < 121^\circ$) than *S. alterniflora* ($9^\circ < F_s - B_s < 61^\circ$) under similar wave action. Drag forces were not directly measured in this study, however stem deformation observations indicate that drag on the *S. patens* stems would be lower due to reductions in frontal area over a large portion of the wave cycle, as well as low relative stem-flow velocity. The inter-species contrast in response to wave action suggests that the two plants could be used to provide complementary flood and erosion control benefits within nature-based hazard management strategies, capitalizing on the cooperative feedback discussed in Schoutens et al. (2020). However, the ecological niche of each species must be considered when designing such strategies, as the optimal elevation zone for providing flood and erosion control may not align with the species' optimal elevation for growth. *S. alterniflora* typically dominates low marsh habitats as it thrives in anoxic environments (Wu et al. 2011; Augustin et al. 2009; Bertness 1991). Contrastingly, *S. patens* frequently colonizes mid- to high marsh habitats, due to its limited ability to oxygenate its rhizosphere in anoxic soils (Bertness 1991). Bertness (1991) investigated species zonation of *S. patens* and *S. alterniflora* in a New England salt marsh, experimenting with transplanting each species to different elevation zones and observing growth and survival. Their study found that *S. patens* that were transplanted to low marsh environments either exhibited significantly stunted growth or died (Bertness 1991). They also found that *S. alterniflora* was restricted from high marsh zones, as a result of interspecies competition rather than physical constraints (Bertness 1991). Ultimately, more research is needed to investigate the feasibility of utilizing *S. patens* and *S. alterniflora* in complementary roles as part of nature-based coastal protection strategies, optimizing their placement for hydrodynamic resistance while balancing ecological constraints.

#### 3.1.4.2 Factors Influencing Motion Response

The influence of planting configuration on live vegetation motion response was investigated in this study through pairwise comparison of bending angles observed between stems planted in isolation and within clusters (planting configurations are shown in **Fig. 3-3**). Statistical analyses indicated that there was a significant difference in forward stem bending between individual and

clustered stem configurations for *S. patens*, and in backward stem bending between individual and clustered stems for *S. alterniflora*. **Fig. 3-10** demonstrates that there was overall more variability in stem bending between individual and clustered stem configurations for *S. patens*, particularly that the stems planted in isolation tend to bend more in both the forward and backward directions in comparison to their clustered counterpart. Some of the variability in bending between stems in isolation versus planted in clusters can be attributed to differences in plant properties between the two tracked stems. As demonstrated in **Table 3-2**, there was more variability in plant properties within the sampled *S. alterniflora* stems, which could account for a large proportion of the variability in stem bending response between the individual and clustered stem observations. For *S. patens* the reduced bending observed for the stems planted in clusters is likely attributed to stem interactions, which could consequently obstruct deformation of adjacent stems or reduce hydrodynamic forces within the cluster. The morphology and flexibility of *S. patens* favors inter-plant interactions within clustered configurations, with many slender stems per plant versus the rigid single-stem morphology of *S. alterniflora*. Stem interactions were observed in the video footage of *S. patens* clusters, but not in the *S. alterniflora* clusters.

The magnitude of stem bending was generally found to increase with wave height for both *S. patens* and *S. alterniflora* (**Fig. 3-11A)**. However, wave height alone was not an effective relative predictor of stem bending. Stem dynamics demonstrated a strong dependence on wave period with longer period waves consistently generating larger bending angles in the forward and backward direction for the same wave height, across both species. This aligns with existing theory that suggests stem motion is dependent on wave excursion, which is a function of both wave period and wave amplitude (*A,* **Eq. 3-6**) (Luhar & Nepf 2016).

Luhar & Nepf (2016) have proposed the parameter *L* to characterize stem reconfiguration in consideration of the ratio of stem length to wave excursion. For small wave excursions ($L > 1$), the linear stem bending angle ($\theta$) is proportional to the ratio of wave excursion to blade length, $\theta \sim A_w/l$ (or $1/L$) (Lei & Nepf 2019). **Fig. 3-11 B**) demonstrates that this approximation holds well for the blade length ratio range investigated in this study ($L > 1.3$). As *L* approaches 1, theoretically a transition from swaying to whip-like stem motion is expected to occur (Rupprecht et al. 2017; Luhar & Nepf 2016). The experimental results of Rupprecht et al. (2017) indicated that this motion transition may occur at a range of *L* values, dependent on plant properties, with the more rigid *P. maritima* first exhibiting whip-like behavior at $L = 0.6$, and the more flexible *E. athericus* at $L = 1.8$ in their study. The symmetry of forward and backward bending angles was used to deduce motion type (swaying vs. whip-like) in the present study, with asymmetry that favors forward bending indicating whip-like motion. Ratios of forward to backward stem bending were compared against the hydrodynamic setting for all tests, however consistently remained close to unity for both species. This indicates that the hydrodynamic forcing was not sufficient to induce whip-like motion in any of tests presented herein, potentially a result of the limited number of tests conducted with *L* near or less than 1.

To incorporate the effects of stem flexibility, stem bending was also plotted against the combined non-dimensional parameter, *CaL*. A value of $Ca < 1$ indicates that the restoring forces due to plant stiffness exceed hydrodynamic forcing, and the plant should remain primarily upright. As values of *Ca* increase to $Ca > 1$, hydrodynamic forces overpower the restoring forces, and initiation of stem bending is expected. Above this threshold for motion, stem bending can be expected to intensify with increasing hydrodynamic forces (increasing *Ca*), however bending will still be limited by the wave excursion (Gosselin 2019). Using the combined parameter *CaL,* the influence of the magnitude of hydrodynamic forces and wave excursion with respect to stem reconfiguration can be examined simultaneously. **Fig. 3-11 C)** demonstrates this relationship for *S. patens,* with $Ca > 1$ in all cases, and bending angles $\propto CaL$.

*S. alterniflora* still showed a strong correlation between stem bending and *CaL* (**Fig. 3-11 D)**) despite being primarily in the range of $Ca < 1$. The flexural rigidity value used to calculate *Ca* for *S. alterniflora* was based on an average of the harvested stem samples that underwent biomechanical testing. Variations in flexural rigidity were observed between the sampled stems of *S. alterniflora* ($EI_{S.alt} = 0.051 +/- 0.015$ Nm$^2$, **Table 3-2**), indicating that the range of *Ca* is likely wider than reported in **Table 3-4,** and thus more of the tests may fall in the range of $Ca > 1$, where increased stem bending is expected. Furthermore, the *S. alterniflora* stems exhibited a high degree of stem tapering, which is expected to be associated with decreasing flexural rigidity along the stem's length. Considering this, the *Ca* values reported for *S. alterniflora* may be an underestimation for upper sections of the tracked stems, where most deformation occurred. Furthermore, Zhang & Nepf (2022) demonstrate that the drag on *S. alterniflora* leaves may contribute to a large portion of the overall drag forces acting on the plant, and that stem motion can be enhanced by leaf drag (Zhang & Nepf 2022; Zhang & Nepf 2021). Consequently, Zhang & Nepf (2022) propose the use of a modified stem Cauchy number that incorporates an additional term inclusive of drag forces acting on the leaves. The neglect of these forces in the *Ca* estimates presented herein could contribute to the discrepancies between the expected theoretical thresholds for stem motion ($Ca > 1$), and the degree of stem bending observed for *S. alterniflora* in this study ($Ca < 1$). Ultimately, testing under a wider range of hydrodynamic conditions could elucidate if the reported relationship between bending and *CaL* for *S. alterniflora* changes significantly as *Ca* increases further above 1, or as more complex plant biomechanics (i.e., height-varying properties) and morphologies (leaves) are considered.

#### 3.1.4.3 Stem Deformation and Wave Attenuation

This study represents a first step towards addressing the logistical challenges and viability of outdoor wave experimental programs with live vegetation, and as such, a full marsh canopy was not planted. Consequently, wave attenuation was not directly measured, and instead this study focused on observations of individual plant motion as a means to infer wave attenuation capacity based on drag force theory and previous experimental studies. Considering the formulation of drag forces acting on plant stems (**Eq. 3-4**), wave energy dissipation is expected to be proportional to plant frontal area, and decrease with increasing plant deflection (i.e., extreme

bending in phase with wave action) (Wang et al. 2021; Lei & Nepf 2019; Paul et al. 2016). Thus, it may be possible to correlate the magnitude of stem deformation to relative wave attenuation capacity.

Based upon measures of stem deformation, it is expected that drag forces on *S. alterniflora* plants would be greater than on *S. patens* under comparable hydrodynamic conditions and canopy densities, and thus *S. alterniflora* could provide greater wave attenuation. However, it should be noted that the attenuation capacity of the two species could be comparable given a high enough density of *S. patens* stems. This was demonstrated in Bouma et al. (2010), who found that wave attenuation was remarkably similar for *S. anglica* and *P. maritima* when compared per unit biomass, despite significant differences in plant morphology and flexibility, similar to that of *S. alterniflora* versus *S. patens.*

Wave period was also found to have a significant influence on the degree of stem bending, with the largest stem excursions recorded for both *S. patens* and *S. alterniflora* attributed to the long-period waves ($T_{s,i}$ > 9 s). This observed influence of wave period is particularly significant as previous physical modeling studies have yielded inconsistent results with respect to the influence of wave period on wave attenuation by vegetation surrogates (Maza et al. 2019; Anderson & Smith 2014). Contrastingly, reductions in frontal area due to extreme bending under longer period waves, as observed in this study, indicate that for flexible vegetation wave attenuation may be limited by wave period, or more accurately, large wave orbital excursions. Overall, this highlights the importance of using surrogates with realistic stiffness characteristics or live vegetation when using physical modeling techniques to assess the performance of vegetation as part of nature-based solutions, ensuring effects that are linked to plant biomechanical properties are captured.

Wave attenuation by flexible vegetation may also rapidly decrease as material thresholds for deformation are exceeded. Irreversible stem deformation (folding or severing) causes a rapid decrease in wave attenuation due to a reduction in plant height (Rupprecht et al. 2017; Vuik et al. 2018), thus, there is an interest in determining these species-specific thresholds for damage. This has previously been investigated by Rupprecht et al. (2017) and Vuik et al. (2018), for *Puccinellia maritima, Elymus athericus, Spartina anglica* and *Scirpus maritimus*. The critical velocity thresholds that result in stem breakage for these species ($U_{crit}$), as determined by Rupprecht et al. (2017) and Vuik et al. (2018), are: $U_{crit}$ > 0.90 m/s (*P. maritima*), $U_{crit}$ = 0.42 m/s (*E. athericus*) (Rupprecht et al. 2017), $U_{crit}$ = 0.86 +/- 0.28 m/s (*S. anglica*), and $U_{crit}$ = 0.59 +/- 0.22 m/s (*S. maritimus*) (Vuik et al. 2018). The critical velocities determined by Rupprecht et al. (2017) were calculated according to linear wave theory, corresponding to a height 15-cm above the bed. Only regular, non-breaking waves were considered in their study (Rupprecht et al. 2017). The values presented by Vuik et al. (2018) were determined from a stem breakage numerical model, that utilized linear wave theory for predictions of critical orbital velocity. No stem folding or breakage was observed during the present experiments, indicating that thresholds for irreversible deformation exceed the maximum velocity conditions presented in **Table 3-4.**

This yields $U_{crit} > 0.37$ m/s for *S. patens* and $U_{crit} > 0.28$ m/s for *S. alterniflora.* Future experiments with *S. patens* and *S. alterniflora* should attempt to identify the exact thresholds through experimental programs with more extreme waves.

#### 3.1.4.4 Stem Tracking Methodologies

Automated stem tracking was initially attempted using the Matlab-based tool *CytoSpectre* (Kartasalo et al. 2015). This tool was previously developed for quantification of orientation and size distributions of cell structures in microscopy images (Kartasalo et al. 2015). The *CytoSpectre* tool was configured to load in an image frame, compute the power spectral density (PSD) using Welch's method (also referred to as the Weighted Overlapped Segment Averaging method), convert the PSD to polar coordinates, and output the complete orientation distribution of identified spectral components (Kartasalo et al. 2015). Peaks of the spectral distribution (i.e., dominant stem orientation angles) were then identified for each frame using *findpeaks* and stored for post-processing. Unfortunately, multiple stems of different orientation (i.e., in the case of the *S. patens*), or the presence of prominent angled blades (*S. alterniflora*) frequently interfered with the analysis, and the tool was unable to consistently identify the peak from the spectral distribution that corresponded to the dominant stem orientation. As a result, stem tracking analysis was performed manually for the experiments presented herein. However, with further development, spectral analysis tools such as *Cytospectre* could yield effective automation of stem bending angle tracking, particularly within vegetation canopies where it is difficult to distinguish individual stems.

### 3.1.5 Conclusions

This paper presents the findings of a large-scale experimental program that investigated the bending response of live salt marsh vegetation to irregular waves. While the data presented in this study, based on individual plants and plant groupings, is not sufficient to derive quantitative relationships for wave attenuation by marsh vegetation at meadow-scale, it directly supports the development of these relationships by providing a validation dataset for future physical and numerical modeling. This study contributes novel quantitative knowledge of plant physical characteristics for two salt marsh species native to the Canadian coast, *S. patens* and *S. alterniflora*, and lays the groundwork for future large-scale experimental programs with live vegetation. The results demonstrate that plant morphology and biomechanical differences between *S. patens* and *S. alterniflora* have an influence on the magnitude of stem deformation under wave action. The more flexible *S. patens* plants consistently exhibited greater stem bending than the more rigid *S. alterniflora* under comparable incident wave conditions ($0.03 \text{ m} < H_{s,i} < 0.28$ m, $T_{s,i} \approx 2$ and 10 s). Neither *S. alterniflora* or *S. patens* exhibited irreversible stem deformation (folding or breakage) during the experiments conducted, indicating that the species are resilient under hydrodynamic forces up to, at minimum, $U_c = 0.37$ m/s for *S. patens* and $U_c = 0.28$ m/s for *S. alterniflora*. The measured plant physical properties, combined with observations of dynamic reconfiguration, indicate that *S. alterniflora* adopts more of a "resistance" strategy when faced with hydrodynamic stress, versus the "avoidance" strategy of *S. patens.* These

distinct behaviors suggest that the two species could work together effectively in nature-based coastal protection strategies, capitalizing simultaneously on the attenuative capacity associated with resistance species and the resilience of avoidance species (Schoutens et al. 2020; Rupprecht et al. 2017; Puijalon et al. 2011). It is recommended that future studies focus on the optimal way of combining these two species, particularly considering their unique ecological requirements.

### 3.1.6 Link to Section 3.2

The study presented here investigated wave-vegetation interactions for two salt marsh species using live vegetation, at prototype-scale. Observations of stem deformation, as well as measured plant physical and biomechanical properties from this study were used to support the development of small-scale modeling methods for one of the tested species, *Spartina alterniflora.* The development and implementation of a downscaled *S. alterniflora* meadow in a higher energy wave program is presented in the following section.

## 3.2 New Insights to the Use of Scaled Surrogate Vegetation for Modelling Nature-Based Solutions

*Preprint of an article submitted to the Journal of Waterway, Port, Coastal and Ocean Engineering.*

### 3.2.1 Introduction

Traditional "hard" shoreline protection structures such as breakwaters, groynes or seawalls have the potential to produce detrimental impacts to coastal environments, including the obstruction of natural sediment transport pathways and limiting ecosystem resilience to anthropogenic and climatic stressors, such as sea-level rise (Temmerman et al., 2013; Bilkovic et al., 2017; Gracia et al., 2018). Furthermore, the static nature of such infrastructure limits its viability in the context of climate change, as changes in the frequency and severity of coastal hazards are expected to demand substantial infrastructure adaptation, replacement, or maintenance, with significant associated costs (Temmerman et al., 2013; Vitousek et al., 2017; Gracia et al., 2018). The coastal protection benefits provided by natural features - such as coastal marshes, mangrove forests and seagrass meadows - has led to growing interest in the conservation and establishment of these features as alternatives to, or in combination with, the deployment of conventional "hard" structures. Under the right hydro-sedimentary conditions, natural systems and features (or hybrid systems combining natural and "hard" features) offer enhanced capacity for wave attenuation, flood protection and erosion prevention by comparison to purely "hard" structural solutions (Spalding et al., 2014; Brooks et al., 2021; Piercy et al., 2021). Thus, the reliance on natural systems as part of coastal protection strategies is advantageous in the context of climate change. Shoreline protection schemes that incorporate the conservation, restoration or planting of coastal vegetation are frequently referred to as examples of "living shorelines" or "nature-based solutions" (NBS) (Bilkovic et al., 2017).

A growing number of studies have endeavored to quantify the coastal protection benefits afforded by coastal marsh vegetation, considering different plant species, planting configurations, and hydrodynamic contexts (e.g., Mendez & Losada, 2004; Lima et al., 2006; Augustin et al., 2009; Anderson & Smith, 2014; Blackmar et al., 2014; Moller et al., 2014; Ozeren et al., 2014; Paul et al., 2016; Wu & Cox, 2016; van Veelen et al., 2020, among others). This knowledge is essential for the development of design guidelines to enable successful incorporation of marsh vegetation into nature-based coastal protection schemes. Physical modelling studies for NBS have aimed to simulate natural coastal systems (or hybrid systems) in laboratory settings, allowing investigation of wave-vegetation interactions in a controlled and accessible manner. Accurate representation of such interactions requires careful model development, including consideration of scale effects and the selection of appropriate vegetation elements. Some studies have utilized live vegetation in full-scale physical modelling studies, collected either through excavation, transplantation of nursery or wild seedlings, or by growing the plants from seed (Fonseca & Calahan, 1992; Tschirky et al., 2000; Moller et al., 2014; Maza et al., 2015; Silinski et al., 2015; Lara et al., 2016; Rupprecht et al., 2017; Poppema et al., 2019;

Paul & Kerpen, 2021; Markov et al., 2022). Lara et al. (2016) provides a thorough overview of the requirements for physical modelling with live vegetation, including experimental design considerations, and growing versus collecting methods.

Growing or excavating live vegetation is not always feasible for physical modelling studies, especially when experiments cannot be conducted at prototype-scale owing to practical laboratory constraints (e.g., maximum wave heights that can be generated in the laboratory). Even where feasible, costs to procure and maintain live vegetation can be significant. To circumvent the challenges with utilizing live vegetation in laboratory settings, surrogate elements are sometimes used to represent live vegetation. Surrogate elements are often selected to mimic the geometric parameters of the target vegetation, including stem/blade length, width, diameter, and planting density (Augustin et al., 2009; Anderson & Smith, 2014; Ozeren et al., 2014; Maza et al., 2019). For small-scale physical models with surrogate vegetation, stem diameters should only be geometrically downscaled if stem Reynolds number (*Re,* **Eq. 3-8**) conditions can be reasonably maintained with respect to prototype conditions, as significant changes to the stem Reynolds range can strongly influence the drag coefficient (Blackmar et al., 2014).

$$Re = \frac{U_c b_v}{v} \quad \textbf{(3-8)}$$

In which $U_c$ =characteristic velocity acting on the plant stem (m/s), $b_v$ = plant stem width (m), and $v$ =kinematic viscosity of water ($10^{-6}$ $m^2/s$).

When modelling flexible vegetation, consideration must also be made for wave-induced vegetation motion (Ghisalberti & Nepf, 2002; Sanchez-Gonzalez et al., 2011; Manca et al., 2012; Koftis et al., 2013; Anderson & Smith, 2014; Lei & Nepf, 2019). The motion of individual, flexible plants in moving water is governed by three primary forces: drag force ($F_D$), a buoyancy force ($F_B$), and a restoring force ($F_R$) (Ghisalberti & Nepf, 2002, Sanchez-Gonzalez et al., 2011). The restoring force is dependent on the rigidity of the plant stem or blade (Ghisalberti & Nepf, 2002). Dynamic similitude may be achieved through matching two independent ratios of these forces: $F_B/F_R$ and $F_R/F_D$ (Ghisalberti & Nepf, 2002). Ghisalberti & Nepf (2002) proposed the following two scale parameters for balancing these force ratios:

$$\lambda_1 = \frac{(\rho_w - \rho_v) l^3}{E b_v^2} \quad \textbf{(3-9)}$$

$$\lambda_2 = \frac{E b_v^3}{l^3 U^2} \quad \textbf{(3-10)}$$

In which $\rho_w$ and $\rho_v$ = densities of water and vegetation ($kg/m^3$), respectively, $U$ = mean in-canopy velocity (m/s), $E$ =modulus of elasticity ($N/m^2$) and $l$ = total stem/blade length (m). There are challenges and uncertainty associated with measurement and quantification of $U$ in $\lambda_2$ (**Eq. 3-10**); thus Ghisalberti & Nepf (2002) recommends selecting $\lambda_1$ as the critical scaling parameter. However, if the prototype plant deflection angles can be accurately represented by the model, $\lambda_{1,p} = \lambda_{1,m}$ (p: prototype, m: model), and the similarity of $\lambda_2$ will also be preserved due to the

assumptions made in the development of the scale parameter equations (Ghisalberti & Nepf, 2002). These scaling parameters were used for physical modelling studies by Ghisalberti & Nepf (2002) and Sanchez-Gonzalez et al. (2011), to mimic the seagrass species *Zostera marina* (full-scale), and *Posidonia oceanica* (1:10 geometric scale), respectively.

Koftis et al. (2013) proposed that the critical scaling parameter, $\lambda_1$, developed by Ghisalberti & Nepf (2002) is not sufficient for vegetation models under steady or oscillatory flow effects, as it does not allow for direct incorporation of flow velocity. As an alternative, Koftis et al. (2013) recommends using the Cauchy number (*Ca*) for scaling of flexible vegetation, defined as the ratio of hydrodynamic (drag) forces to the plant restoring forces (material stiffness) (**Eq. 3-11**):

$$Ca = \frac{\rho_w b_v U_c^2 l^3}{EI} \quad \textbf{(3-11)}$$

In which *EI* = stem flexural rigidity ($Nm^2$), defined by the product of elastic modulus (*E)* and *I* = 2nd moment of inertia ($m^4$) (Koftis et al., 2013; Luhar & Nepf, 2016; Rupprecht et al., 2017).

Other studies have used more simplified approaches to consider plant flexibility for physical modelling of coastal vegetation. Anderson & Smith (2014) identified posture and motion as the two most important parameters when selecting plant mimics, and accordingly selected surrogate elements considering stem material density and modulus of elasticity for accurate reproduction of the wave-induced swaying motion of *Spartina alterniflora*, while also ensuring an upright position in shallow waters (Anderson & Smith, 2014). Surrogate plants were similarly selected for experiments performed by Lima et al. (2006), Augustin et al. (2009) and Manca et al. (2012).

Luhar & Nepf (2016) proposed an alternative method for consideration of flexible vegetation motion in modelling wave-vegetation interactions, using the concept of an effective stem length. The effective length, $l_e$, is defined as the equivalent rigid stem length that may produce the same drag forces as a flexible blade of length *l* (Luhar & Nepf, 2016). Zhang & Nepf (2021) found that the effective length can be reasonably defined using non-dimensional parameters *Ca* and *L*, the ratio of stem length to wave orbital excursion (**Eq. 3-12**), through **Eq. 3-13**.

$$L = \frac{l}{A}, A = \frac{U_c}{\omega} \quad \textbf{(3-12)}$$

$$\frac{l_e}{l} = (CaL)^{-1/4} \quad \textbf{(3-13)}$$

In which *A* = wave orbital excursion (m), and $\omega$ = wave angular frequency ($\omega = 2\pi/T$, rad/s) (Luhar & Nepf, 2016; Rupprecht et al., 2017). This effective length formula applies for unsteady flow with small excursions ($L \gg 1$) and assumes that drag is dominantly responsible for hydrodynamic forcing. Using this relationship, an equivalent rigid element may be used to represent the drag induced by flexible marsh plants in numerical or physical modelling studies.

Furthermore, vegetation canopies for some marsh species may be successfully mimicked using arrays of rigid elements such as aluminum rods or wooden dowels, despite the live plants exhibiting some degree of flexibility (Augustin et al., 2009; Wu, et al., 2011; Hoque et al., 2018;

Maza et al., 2019; van Veelen et al., 2020). For example, Augustin et al. (2009) modelled *Spartina alterniflora* using both rigid and flexible elements at prototype-scale and found that the two models produced similar attenuation effects for the tested flow conditions ($H_s$ = 0.085 m, 1.5 s < $T_p$ < 2.0 s). Thus, the necessity for consideration of vegetation motion using flexible surrogate elements may be species-specific, and/or depend on the experimental hydrodynamic conditions and scale.

**Table 3-6.** Summary of physical modelling studies for coastal marsh-based NBS under wave action.

| Study | Target Species | Model Material | Scale | Flat / Slope | Stem density | Canopy submergence | Wave Conditions (prototype scale) | Wave Type | Re | KC |
|---|---|---|---|---|---|---|---|---|---|---|
| ***Anderson & Smith (2014)*** | *Spartina alterniflora* | XLPO tubing | 1:1 | Flat | 200-400 stems/m$^2$ | Emergent, submerged | 1.25 s < $T_p$ < 2.25 s<br>0.05 m < $H_s$ < 0.192 m | Irregular (TMA) | 533-2296 | 26-112 |
| ***Augustin et al. (2009)*** | *Spartina alterniflora* | Cylindrical wooden dowels, polyethylene foam tubing | 1:1 | Flat | 97 – 194 stems/m$^2$ | Emergent, submerged | 1.5 s < $T_p$ < 2.0 s<br>$H_s$ = 0.085 m | Irregular (TMA) | 3300-8500 | 40-105 |
| ***Paul et al. (2016)*** | *n/a* | Plastic strips (Lexaan plates) | 1:1 | Flat | n/a | Submerged | 1.4 s < $T_p$ < 5.1 s<br>0.1 m < $H_s$ < 0.9 m | Regular; Irregular (JONSWAP) | n/a | n/a |
| ***Ozeren et al. (2014)*** | *Spartina alterniflora, Juncus roemerianus* | EPDM foam-rubber cords, live plants | 1:1 | Flat | 156-2857 stems/m$^2$ | Emergent, submerged | 0.7 s < $T_p$ < 2.0 s<br>0.03 m < $H_s$ < 0.15 m | Regular; Irregular (JONSWAP) | 200-4500 | 2-80 |
| ***Wu & Cox (2016)*** | *Schoeno-plectus pungens* | Plastic strips (zip ties) | 1:4* | Flat | 1618-3236 stems/m$^2$ | Emergent | 0.8 s < $T_p$ < 2.8 s<br>0.06 m < $H_s$ < 0.14 m | Irregular (JONSWAP) | 590-810 | 19-45 |
| ***Blackmar et al. (2014)*** | *Schoeno-plectus pungens* | Flexible artificial vegetation (material not specified) | 1:4* | Flat | 556-5000 stems/m$^2$ | Emergent, submerged | 1.2 s < $T_p$ < 1.6 s<br>0.072 m < $H_s$ < 0.12 m | Irregular (JONSWAP) | 200-1700 | n/a |
| ***Lima et al. (2006)*** | *Brachiaria subquadripara* | Braided nylon rope | 1:1 | Flat | 400-1600 stems/m$^2$ | Submerged | 1.00 s < $T$ < 1.50 s<br>0.05 < $H$ < 0.15 m | Regular | n/a | n/a |
| ***van Veelen et al. (2020)*** | *n/a* | Bamboo dowels, silicon sealants | 1:1 | Flat | 1111 stems/m$^2$ | Emergent, submerged | 1.4 s < $T$ < 2.0 s<br>0.08 m < $H$ < 0.2 m | Regular | 779-1658 | 53-133 |
| ***Yin et al. (2019)*** | *n/a* | Rigid cylinders | 1:4 | Slope (1:6) | 462 stems/m$^2$ | Emergent | 3.0 s < $T$ < 6.0 s<br>0.24 m < $H$ < 0.48 m | Regular | n/a | n/a |
| ***Keimer et al. (2021)*** | *n/a* | PVC rods | 1:10 | Flat | 200-400 stems/m$^2$ | Submerged | 3.2 s < $T_{p,1}$ < 15.8 s<br>0.8 m < $H_{m0,1}$ < 2.0 m | Irregular | n/a | n/a |
| ***Wang et al. (2022)*** | *Spartina alterniflora* | Polyethylene flexible cylinders | 1:1 | Flat | 133-444 stems/m$^2$ | Emergent, submerged | 1.0 s < $T$ < 1.5 s<br>0.08 m < $H$ < 0.14 m | Regular | 1500-8000 | 15-75 |
| ***Baker et al. (2022)*** | *Spartina alterniflora* | Birch dowels, flexible Tygon tubing | 1:20 | Flat | 150-550 stems/m$^2$ | Emergent, submerged | 3 s < $T_p$ < 15 s<br>1.0 m < $H_{m0}$ < 2.0 m | Irregular | 5026-23121 | 241-5359 |

*Stem diameter not scaled to maintain reasonable stem Reynolds conditions

Various surrogate materials have been used to represent salt marsh species in physical modelling studies (**Table 3-6**). Many of these vegetation surrogates were developed at prototype-scale to avoid errors associated with downscaling and Froude similitude assumptions (Lima et al., 2006; Augustin et al., 2009; Manca et al., 2012; Anderson & Smith, 2014; Ozeren et al., 2014). Few studies have utilized vegetation surrogates at small-scale, namely Sanchez-Gonzalez et al. (2011), Blackmar et al., (2014), Maza et al. (2017), Hoque et al. (2018), Maza et al. (2019), Vettori & Nikora (2020) and Baker et al. (2022), requiring additional scaling of the selected surrogate elements. Hoque et al. (2018), Maza et al., (2017) and Maza et al. (2019) developed downscaled (1:25, 1:12, 1:6, respectively) models of mature *Rhizophora* (mangrove) trees.

Hoque et al. (2018) and Maza et al. (2017) downscaled the *Rhizophora* models purely geometrically, while Maza et al. (2019) noted that the trunk and root diameters were selected to ensure turbulent wake structures for both $Re_{trunk}$ and $Re_{roots}$ conditions were maintained at model scale. Sanchez-Gonzalez et al. (2011) and Vettori & Nikora (2020) developed reduced-scale model elements representative of the seagrass species *Posidonia oceanica* and *Saccharina latissima,* respectively. For both studies, surrogates were downscaled considering geometric similarity (1:10, Sanchez-Gonzalez et al., 2011; 1:5, Vettori & Nikora, 2020). Blackmar et al. (2014) and Wu & Cox (2016) developed vegetation models for a reduced scale (1:4) experimental wave program, based on the plant properties of the coastal marsh species *Schoenoplectus pungens.* All plant properties were scaled geometrically except the plant diameter, which was maintained to ensure reasonable stem Reynolds conditions at model scale (Blackmar et al., 2014; Wu & Cox, 2016). Yin et al. (2019) performed reduced-scale (1:4) testing with emergent mimic vegetation on a slope, however the idealized vegetation was not selected to be representative of a target species, and thus their study provides little insight for methods of downscaling vegetation surrogates. Keimer et al. (2021) investigated wave-vegetation interactions on vegetated foreshores at sea dikes at reduced scale (1:10), however similarly did not aim to reproduce a specific vegetation species. Baker et al. (2022) modelled wave attenuation across a downscaled artificial salt marsh (1:20). In their study, Baker et al. (2022) modelled the marsh using surrogate vegetation with enlarged diameters but reduced stem density (i.e., increased stem spacing), maintaining an equivalent solid volume fraction with prototype-scale conditions. This was done to overcome the practical challenges of constructing model vegetation canopies at such a small-scale, which would have required thousands of very narrow elements, as well as to preserve reasonable stem Reynolds number similarity (Baker et al., 2022).

Overall, few physical modelling studies have been performed with vegetation surrogates at reduced scale, owing to uncertainties in scale effects and appropriate methodologies for downscaling. Studies that have been performed with downscaled vegetation surrogates have not demonstrated clear guidelines for appropriate methods of downscaling, or the sensitivities of these methods to the selection of stem diameter. Large-scale and/or live vegetation studies are costly and often not feasible, with few experimental facilities that can support such programs. To enhance the accessibility and practicality of physical modelling of coastal vegetation to inform NBS design and deployment, significant knowledge gaps must be addressed to improve experimental methods, particularly for modelling coastal vegetation at reduced scale.

To address some of these knowledge gaps, irregular wave experiments were conducted with a downscaled surrogate marsh in the Steel Wave Flume of the National Research Council Canada's Ocean, Coastal and River Engineering (NRC-OCRE) Research Centre, in Ottawa, Canada. Surrogate elements were selected to represent *S. alterniflora* (smooth cordgrass), a coastal marsh species native to the Atlantic coast of Canada, dominant within the Bay of Fundy in Nova Scotia and New Brunswick (Natural Resources Conservation Service, 2021). The

experimental program investigated the wave attenuation provided by a simulated *S. alterniflora* meadow under increasingly severe wave conditions, for realistic constructed marsh scenarios (i.e., mildly sloping shoreline, irregular waves). Primary objectives were to:

1. Investigate methods for downscaling live vegetation in laboratory settings, including sensitivities to the selection of model element diameter and spacing.
2. Compare the performance of various surrogate proxies for the semi-flexible *Spartina alterniflora*, to inform guidelines for vegetation surrogate selection.

The remainder of this paper is organized as follows. Section 3.2.2 provides a comprehensive overview of the development of various surrogate elements and configurations considered for simulation of the downscaled *S. alterniflora* marsh. Section 3.2.3 focuses on the physical setup of the experimental program, including details on hydrodynamic testing conditions and instrumentation. Section 3.2.4 presents results from the experimental program that demonstrate the wave attenuation provided by the downscaled marsh. Wave attenuation results from the different surrogate array configurations and elements are then compared and discussed in Section 3.2.5. Section 3.2.5 also provides recommendations for physical modelling of vegetation at reduced scale to inform NBS design, based upon the experimental findings. Finally, conclusions are presented in Section 3.2.6.

### 3.2.2 Surrogate Development

There is significant intra-species variation in the physical properties of coastal marsh plants (Puijalon et al., 2011; Rupprecht et al., 2017; Zhu et al., 2020; Zhang & Nepf, 2021). Previous studies investigating wave-vegetation interactions with *S. alterniflora*, the target species for the experiments described here, have reported average stem diameters between 4.3 mm and 8.0 mm (Knutson et al., 1982; Chatagnier et al., 2012), and average stem lengths between 32 cm and 84 cm (Knutson et al., 1982; Ysebaert et al., 2011). The biomechanical properties of *S. alterniflora* have also been reported to range across orders of magnitude, with lower estimates of $E$ = 159.8 MPa by Chatagnier et al. (2012) and upper estimates of $E$ = 1410 MPa by Feagin et al. (2011). Several factors contribute to the differences in plant properties amongst mature *S. alterniflora* plants, including but not limited to geography, climate, hydrodynamic setting, and season (Neumeier, 2005; Liu et al., 2015; Schulze et al. 2019; Schoutens et al. 2020). As a result, it is difficult to develop surrogate elements entirely representative of the *S. alterniflora* marsh species and it is more appropriate to identify the target region and/or season for replication. For this study, surrogates were developed based on the live vegetation parameters reported from the full-scale experiments performed by Markov et al. (2022). The *S. alterniflora* plants used in their study were sourced from a marsh along the St. Lawrence River near Trois-Pistoles, Québec, Canada. Plant physical characteristics were measured in summer (August 2021) following transplantation into an outdoor wave flume, and further details on the plant husbandry methods and stem measurements are provided by Markov et al. (2022). A summary of measured parameters for the live *S. alterniflora* plants from Markov et al. (2022) is provided in **Table 3-7**, along with measurements from other *S. alterniflora* studies (non-exhaustive) for comparison.

**Table 3-7.** Summary of live *S. alterniflora* plant parameters from various field and experimental studies. Surrogate development for the present study was based upon the reported values of Markov et al. (2022).

| **Study** | **Markov et al. (2022)** | **Feagin et al. (2011)** | **Chatagnier et al. (2012)** | **Knutson et al. (1982)** | **Ysebaert et al. (2011)** |
|---|---|---|---|---|---|
| **Geography** | *Quebec, Canada* | *Texas, United States* | *Louisiana, United States* | *Virginia, United States* | *Yangtze estuary, China* |
| Stem width, $b_v$ (mm) | 4.47 +/- 0.89 | 4.3 | 7.97 | 5.2-6.4 | 5.2+/-1.7 |
| Stem height, $l$ (cm) | 62 +/- 18 | 51.67 | 71.6 | 18-32 | 84+/-63 |
| Elastic modulus, $E$ (MPa) | 230 +/- 40 | 1410 +/- 710 | 159.8 | n/a | n/a |
| Flexural rigidity, $EI$ (Nm$^2$) | 0.051 +/- 0.015 | n/a | 0.0341 | n/a | n/a |

#### 3.2.2.1 Downscaling Vegetation Meadows via Solid Volume Fraction

Wave tests were conducted at a 1:4 geometric scale considering Froude similitude. This scale was selected based upon the dimensions of the experimental facility and optimization of the wave generation capabilities. Stem length was scaled geometrically to 15.5 cm, corresponding to the average live *S. alterniflora* stem length from Markov et al. (2022). Stem diameters were not downscaled geometrically considering the 1:4 scale, to avoid potential errors associated with significant changes to the stem Reynolds conditions relative to prototype-scale (Blackmar et al., 2014; Wu & Cox, 2016; Keimer et al., 2021). Instead, selection of a stem diameter that maintained the prototype-scale stem Reynolds range was prioritized, and the stem density ($N_v$, stems/m$^2$) was adjusted for downscaling. A solid volume fraction scaling factor ($\alpha$) was used in this approach **(Eq. 3-14):**

$$\alpha = \frac{\pi}{4} b_v^2 * l * N_v \quad \textbf{(3-14)}$$

Previous experimental studies have demonstrated a strong relationship between wave damping and the solid volume fraction of vegetation encountered by the waves, providing evidence to support the use of this scaling approach (Augustin et al., 2009; Phan et al., 2019; Tang et al., 2022). The solid volume fraction has been used for surrogate development (prototype-scale) in a study by Phan et al. (2019), and in a downscaled (1:20) surrogate study by Baker et al. (2022). However, the validity of this approach, as well as its sensitivity to stem diameter selection, has never been directly investigated to the authors' knowledge.

Based on the selected wave protocol, prototype-scale stem Reynolds conditions were expected to be between $1600 < Re < 5000$. Maintaining this $Re$ range under scaled hydrodynamic conditions yielded a model stem diameter of $b_v = 9.5$ mm. To test the method's sensitivity to stem diameter selection, an additional diameter of $b_v = 4.75$ mm was selected. Applying the scaling factor $\alpha$, considering a 1:4 scale and stem length ($l$) of 15.5 cm, the resultant stem densities were 50 stems/m$^2$ and 204 stems/m$^2$, respectively, both representative of a prototype-scale marsh of $N_v$ = 51 stems/m$^2$ (stem spacing, $\lambda$ = 15-cm). Rigid wooden dowels were used for these two surrogate test series, to investigate the sensitivity of the downscaling method to surrogate diameter and stem spacing while eliminating influences associated with element flexibility. The test series with rigid surrogates are hereafter referred to as TS-R1 (wooden dowel, $l$=15.5 cm, $b_v$ = 9.5 mm,

$N_v$ = 51 stems/m$^2$), and TS-R2 (wooden dowel, $l$=15.5 cm, $b_v$ = 4.75 mm, $N_v$ = 204 stems/m$^2$). An additional three surrogate configurations were developed to investigate the influence of flexibility on the experimental outcomes, described in the following section.

#### 3.2.2.2 Flexibility Considerations in Surrogate Selection

Stem flexibility was considered in the development of additional *S. alterniflora* surrogate meadows both directly, through selection of a flexible surrogate material, and indirectly, through application of the effective length theory proposed by Luhar & Nepf (2016). All surrogates that considered flexibility through either method were developed in alignment with the geometry and stem configuration (planting density) of TS-R1.

##### *Flexible Element Selection*

Flexible surrogate elements were selected in an attempt to match the bending response of live *S. alterniflora* under irregular wave action, similar to the methods utilized by Lima et al. (2006), Augustin et al. (2009), Manca et al. (2012), and Koftis et al. (2013). Application of Cauchy similitude was not employed due to significant variation and uncertainties associated with the biomechanical properties (i.e., *EI*) of *S. alterniflora.* Various flexible surrogate materials were investigated, prioritizing bending similarity to *S. alterniflora* and surrogate posture. With respect to the latter criterion, only flexible elements that could remain upright under their self-weight were deemed viable, to avoid significant buoyancy effects.

Two candidate surrogate elements - silicone tubing and latex rubber tubing - were exposed to irregular waves with spectral significant wave heights in the range 0.025 < $H_{m0}$ < 0.05 m, and peak wave periods of $T_p$ = 1.25 s, in a small wave flume (13 m x 0.3 m x 0.3 m) at the Institut National de la Recherche Scientifique (INRS) in Quebec, Canada. A water depth of 22.5 cm was selected to create stem submergence conditions ($l/d$ = 0.78) comparable to Markov et al. (2022). The outer diameter and stem length of the surrogates were selected to match the TS-R1 surrogates, with $l$ = 15.5 cm and $b_v$ = 9.5 mm (3/8”). A video camera stationed outside of the wave flume captured motion of the surrogate candidates under various irregular wave scenarios. Stem bending angle tracking was performed for each video in Matlab, through a frame-by-frame analysis using the *pointTracker* function (MATLAB, 2021). Summary statistics from stem bending angle tracking were subsequently obtained following the methods of Markov et al. (2022), extracting significant bending angles (average of the highest one-third angles) in both the forward (direction of wave travel) and backward directions, $F_s$ and $B_s$, respectively. Results from the bending angle analysis performed on the candidate surrogate materials were compared to the bending response of live *S. alterniflora* from Markov et al. (2022) under comparable prototype-scale hydrodynamic settings (offshore wave conditions: 0.1 m < $H_{m0}$ < 0.2 m, $T_p$ = 2.5 s; stem submergence: 0.60 < $l/d$ < 0.94). This comparison is provided in **Fig. 3-12**.

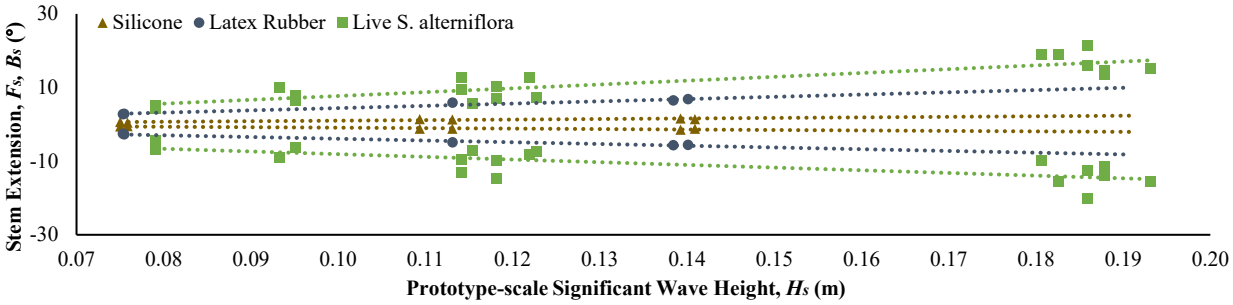


**Fig. 3-12.** Comparison of surrogate element bending (silicone tubing, latex rubber tubing) under scaled wave conditions, to live *S. alterniflora* bending from Markov et al. (2022). Plot displays stem bending summary statistics in the forward and backward directions ($F_s$ and $B_s$, respectively) versus wave height (all converted to prototype-scale).

As illustrated by **Fig. 3-12**, neither surrogate material was able to exactly replicate the same magnitude of stem bending observed for the live *S. alterniflora* stems. More flexible materials may have been able to yield more comparable bending, however such elements could not maintain an upright posture under their self-weight. The latex rubber tubing was selected as the preferred flexible surrogate, having exhibited bending responses most similar to live *S. alterniflora* (TS-F1).

### *Effective Length*

Several studies have demonstrated that wave attenuation by flexible vegetation canopies varies with hydrodynamic conditions, partly as a response to changes in vegetation motion, whereas wave attenuation by rigid vegetation canopies is independent of plant biomechanical properties (Bradley & Houser, 2009; van Veelen et al., 2020). This is considered in the effective length formula produced by Luhar & Nepf (2016), as both $Ca$ and $L$ change with $U_c$. While convenient for numerical models, where calculation of $l_e$ can be intrinsically built into the model execution considering changing hydrodynamic conditions, this iterative formulation is not as easily implemented for physical modelling. In the present study, two different rigid element lengths were selected, based upon calculations of $l_e$ via **Eq. 3-13**, to cover the range of hydrodynamic conditions investigated experimentally. The calculation of $l_e$ utilized prototype-scale *S. alterniflora* parameters from Markov et al. (2022) ($EI$ = 0.051 Nm$^2$, $l$ = 0.62 m, $b_v$ = 0.00447 m) and prototype-scale experimental test conditions. Effective lengths computed using **Eq. 3-13** with prototype-scale values were then scaled geometrically considering the 1:4 model scale. The selected effective lengths were $l_e$ = 7.8 cm (TS- E1) and $l_e$ = 5.5 cm (TS- E2), corresponding to $l_e$ = 31 cm and $l_e$ = 22 cm at prototype-scale. This selection covers prototype-sale $CaL$ values in the range of 16 to 59, and $U_c$ in the range of 0.5 m/s to 1.8 m/s, as demonstrated in **Fig. 3-13**.

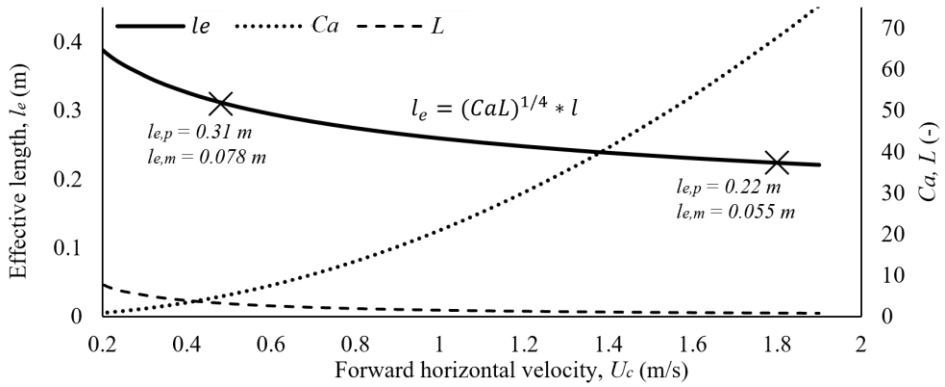


**Fig. 3-13.** Selection of effective lengths for rigid elements (marked with 'X' on the $l_e$ plot).

### 3.2.2.3 Summary of Surrogate Elements

Overall, five test series with surrogate arrays were developed to simulate the *S. alterniflora* field. Comparative assessment of the various test series allows investigation of the downscaling method (solid volume fraction, $\alpha$), as well as the importance of, and methods for, considering element flexibility in downscaled models of vegetation canopies with plant surrogates. **Fig. 3-14** summarizes all surrogate elements and configurations considered in the downscaled experimental program.

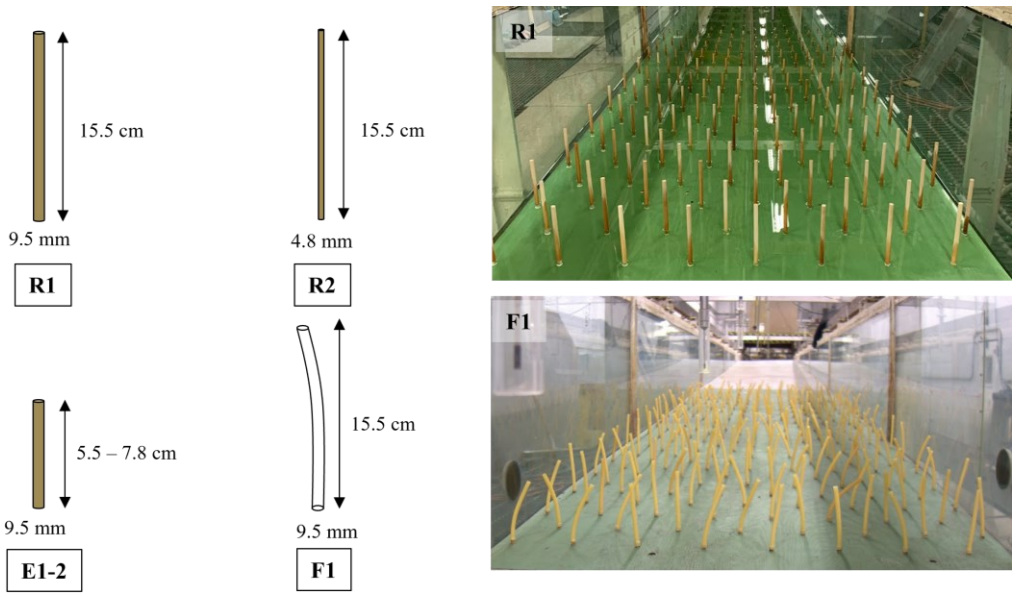


| Surrogate | Material | Rigid / Flexible | Length (cm) | Diameter (mm) | Planting Density (stems/m$^2$) |
|---|---|---|---|---|---|
| R1 | Wooden dowel | Rigid | 15.5 | 9.5 | 50 |
| R2 | Wooden dowel | Rigid | 15.5 | 4.8 | 204 |
| F1 | Latex rubber tubing | Flexible | 15.5 | 9.5 OD, 6.4 ID | 50 |
| E1,2 | Wooden dowel | Rigid* | 7.8, 5.5 | 9.5 | 50 |

*Indirectly considers flexibility through consideration of the effective length of flexible vegetation (Zhang & Nepf, 2021)

**Fig. 3-14.** Summary of all surrogate vegetation test series: R1, R2, F1, E1 and E2. Images of R1 and F1 panels show the two different surrogate materials: rigid wooden dowels (top right), and flexible latex rubber tubing (bottom right).

## 3.2.3 Experimental Program

### 3.2.3.1 Sloping Shoreline Installation

Experiments were conducted in the Steel Wave Flume of the National Research Council of Canada's Ocean, Coastal and River Engineering Research Centre, located in Ottawa, Canada. The wave flume measures 64 m long by 1.2 m wide and 1.2 m deep and utilizes a piston-type wave generator. A 1:20 concrete slope was installed in the wave flume with the slope toe located at a distance of 30 m from the wave paddle. Interchangeable panels were constructed using 1.2 m by 2.4 m plywood sheets to facilitate transitions between test series with surrogate vegetation. These interchangeable panels were fixed to a wooden frame embedded in the concrete slope.

Surrogate vegetation panels were constructed by drilling holes into the plywood sheets in a staggered arrangement (see **Fig. 3-15**), with stem spacing ($\lambda$) selected to obtain two different stem densities ($N_v$) of 50 stems/m$^2$ (R1, E1, E2, F1) and 204 stems/m$^2$ (R2). The relationship between $\lambda$ and $N_v$ is provided in **Fig. 3-15.** For rigid surrogate elements (R1, R2, E1, E2), the wooden dowels were inserted into the drilled holes, and fixed with small amounts of wood glue. For flexible elements (F1), a short wooden dowel was inserted into the latex rubber tubing, and this wooden peg was then fixed to the drilled plywood panel in the same manner as for the rigid surrogate elements.

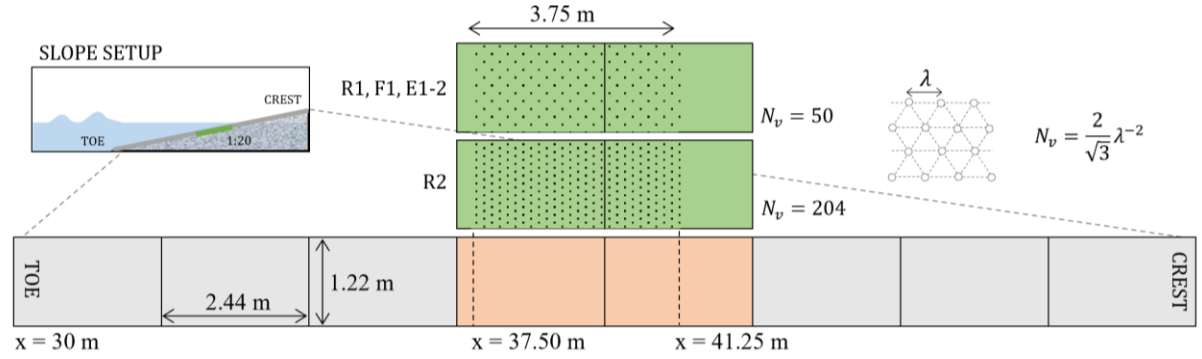


**Fig. 3-15.** Slope setup with interchangeable plywood panels for transitions between surrogate test series. The interchangeable panel locations on the slope are indicated in orange. Cross-shore distances (in the x-direction) are measured relative to the wavemaker.

Prior to surrogate vegetation testing, all wave conditions were measured across a bare slope to establish a base (unvegetated) case for wave height evolution. For the bare slope experiments, eight undrilled plywood panels were fixed to the concrete slope. For the experiments with model vegetation canopies, two of the undrilled panels were swapped for surrogate vegetation panels. These two panels were partially drilled, to create a marsh 3.75 m in length, starting 7.5 m from the slope toe. Interchangeable panel configurations for all test series are shown in **Fig. 3-15.**

### 3.2.3.2 Wave Conditions

Wave conditions were synthesized from JONSWAP spectra to generate incident waves with zeroth-moment wave heights in the range 0.075 m < $H_{m0}$ < 0.230 m, and target peak wave periods ($T_p$) of either 2.00 s, 2.75 s, or 3.25 s (prototype-scale: 0.30 m < $H_{m0}$ < 0.92 m, $T_p$ = 4.0 s,

5.5 s and 6.5 s). Wave heights were selected to capture a range of hydrodynamic conditions, from moderate wave conditions that may be experienced in natural marsh environments (Roland & Douglass, 2005), up to more extreme waves expected under storm conditions or for more hydrodynamically-exposed engineered vegetated dyke structures. These wave conditions were generated for two different water depths: $d_1$ = 0.60 m and $d_2$ = 0.75 m (prototype-scale: $d$ = 2.40 m and 3.00 m). The resultant relative stem submergence is schematized for each test series in **Fig. 3-16**, with the marsh partially emergent for $d_1$ and fully submerged for $d_2$**.** The bare slope was first subjected to the wave protocol to establish an unvegetated base case for wave transformations across the slope. All test surrogate vegetation configurations were then subjected to the same wave protocol, which consisted of 17 wave tests, each with a non-repeating sequence of approximately 600 irregular waves.

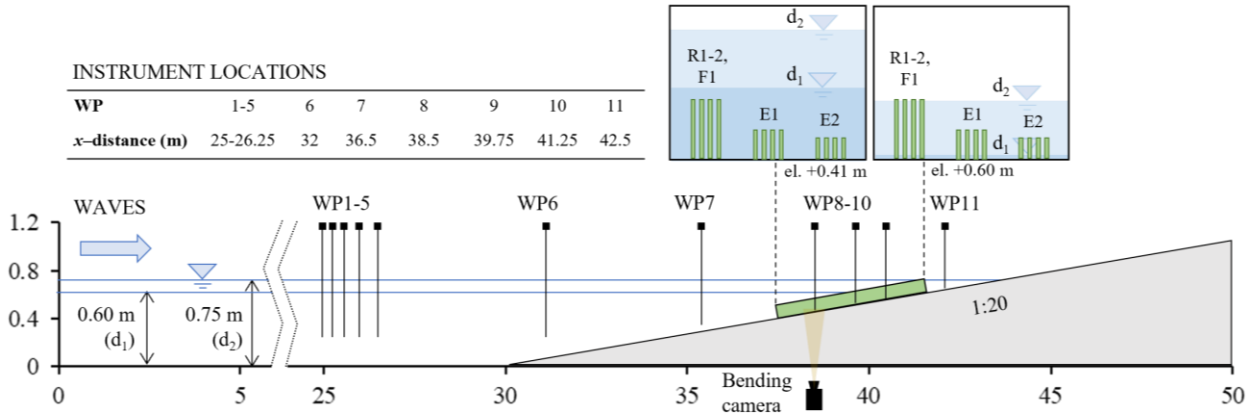


**Fig. 3-16.** Experimental setup in the wave flume (width 1.2 m) with interchangeable surrogate vegetation field at x-shore distance of 7.5 m from the slope toe (1:20), as well as instrument locations relative to the wave paddle (WP = wave probe), and schematic representation of stem submergence for all surrogate heights and water level scenarios.

#### 3.2.3.3 Instrumentation

Five fixed wave gauges were deployed between the wavemaker and the slope toe. These wave gauges formed a Goda-type array ($\Delta x_2$ = 0.18 m, $\Delta x_3$ = 0.40 m, $\Delta x_4$ = 0.66 m, $\Delta x_5$ = 1.25 m) for estimation of wave reflection and offshore wave conditions during testing (Lin & Huang, 2004). For the test series performed at a water depth of 0.60 m, four fixed wave gauges were deployed on the slope. For experiments conducted at a depth of 0.75 m, two additional wave gauges were deployed shoreward, for a total of six wave gauges on the slope. A stationary camera was also deployed outside of the flume to capture footage of flexible surrogate motion through glass windows in the side of the flume. Instrument locations are provided in **Fig. 3-16**.

### 3.2.4 Results

#### 3.2.4.1 Hydrodynamic Conditions

The five-gauge offshore array was used to obtain incident and reflected wave parameters for each wave test, according to Mansard & Funke (1980). For all tests, wave reflection coefficients $C_r$ were between 8.6% and 20.2%, generally increasing with wave height and wave period. Wave heights and wave periods were analyzed both in the spectral and time domain. Analysis in the

spectral domain consisted of application of the fast Fourier transform (FFT) technique, in order to obtain the zeroth-moment wave height $H_{m0}$ (**Eq. 3-15**), as well as the wave period corresponding to the frequency of the spectral peak, $T_p$.

$$H_{m0} = 4\sqrt{m_0} \approx 4\sqrt{\sum_{i=1}^{n} S(f)\Delta f} \quad \textbf{(3-15)}$$

In which $m_0$ is the zeroth moment of the wave spectrum, $S(f)$ is the spectral density contained within each discrete frequency bands (numbered from $i$ = 1 to $n$), and $\Delta f$ is the frequency bandwidth.

The zero-downcrossing method was used to obtain wave summary statistics in the time domain, where the significant wave height $H_s$ was calculated as the average height of the highest one-third of all waves ($H_s = H_{1/3}$). A summary of the generated irregular waves (from analysis of WPs 1-5) is provided in **Table 3-8**, along with estimates of the Iribarren number ($\xi$) and associated classification of wave breaker type. The values provided in **Table 3-8** represent an average of the generated wave conditions, as the wave program (consisting of the 17 test conditions in **Table 3-8**) was repeated for each test series. The Irribaren number was estimated using **Eq. 3-16** (Holthuijsen, 2007):

$$\xi = \frac{\tan\theta}{\sqrt{\frac{H_{m0}}{L_0}}}, L_0 = \frac{9.81T_p^2}{2\pi}\tanh\frac{2\pi d}{L_0} \quad \textbf{(3-16)}$$

In which $\tan\theta$ = beach slope (1/20) and $L_o$ = offshore wavelength (m). Offshore zeroth-moment wave heights $H_{m0,}$ corresponding peak wave periods $T_p$, and offshore water depths $d$ were used in the estimation of $L_o$.

**Table 3-8.** Summary of generated wave conditions, measured by offshore wave gauge array (average of WPs 1-5).

| Water Depth at Slope Toe, $d$ (m) | $H_{m0}$ (m)* | | | $H_{s,o}$ (m) | $T_p$ (s) | $C_r$ (%) | Number of Waves | $\xi$ (-) | Breaker type |
|---|---|---|---|---|---|---|---|---|---|
| 0.60 | 0.074 | +/- | 0.002 | 0.072 | 1.99 | 8.6 | 643 | 0.38 | Spilling |
| | 0.073 | +/- | 0.002 | 0.072 | 3.22 | 9.6 | 685 | 0.51 | Plunging |
| | 0.111 | +/- | 0.003 | 0.109 | 2.00 | 9.3 | 643 | 0.31 | Spilling |
| | 0.108 | +/- | 0.003 | 0.107 | 3.23 | 11.8 | 687 | 0.42 | Spilling |
| | 0.149 | +/- | 0.003 | 0.147 | 2.02 | 10.5 | 636 | 0.27 | Spilling |
| | 0.145 | +/- | 0.003 | 0.144 | 3.23 | 14.4 | 697 | 0.36 | Spilling |
| | 0.186 | +/- | 0.002 | 0.182 | 2.03 | 11.5 | 603 | 0.24 | Spilling |
| 0.75 | 0.074 | +/- | 0.001 | 0.072 | 1.99 | 9.1 | 631 | 0.40 | Spilling |
| | 0.073 | +/- | 0.001 | 0.071 | 3.21 | 11.7 | 669 | 0.53 | Plunging |
| | 0.112 | +/- | 0.001 | 0.108 | 2.00 | 9.5 | 631 | 0.33 | Spilling |
| | 0.109 | +/- | 0.002 | 0.107 | 3.21 | 12.8 | 670 | 0.44 | Spilling |
| | 0.149 | +/- | 0.001 | 0.146 | 2.01 | 10.1 | 625 | 0.28 | Spilling |
| | 0.144 | +/- | 0.003 | 0.143 | 3.22 | 14.2 | 667 | 0.38 | Spilling |
| | 0.187 | +/- | 0.001 | 0.184 | 2.02 | 11.4 | 608 | 0.25 | Spilling |
| | 0.181 | +/- | 0.004 | 0.178 | 3.23 | 15.9 | 653 | 0.34 | Spilling |
| | 0.225 | +/- | 0.002 | 0.224 | 2.03 | 12.6 | 588 | 0.23 | Spilling |
| | 0.224 | +/- | 0.003 | 0.222 | 2.77 | 20.2 | 775 | 0.28 | Spilling |

*Values provided following '+/-' indicate standard deviations in the generated wave conditions across all test series

### 3.2.4.2 Vegetation Effects on Wave Propagation

Significant wave heights, as measured by on-slope wave probes within or directly proximate to the vegetation field (WPs 7-10), were compared between test series to investigate vegetation

impacts on wave height evolution, as well as differences between test series with different surrogate elements/configurations. The beach slope was subjected to a wide range of hydrodynamic conditions under both bare and vegetated conditions. For tests with surrogate vegetation, meadow submergence was also varied as a result of wave testing at two water depths ($d_1$ = 0.60 m, $d_2$ = 0.75 m). Consequently, the testing program enabled isolation of the different processes contributing to wave transformation (e.g., shoaling, breaking, vegetation-induced attenuation). **Fig. 3-17** shows the results of normalized significant wave height evolution for all wave tests. All wave heights were normalized by offshore significant wave height ($H_{s,o}$) to account for slight variations in incident wave conditions between test series. The black dotted lines in **Fig. 3-17** demonstrate the effects of the bare (unvegetated) slope on cross-shore wave transformation (e.g., including wave shoaling and breaking processes) as no surrogate vegetation was present for these tests (TS-0). For the colored lines in **Fig. 3-17**, wave damping due to the presence of surrogate vegetation is evident from the reduced significant wave heights compared to the bare slope tests.

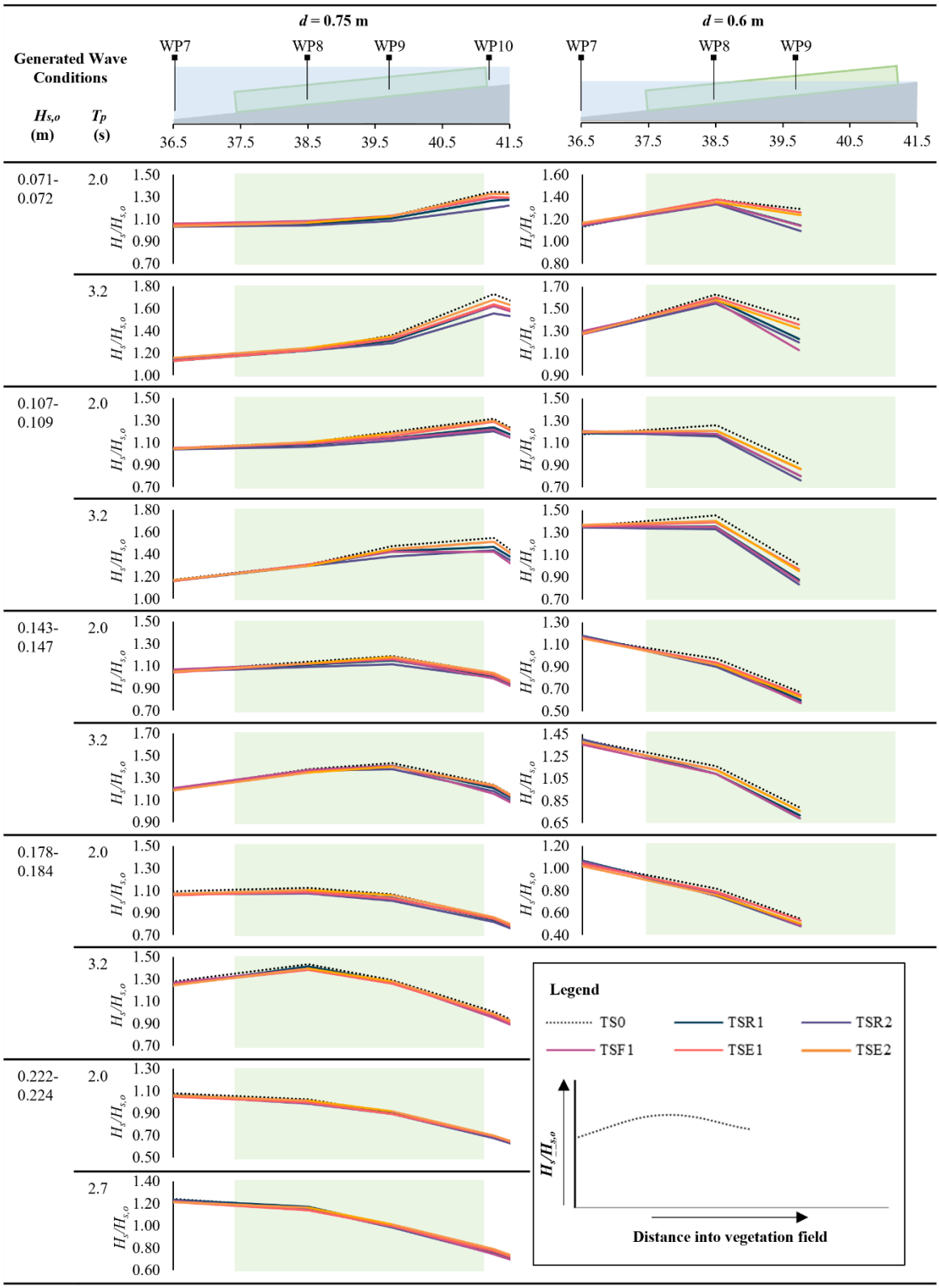


**Fig. 3-17.** Significant wave height evolution across the 1:20 beach slope for all TS under varying incident wave conditions. The base case (unvegetated, TS-0) is indicated by the black dotted line, and all TS with surrogate vegetation are in colour.

Wave breaking height, $H_b$, was estimated from the maximum significant wave height recorded on-slope by one of WPs 7-10. **Table 3-9** summarizes results of $H_b$ as well as wave breaking location, $x_b$ (in distance from slope toe and as wave probe location), for each test series and wave condition. For wave tests at $d$ = 0.75 m, $H_b$ (wave breaking associated with $H_s$) is recorded after or within the vegetation field for offshore wave heights between 0.07 m < $H_{s,o}$ < 0.19 m, and both tested wave periods. For wave tests at $d$ = 0.60 m, $H_b$ occurs primarily around WP8 within the vegetation field when offshore $H_{s,o}$ < 0.14 m, and before the vegetation field for all larger incident wave conditions. For most cases, results presented in **Fig. 3-17** and **Table 3-9** indicate that the presence of surrogate vegetation influenced the peak significant wave height recorded prior to breaking, but not the location. For some cases, the peak significant wave height appears to occur farther onshore, in alignment with the results presented in Mendez & Losada (2004). It is hypothesized with hindsight that delayed wave breaking may have been more clearly observed had more wave probes been positioned in the vicinity of the breaker zone.

The influence of vegetation on significant wave height evolution across the 1:20 slope differed for the various surrogate elements and configurations tested, as illustrated by **Fig. 3-17** and **Table 3-9**. Differences in the results for test series with different surrogate vegetation characteristics were more pronounced for smaller waves, where the effects of vegetation-induced wave damping were clearly evident. The surrogate meadow used in TS-R2 consistently yielded the greatest reduction in significant wave height compared to the unvegetated case (TS-0), followed by TS-R1 and TS-F1; the rigid surrogate array of TS-R1 and the flexible surrogate array of TS-F1 produced very similar results with respect to significant wave height reduction across the slope. The surrogate meadows of TS-E1 and TS-E2 produced significantly more minor reductions in significant wave height evolution than the other three test series with surrogate vegetation. The 2-cm change in surrogate element length between TS-E1 and TS-E2 did not equate to significantly different results in the surrogate meadows' impact on significant wave height evolution, with similar results for both test series. A comparison of the results between test series with surrogate vegetation is discussed in more detail in Section 5.0. Overall, vegetation-induced damping was barely observable in the results for tests with incident significant wave heights exceeding $H_{s,o}$ > 0.184 m.

**Table 3-9.** Summary of wave transformations across the 1:20 slope for all test series: TS-0 (base/no vegetation), TS-R1, TS-R2, TS-F1, TS-E1, and TS-E2. All $H_b/H_0$ values were calculated using values of $H_s = H_{1/3}$. Locations are measured relative to the slope toe (+30 m from wavemaker).

| Offshore Wave Conditions | | | | TEST SERIES | | | | | | | | | | | | | | | | | | | |
|---|---|---|---|---|---|---|---|---|---|---|---|---|---|---|---|---|---|---|---|---|---|---|---|
| | | | | 0 (base) | | | R1 | | | R2 | | | E1 | | | E2 | | | F1 | | |
| $d$ (m) | $H_{m0}$ (m) | $H_{s,o}$ (m) | $T_p$ (s) | $H_b/H_{s,o}$ | $x_b$ (m / WP) | | $H_b/H_{s,o}$ | $x_b$ (m / WP) | | $H_b/H_{s,o}$ | $x_b$ (m / WP) | | $H_b/H_{s,o}$ | $x_b$ (m / WP) | | $H_b/H_{s,o}$ | $x_b$ (m / WP) | | $H_b/H_{s,o}$ | $x_b$ (m / WP) | |
| 0.6 | 0.074 | 0.072 | 1.99 | 1.38 | 8.5 | WP8 | 1.35 | 8.5 | WP8 | 1.33 | 8.5 | WP8 | 1.38 | 8.5 | WP8 | 1.35 | 8.5 | WP8 | 1.34 | 8.5 | WP8 |
| 0.6 | 0.111 | 0.109 | 2.00 | 1.26 | 8.5 | WP8 | 1.19 | 6.5 | WP7 | 1.20 | 6.5 | WP7 | 1.21 | 8.5 | WP8 | 1.21 | 8.5 | WP8 | 1.21 | 6.5 | WP7 |
| 0.6 | 0.149 | 0.147 | 2.02 | 1.16 | 6.5 | WP7 | 1.18 | 6.5 | WP7 | 1.17 | 6.5 | WP7 | 1.16 | 6.5 | WP7 | 1.16 | 6.5 | WP7 | 1.17 | 6.5 | WP7 |
| 0.6 | 0.186 | 0.182 | 2.04 | 1.05 | 6.5 | WP7 | 1.07 | 6.5 | WP7 | 1.06 | 6.5 | WP7 | 1.05 | 2 | WP6 | 1.04 | 2 | WP6 | 1.05 | 6.5 | WP7 |
| 0.6 | 0.073 | 0.072 | 3.22 | 1.63 | 8.5 | WP8 | 1.58 | 8.5 | WP8 | 1.55 | 8.5 | WP8 | 1.60 | 8.5 | WP8 | 1.58 | 8.5 | WP8 | 1.56 | 8.5 | WP8 |
| 0.6 | 0.108 | 0.107 | 3.23 | 1.45 | 8.5 | WP8 | 1.35 | 8.5 | WP8 | 1.35 | 6.5 | WP7 | 1.39 | 8.5 | WP8 | 1.40 | 8.5 | WP8 | 1.36 | 6.5 | WP7 |
| 0.6 | 0.145 | 0.144 | 3.23 | 1.40 | 6.5 | WP7 | 1.40 | 6.5 | WP7 | 1.40 | 6.5 | WP7 | 1.37 | 6.5 | WP7 | 1.38 | 6.5 | WP7 | 1.36 | 6.5 | WP7 |
| 0.75 | 0.073 | 0.072 | 1.99 | 1.13 | 9.75 | WP10 | 1.10 | 9.75 | WP11 | 1.08 | 9.75 | WP11 | 1.13 | 9.75 | WP10 | 1.13 | 9.75 | WP10 | 1.13 | 9.75 | WP11 |
| 0.75 | 0.109 | 0.108 | 2.01 | 1.20 | 9.75 | WP10 | 1.14 | 9.75 | WP10 | 1.12 | 9.75 | WP10 | 1.16 | 9.75 | WP10 | 1.18 | 9.75 | WP10 | 1.14 | 9.75 | WP10 |
| 0.75 | 0.144 | 0.146 | 2.01 | 1.19 | 9.75 | WP9 | 1.15 | 9.75 | WP9 | 1.12 | 9.75 | WP9 | 1.17 | 9.75 | WP9 | 1.18 | 9.75 | WP9 | 1.16 | 9.75 | WP9 |
| 0.75 | 0.181 | 0.184 | 2.02 | 1.13 | 8.5 | WP8 | 1.09 | 8.5 | WP8 | 1.07 | 8.5 | WP8 | 1.09 | 8.5 | WP8 | 1.11 | 8.5 | WP8 | 1.08 | 8.5 | WP8 |
| 0.75 | 0.225 | 0.224 | 2.02 | 1.08 | 6.5 | WP7 | 1.06 | 6.5 | WP7 | 1.06 | 6.5 | WP7 | 1.05 | 6.5 | WP7 | 1.06 | 6.5 | WP7 | 1.06 | 6.5 | WP7 |
| 0.75 | 0.073 | 0.071 | 3.22 | 1.36 | 9.75 | WP10 | 1.31 | 9.75 | WP10 | 1.29 | 9.75 | WP10 | 1.33 | 9.75 | WP10 | 1.35 | 9.75 | WP10 | 1.33 | 9.75 | WP10 |
| 0.75 | 0.109 | 0.107 | 3.22 | 1.47 | 9.75 | WP10 | 1.43 | 9.75 | WP10 | 1.38 | 9.75 | WP10 | 1.44 | 9.75 | WP10 | 1.45 | 9.75 | WP10 | 1.42 | 9.75 | WP9 |
| 0.75 | 0.144 | 0.143 | 3.22 | 1.43 | 9.75 | WP9 | 1.41 | 9.75 | WP9 | 1.38 | 9.75 | WP9 | 1.40 | 9.75 | WP9 | 1.40 | 9.75 | WP9 | 1.41 | 9.75 | WP9 |
| 0.75 | 0.181 | 0.178 | 3.24 | 1.44 | 8.5 | WP8 | 1.41 | 8.5 | WP8 | 1.40 | 8.5 | WP8 | 1.38 | 8.5 | WP8 | 1.39 | 8.5 | WP8 | 1.40 | 8.5 | WP8 |
| 0.75 | 0.224 | 0.222 | 2.78 | 1.24 | 6.5 | WP7 | 1.23 | 6.5 | WP7 | 1.23 | 6.5 | WP7 | 1.22 | 6.5 | WP7 | 1.21 | 6.5 | WP7 | 1.22 | 6.5 | WP7 |

#### 3.2.4.3 Wave Attenuation by Surrogate Vegetation

Wave attenuation was quantified for every test series with surrogate vegetation, considering reduction of the breaking wave height (approximated as the maximum significant wave height $H_s$ measured across the slope, by WPs 6-11) in comparison to the bare (unvegetated) slope test results (TS-0). An attenuation coefficient ($\mu_{H_b}$) was calculated for each test using the following equation:

$$\mu_{H_b} = \frac{(H_b/H_{s,0})_{TS0} - (H_b/H_{s,0})_{TSveg}}{(H_b/H_{s,0})_{TS0}} \quad \textbf{(3-17)}$$

In which the *TS0* and *TSveg* subscripts denote test series incorporating the bare slope (TS-0) and surrogate vegetation fields (R1, R2, F1, E1 or E2), respectively.

Wave attenuation was also quantified for the wave probe located deepest within the vegetation field (i.e., the most shoreward position) to investigate the overall influence of the entire surrogate vegetation field on significant wave height evolution. For $d$ = 0.75 m, wave height attenuation was quantified at WP10, located at the shoreward end of the vegetation field (3.75 m total encountered marsh length). For $d$ = 0.60 m, wave height attenuation was quantified at WP9, located at a distance 9.75 m shoreward of the toe of the slope, within the surrogate vegetation

field (2.25 m total encountered marsh length). Note that wave breaking (characterized by the peak significant wave height) occurred at or before these wave probe locations for all wave conditions tested. Total wave attenuation, $\mu_{total}$, was quantified in the same manner as **Eq. 3-17**, replacing $H_b$ with $H_s$ as measured at WP9 ($d$ = 0.60 m) or WP10 ($d$ = 0.75 m). The results from wave attenuation analysis ($\mu_{H_b}$ and $\mu_{total}$) are presented in **Fig. 3-18**.

**A**

| Offshore Conditions | | | Surrogate Test Series $\mu_{H_b}$ | | | | |
|---|---|---|---|---|---|---|---|
| $d$ (m) | $H_{s,o}$ (m) | $T_p$ (s) | R1 | R2 | F1 | E1 | E2 |
| 0.6 | 0.072 | 1.99 | 0.021 | 0.031 | 0.025 | 0.000 | 0.017 |
| | 0.072 | 3.22 | 0.027 | 0.049 | 0.041 | 0.017 | 0.031 |
| | 0.109 | 2.00 | 0.057 | 0.047 | 0.041 | 0.041 | 0.038 |
| | 0.107 | 3.23 | 0.069 | 0.073 | 0.066 | 0.041 | 0.034 |
| | 0.147 | 2.02 | 0.000 | 0.000 | 0.000 | 0.003 | 0.002 |
| | 0.144 | 3.23 | 0.000 | 0.000 | 0.031 | 0.018 | 0.015 |
| | 0.182 | 2.03 | 0.000 | 0.000 | 0.001 | 0.000 | 0.012 |
| 0.75 | 0.072 | 1.99 | 0.020 | 0.039 | 0.000 | 0.000 | 0.000 |
| | 0.071 | 3.21 | 0.038 | 0.055 | 0.023 | 0.027 | 0.010 |
| | 0.108 | 2.01 | 0.047 | 0.066 | 0.052 | 0.031 | 0.013 |
| | 0.107 | 3.22 | 0.032 | 0.063 | 0.034 | 0.021 | 0.017 |
| | 0.146 | 2.02 | 0.033 | 0.061 | 0.027 | 0.015 | 0.006 |
| | 0.143 | 3.23 | 0.017 | 0.038 | 0.015 | 0.021 | 0.022 |
| | 0.184 | 2.02 | 0.032 | 0.048 | 0.042 | 0.032 | 0.018 |
| | 0.178 | 3.23 | 0.015 | 0.027 | 0.028 | 0.036 | 0.028 |
| | 0.224 | 2.03 | 0.013 | 0.018 | 0.019 | 0.029 | 0.018 |
| | 0.222 | 2.77 | 0.008 | 0.012 | 0.017 | 0.022 | 0.023 |

Wave breaking before vegetation

**B**

| Offshore Conditions | | | Surrogate Test Series $\mu_{total}$ | | | | |
|---|---|---|---|---|---|---|---|
| $d$ (m) | $H_{s,o}$ (m) | $T_p$ (s) | R1 | R2 | F1 | E1 | E2 |
| 0.6 | 0.072 | 1.99 | 0.113 | 0.153 | 0.117 | 0.024 | 0.043 |
| | 0.072 | 3.22 | 0.124 | 0.147 | 0.195 | 0.035 | 0.059 |
| | 0.109 | 2.00 | 0.117 | 0.157 | 0.115 | 0.049 | 0.044 |
| | 0.107 | 3.23 | 0.133 | 0.173 | 0.148 | 0.038 | 0.053 |
| | 0.147 | 2.02 | 0.102 | 0.123 | 0.144 | 0.035 | 0.062 |
| | 0.144 | 3.23 | 0.089 | 0.123 | 0.119 | 0.038 | 0.038 |
| | 0.182 | 2.03 | 0.094 | 0.121 | 0.114 | 0.029 | 0.075 |
| 0.75 | 0.072 | 1.99 | 0.060 | 0.108 | 0.040 | 0.033 | 0.012 |
| | 0.071 | 3.21 | 0.063 | 0.102 | 0.062 | 0.054 | 0.030 |
| | 0.108 | 2.01 | 0.059 | 0.086 | 0.072 | 0.020 | 0.016 |
| | 0.107 | 3.22 | 0.053 | 0.075 | 0.082 | 0.024 | 0.024 |
| | 0.146 | 2.02 | 0.022 | 0.036 | 0.047 | 0.015 | 0.000 |
| | 0.143 | 3.23 | 0.025 | 0.047 | 0.063 | 0.008 | 0.002 |
| | 0.184 | 2.02 | 0.020 | 0.041 | 0.000 | 0.011 | 0.000 |
| | 0.178 | 3.23 | 0.033 | 0.036 | 0.055 | 0.031 | 0.018 |
| | 0.224 | 2.03 | 0.016 | 0.021 | 0.000 | 0.000 | 0.000 |
| | 0.222 | 2.77 | 0.029 | 0.049 | 0.054 | 0.019 | 0.000 |

Wave height attenuation, $\mu$: 0.0 — 0.20

**Fig. 3-18.** Results from wave height attenuation analysis for all test series with surrogate vegetation, with darker red cells associated with higher estimates of wave attenuation. (A) Attenuation of breaking wave heights, $\mu_{H_b}$. Cells in gray represent cases in which wave breaking occurred without vegetation influence (i.e., prior to encountering the surrogate field). (B) Total wave attenuation, $\mu_{total}$, estimated from significant wave heights at WP9 (d = 0.6 m) and WP10 (d = 0.75 m).

#### 3.2.4.4 Flexible Surrogate Motion

Video data collected during TS-F1 was processed to quantify flexible surrogate motion. Prior to analysis, potential lens distortion was investigated using *estimateFisheyeParamaters* (MATLAB 2021). Lens distortion was negligible with average polynomial distortion coefficients of $a_2 = 2.8\text{x}10^{-3}$, $a_3 = -6.2\text{x}10^{-6}$, and $a_4 = 3.5\text{x}10^{-9}$, and thus no correction was applied. Video footage was resampled from 30 Hz to a frame rate between 4 and 6 Hz, selected to optimize computation time without compromising stem tracking accuracy (considering the magnitude and period of motion). Control points marked along the surrogate elements facilitated stem tip tracking, which was performed manually frame-by-frame in Matlab, for a single element per wave test. The stem base was selected in the first frame, and for every proceeding resampled frame the control point located at the stem tip was selected. Due to the computational requirements associated with manual stem tracking, a subset of 20 waves was analyzed for each TS-F1 wave test. For one of the videos, stem tracking was performed for an additional 20-wave segment; minimal differences were observed in the results of this duplicate analysis, indicating that 20 waves are a sufficiently representative subsample of the full 600+ wave series for each test condition.

As stems bend in response to oscillatory wave forcing, there is a periodic reduction in vegetation canopy height and thus a potential for reduced wave energy dissipation in comparison to a rigid, upright canopy. To investigate this, stem tip coordinates obtained from tracking were used to quantify the temporal reduction in canopy height over the 20-wave cycle. Upright canopy height ($h_v$) was first defined as the vertical distance from the stem tip under stillwater conditions ($y_o$) to the stem base ($y_b$). Stem tip coordinates were then used to calculate the canopy height evolution per frame as $y_n - y_b$, where $y_n$ represents the y-location of the stem tip for any frame within the 20-wave analysis period. A cumulative probability distribution was then constructed from the canopy height dataset to obtain the canopy height sustained for at least 50% ($h_{0.5}$), 70% ($h_{0.7}$) and 90% ($h_{0.9}$) of the 20-wave cycle. These values were calculated with respect to the initial, undisturbed canopy height:

$$c50 = \frac{h_{0.5}}{h_v}, c70 = \frac{h_{0.7}}{h_v}, c90 = \frac{h_{0.9}}{h_v} \quad \textbf{(3-18)}$$

In which $h_v = y_o - y_b$. Results from analysis of flexible surrogate motion and canopy height reduction are presented in **Fig. 3-19**.

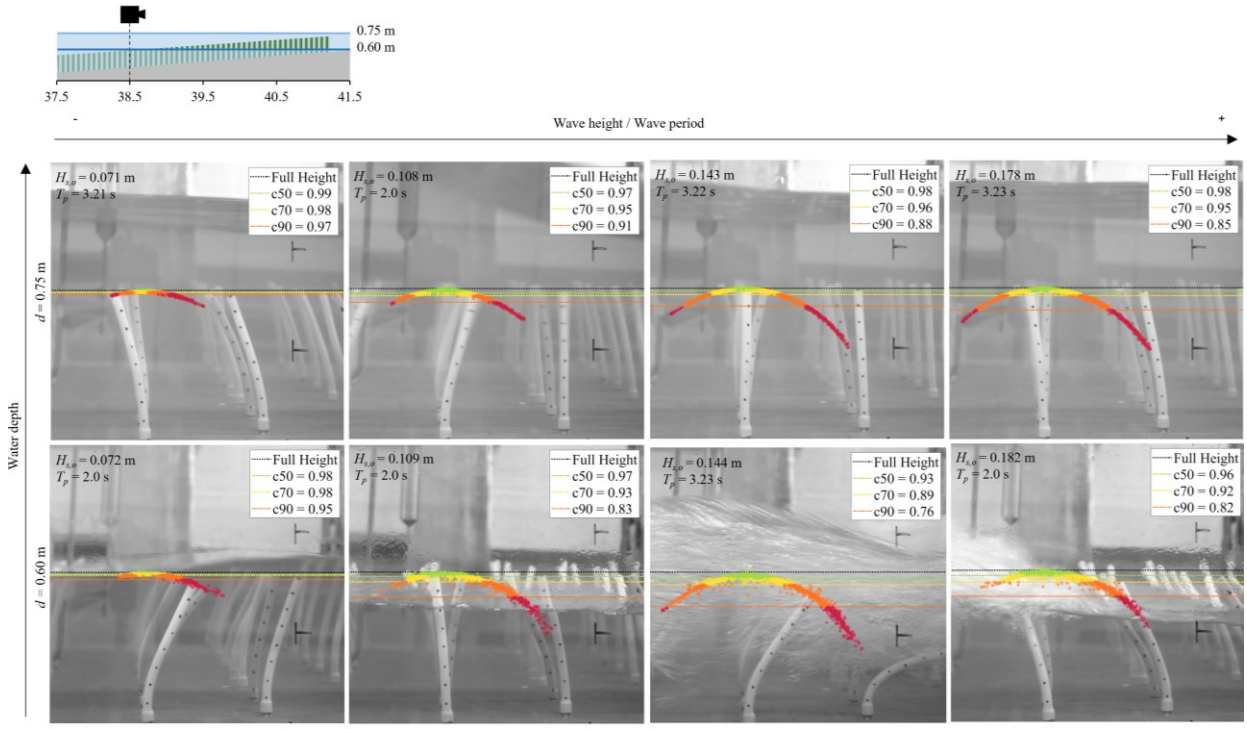


**Fig. 3-19.** Results from flexible surrogate tracking. Stem tip tracking points are colored based upon the cumulative probability distributions of canopy height, e.g., green points represent the zone within which the stem tip resides throughout 50% of the 20-wave analysis.

## 3.2.5 Discussion

### 3.2.5.1 Methods for Downscaling Live Vegetation

There have been few experimental studies of wave-vegetation interactions using surrogate plants at a reduced scale, and among such studies there is not a consistent method used for downscaling

vegetation meadows. In the present study, a solid volume fraction approach was applied to model a field of *S. alterniflora* at reduced scale (1:4) using various surrogate proxies. Two surrogate diameters were selected, resulting in two different stem densities to maintain the same solid volume fraction (TS-R1 and TS-R2). Through this selection, the validity of the applied downscaling method ($\alpha$, **Eq. 3-14**) may be investigated.

Results indicate that the downscaling of surrogate vegetation using the solid volume fraction approach is sensitive to the selection of element diameter. This can be seen through comparison of significant wave height evolution (**Fig. 3-17**) as well as the reduction of $H_b$ (**Fig. 3-18**) in TS-R2 compared to TS-R1. The more slender elements ($b_v$ = 4.5 mm), placed at higher stem densities (smaller spacing) in TS-R2 consistently yielded greater wave damping effects compared to the more sparsely distributed, thicker-stemmed ($b_v$ = 9.5 mm) surrogate elements of TS-R1, despite identical solid volume fractions. These findings are contrary to the expectations of the percent volume fraction downscaling approach, which relies upon the assumption that if the solid volume fraction of vegetation is maintained, so should the magnitude of vegetation-induced wave damping. To enhance understanding of the sensitivities of the solid volume fraction scaling approach, and improve upon methods for downscaling surrogate vegetation, potential causes for the discrepancy in results between TS-R1 and TS-R2 are discussed as follows.

### *Influence of Frontal Area*

One factor that may have contributed to the discrepancy in wave damping between TS-R1 and TS-R2 is the change in frontal area per unit volume. The wave-induced bulk drag force ($F_D$) per unit volume of marsh meadow can be estimated as:

$$F_D = \frac{1}{2}\rho C_D A_P U_c^2 \qquad \textbf{(3-19)}$$

In which $\rho$ is the fluid density, $C_D$ is the bulk drag coefficient and $A_p$ is the projected frontal area per submerged unit volume of the meadow ($A_p = b_v * N_v$) (Ozeren et al., 2014). Considering this equation, two main factors may contribute to a difference in the vegetation drag-induced wave damping between TS-R1 and TS-R2: changes to the bulk drag coefficient $C_D$, or to the projected meadow frontal area $A_p$. While the solid-volume fraction is maintained between the two tests series ($\alpha \propto b_v^2 N_v$, **Eq. 3-14**), frontal area per unit volume $A_p$ is effectively doubled for TS-R2 compared with TS-R1 ($A_p \propto b_v N_v, b_{v,R1} = 2b_{v,R2}, N_{v,R1} = \frac{1}{4}N_{v,R2}$). Considering this, and excluding potential changes in $C_D$ between test series, TS-R2 would be expected to yield twice as much wave damping due to vegetation drag compared to TS-R1. However, this direct linear relationship between wave attenuation and frontal area was not observed, with wave attenuation associated with TS-R2 between 0.8 and 2.2 times that of TS-R1. One potential cause for this is a difference in the degree of stem sheltering between the surrogate meadows of each test series. Stem sheltering effects increase as the ratio of wave excursion to stem spacing increases (Lei & Nepf, 2019). Consequently, it is expected that stem sheltering would be more significant for TS-

R2, as the stems are more closely spaced than TS-R1. However, no consistent trend between the relative wave damping of TS-R2 vs. TS-R1 and wave excursion was found. Thus, it is unclear to what degree stem sheltering plays a role in the present study, and ultimately to the strength of the relationship between meadow frontal area (per unit submerged volume) and wave damping, as opposed to meadow volume and wave damping. Large-scale studies that have suggested solid volume fraction (or, similarly, biomass) as the primary controller for wave damping are conducted with higher array densities than those considered herein, where stem sheltering and flow interactions would be much more likely (e.g., Maza et al., 2022). For low array densities, frontal area may be the more important parameter to consider. Overall, the comparative validity of downscaling by frontal area per unit meadow volume, versus by solid volume fraction, could be dependent on meadow properties such as stem density, and wave conditions, each of which have the potential to influence adjacent stem interactions such as sheltering. Ultimately, these relationships in downscaled models require further investigation.

### *Influence of Stem Spacing and Diameter*

Another factor that could have yielded enhanced wave damping in TS-R2 vs. TS-R1 despite equivalent solid volume fractions is the change in stem spacing. Paul et al. (2016) observed enhanced drag forces within a surrogate vegetation field when stems were more closely spaced laterally, suggesting edge turbulence interactions between adjacent stems as the cause. Supporting this, an experimental study of force loading on closely-spaced rigid cylinders found that a decrease in lateral spacing caused amplification effects on central cylinder loading under wave attack (Sparboom et al., 2006). Similar amplification effects were reported by Bonakdur et al. (2015), who also investigated force amplification on individual elements within cylinder arrays, including staggered arrangements. However, both Sparboom et al. (2006) and Bonakdur et al. (2015) investigated the influence of lateral spacing on central cylinder loading considering only changes in relative spacing $P^*$, the ratio of cylinder spacing to diameter ($P^*=\lambda/b_v$). Thus, it is difficult to extend their findings to the present study in which $P^*$ does not change between TS-R1 and TS-R2.

The decrease in diameter between TS-R1 and TS-R2 also has the potential to influence wake interactions within the surrogate array, due to related changes to the stem Reynolds number (**Eq. 3-8**). Overall, the stem Reynolds range for both test series are approximately $1600 < Re < 5600$ (TS-R1) and $800 < Re < 2800$ (TS-R2), with Re effectively doubled for TS-R1 versus TS-R2. In this range, fully turbulent wakes of a vortex street appearance ($300 < Re < 3x10^5$, Sumer & Fredsøe, 2006) are expected to develop around individual surrogate elements for both test series. However, this does not consider the potential for wake interactions between adjacent surrogate elements, which can dominate the flow pattern in multicylinder arrays (Schoneboom et al., 2011). Zhou et al. (2009) performed an experimental study to investigate the effects of Re on wake interactions between cylinders in various staggered arrangements, at a range of $P^*$. Zhou et al. (2009) categorized numerous tested flow scenarios and array configurations into four relationship types, for which different wake interactions between adjacent staggered elements

would be expected. This categorization was developed in primary consideration of $P^*$, and secondary consideration of the angle of flow relative to the center-to-center connection between adjacent staggered elements. Zhou et al. (2009) then presents the influence of Reynolds number on wake interactions for each relationship type. Considering the regimes presented by Zhou et al. (2009), the surrogate configurations for both TS-R1 and TS-R2 fall within a type 4 relationship, generally corresponding to larger $P^*$ values ($P^*$>2.2). The angle of flow relative to the staggered element axis is 30° in this study, which falls within the 4B relationship presented by Zhou et al. (2009). For type 4B scenarios, Zhou et al. (2009) demonstrate a sensitivity in flow structure with respect to Re, with more street interactions between adjacent staggered elements at low Re (Re = $O(10^3)$). As Re increases, vortex streets interact less intensively and flow structures beginning to resemble that of isolated cylinders (Re = $O(10^4)$) (Zhou et al., 2009). Considering this, more wake interactions could be expected for TS-R2 in comparison with TS-R1 under the same wave conditions. However, the value of $P^*$ considered in the present study (~15) is significantly greater than the range considered by Zhou et al. (2009) ($1.2 < P^* < 4.0$), so it is unclear if the potential differences in wake structure interactions between TS-R1 and TS-R2, as induced by differences in the Re regime, could be significant enough to contribute to the enhanced wave damping observed for TS-R2 in comparison to TS-R1.

#### 3.2.5.2 Flexibility Considerations with Downscaled Vegetation

*S. alterniflora* is a semi-flexible marsh species that is expected to experience deformation under the wave conditions tested herein (Markov et al., 2022). Two methods were used in this study to consider vegetation flexibility in the physical models: flexible surrogate elements (latex rubber tubing), and rigid elements with a reduced (effective) length, as defined by Luhar & Nepf (2016). Flexible surrogate elements (TS-F1) were selected to match the degree of bending experienced by live *S. alterniflora* under the same hydrodynamic conditions (downscaled, 1:4), and the two effective lengths selected (TS-E1, TS-E2) were based upon live *S. alterniflora* biomechanical properties as well as to cover the range of hydrodynamic conditions tested.

TS-F1 and TS-R1 shared the same geometric properties (including lengths) and surrogate configurations. Thus, comparison of results between the two can provide insight to the use of flexible versus rigid surrogate elements in downscaled models of *S. alterniflora* fields. For incident wave tests where the offshore wave heights exceeded $H_{s,o} > 0.15$ m, surrogate vegetation (all test series) had very little influence on significant wave height evolution due to the dominance of wave shoaling and/or breaking (see **Fig. 3-17**). In the cases where vegetation effects on wave attenuation were more prominent, results indicate that TS-R1 and TS-F1 produced similar wave damping effects (as quantified by cross-shore decreases in significant wave heights), despite the occurrence of measurable stem bending for the flexible elements. As demonstrated in **Fig. 3-19**, stem bending does not result in a significant reduction in overall canopy height for the majority of the wave test duration. For example, over 70% of the test duration, canopy height was reduced only by 2% for $H_{s,o} = 0.071$ and $T_p = 3.21$ s, up to 4% for $H_{s,o} = 0.143$ m and $T_p = 3.22$ s ($d = 0.75$ m tests, **Fig. 3-19**). Canopy height reductions were

observed to be more significant for the tests conducted at $d$ = 0.60 m, however this is likely due to waves breaking very close to the tracked surrogate element, which caused occasional extreme deformation.

Augustin et al. (2009) similarly compared the wave damping effects of *S. alterniflora* as modelled by rigid versus flexible elements and found that the two models produced similar effects. Augustin et al. (2009) considered wave heights of $H_s$ = 0.085 m and wave periods between $T_p$ = 1.5-2.0 s, more mild than the range of hydrodynamic conditions considered in the present study. The similarity in wave attenuation performance of the flexible versus rigid elements in Augustin et al. (2009) could therefore be a result of minimal wave-induced flexible element bending. No comment on observations of element motion were provided in their study, however, for live *S. alterniflora* plants Markov et al. (2022) shows minimal stem bending in the range of hydrodynamic conditions tested by Augustin et al. (2009). In general, stem bending is expected to increase with increasing wave height and wave period, with several studies indicating a strong correlation between plant motion and wave orbital excursion (Luhar & Nepf, 2016; Rupprecht et al., 2017; Markov et al., 2022). As stem bending increases, a divergence in the attenuation provided by flexible versus rigid surrogate elements is expected. In the present study, larger wave heights than those considered in Augustin et al. (2009) are used, with evidence of stem bending. However, due to the relatively low orbital excursion associated with the wave conditions tested herein (small wave periods), and short element length, stem bending did not result in a significant reduction in canopy height. Furthermore, at the beach slope considered (1:20), wave shoaling and breaking dominated significant wave height evolution for many of the test conditions, making it difficult to discern the importance of using flexible versus rigid elements under conditions of more extreme stem bending.

Overall, the comparison of the results between TS-R1 and TS-F1 indicate that, for the present hydrodynamic conditions, scale (1:4) and beach slope (1:20) considered, rigid elements may be sufficient to capture the effects of a downscaled *S. alterniflora* meadow. However, more testing is needed to investigate if this holds for 1) different scales, and 2) different beach slopes where shoaling and breaking effects may be less dominant, and flexible element bending has more importance.

The test series that was designed based on the effective length theory proposed by Luhar & Nepf (2016) to consider vegetation flexibility by using shorter, rigid element arrays, resulted in wave damping effects that were less significant than expected, based on corresponding flexible elements. This is evident from a comparison of the results from TS-F1 with TS-E1 and TS-E2, in **Fig. 3-17** or **Fig. 3-18**. Otherwise, the results from TS-E1 and TS-E2 are as expected, with a reduction in rigid surrogate element length yielding a reduction in wave energy dissipation due to the artificial meadow. The effective length approach may be more appropriate for simulating wave damping by flexible vegetation using rigid surrogates under conditions where more extreme stem bending occurs, possibly including stem breakage. Breakage would be likely for the higher energy wave conditions tested herein but could not be captured by the flexible

surrogate elements, as the flexural strength of latex rubber tubing exceeds that of live *S. alterniflora* stems. However, in the context of the present study, breakage conditions would likely occur for the same wave tests where wave shoaling and breaking dominate wave height evolution, and minimal impact of surrogate vegetation for any test series was observed.

#### 3.2.5.3 Experimental Limitations

To maintain stem Reynolds conditions reasonably similar to prototype-scale, flexible surrogate diameters were increased relative to live *S. alterniflora* stems. To achieve bending similitude, a surrogate element with much higher flexibility (lower stiffness) in comparison to live *S. alterniflora* was required. This was difficult to achieve while also limiting buoyancy effects, as only self-supporting materials were considered. Ultimately, the selected surrogate material - latex rubber tubing - was still not flexible enough to match the live *S. alterniflora* bending observed in Markov et al. (2022), and thus live plants may experience more deformation under the tested hydrodynamic conditions (at prototype-scale) than reported for TS-F1. Furthermore, it is expected that for the more extreme wave heights considered, live plants would experience damage, ultimately altering the wave damping potential of the marsh. No critical thresholds for irreversible deformation (folding or stem breakage) of *S. alterniflora* stems have been reported in the literature, to the authors' knowledge, however Vuik et al. (2018) reported $u_{crit}$ = 0.58 +/ 0.13 m/s as the critical velocity for stem damage for a similar *Spartina* species, *Spartina anglica*. This threshold was exceeded by the current experimental program, and thus damage would be expected for live *S. alterniflora*, which could not be captured via the present surrogate vegetation due to differences in flexural strength. An additional limitation of the present study is that all test series were not conducted simultaneously, introducing some inconsistencies in the wave program between test series. Such variability is quantified in **Table 3-8**, with standard deviations in generated wave heights around 0.5% to 2.8% between test series. This minimal variability is not expected to have significant effects on the findings presented herein but is noted for any uncertainty it may have contributed to the experimental results. Overall, comparison of results between the different test series with surrogate vegetation was limited due to the minimal overall influence of surrogate vegetation on wave height evolution. This is partially due to the dominance of wave shoaling and breaking for the wave conditions and beach slope considered. It could also be a result of the vegetation meadow properties, particularly the stem density or the cross-shore length of the vegetation field. The results indicate that an extension of the vegetation field would not yield significantly more vegetation-induced wave damping due to significant meadow submergence. However, an increase in stem density could yield greater vegetation-induced wave damping, potentially providing more insight to the differences in wave attenuation provided by the different methods of surrogate downscaling. Finally, this study would benefit from direct comparison to a similar experimental program conducted at prototype-scale with live *S. alterniflora,* to gain further insight on scale effects. Conclusions drawn from the present study can only compare between downscaling methods to infer how they perform relative to each other, but the accuracy with which each captures the target full-scale live vegetation meadow is still uncertain. This is a critical next step to the present research, currently underway.

#### 3.2.5.4 Recommendations for Physical Modelling with Downscaled Vegetation

Based upon the results of the experimental program presented herein, the following recommendations for physical modelling with downscaled vegetation are made, along with identification of areas for future study that could supplement the continued development of such physical modelling methods. These recommendations are made in consideration of the experimental objectives and findings of the present study, which were predominantly focused on investigations of wave attenuation.

a. It may not be possible to accurately scale both plant flexural rigidity and motion response simultaneously. The reduction in flexural rigidity required for surrogate elements to achieve an equivalent bending response at small scales, relative to live vegetation at full-scale, yields practical implications in that the surrogates are no longer self-supporting. Consequently, it is recommended that accurate scaling of flexural rigidity versus bending response be prioritized in consideration of the experimental objectives. In this study, self-supporting elements were prioritized over bending accuracy to reduce buoyancy effects, sacrificing some accuracy in the motion response.

b. Downscaling salt marsh meadows using a solid volume fraction approach is sensitive to the selection of stem diameter, with two meadows of equivalent $\alpha$ and $P^*$ exhibiting different wave attenuation capacities. Careful selection of the surrogate stem diameter should be made to ensure a balance of both reasonable stem spacing, and appropriate stem Reynolds conditions. Downscaling by frontal area per unit volume may be more suitable for certain hydrodynamic conditions (e.g., short orbital excursion) and low stem array densities, where stem sheltering effects are minimized, although this requires further study.

c. Selection of appropriate surrogate elements to represent target marsh plants at reduced scales can introduce significant complexities to physical models of wave-vegetation interactions, particularly when vegetation flexibility is considered. This study has demonstrated that an array of rigid cylinders can provide suitable surrogates for *S. alterniflora* meadows in downscaled physical models intended to investigate wave attenuation by vegetation, thus reducing such complexity. Moderate- to high-energy wave conditions (in the context of natural marsh environments) were considered in this study, where stem bending was observed for flexible elements, but had minimal overall impact on wave damping effects in comparison to their rigid counterparts. It is recommended that these findings be tested for extension to other species, hydrodynamic conditions, beach slopes and scale factors.

d. Rigid surrogate elements with effective lengths as defined in Luhar & Nepf (2016) did not provide suitable proxies for flexible vegetation canopies in this study. However, it is recommended that this method be tested further in physical modelling applications, particularly for flat, or gently sloping beaches to minimize contamination of the data by

wave shoaling and breaking effects that obscure contributions of vegetation to wave attenuation, or for cases where extreme stem bending is expected for the target live vegetation (e.g., highly flexible plant species, or large wave excursions).

### 3.2.6 Conclusions

Several methods were applied for modelling wave damping of a *S. alterniflora* meadow at reduced scale (1:4) on a 1:20 beach slope and using surrogate vegetation. Hydrodynamic conditions were selected to cover moderate to high energy wave scenarios (0.075 m < $H_{m0}$ < 0.23 m, $T_p$ = 2 and 3.25 s) expected as low-frequency, high-energy events for natural salt marsh environments, or realistic design scenarios for engineered coastal structures with marsh vegetation. Surrogate elements were selected to consider vegetation flexibility directly (flexible elements: latex rubber tubing), indirectly (effective length, after Luhar & Nepf, 2016) or not at all (rigid elements). A percent volume fraction approach was applied to downscale surrogate elements based upon live *S. alterniflora* plant properties available in literature. Comparison of wave height transformations for test series with surrogate vegetation against results from unvegetated slope tests yielded practical insight for downscaling methodologies, and surrogate element selection for modelling semi-flexible *S. alterniflora* under a relatively high-energy wave regime. The current results would benefit from comparisons with a prototype-scale meadow of live *S. alterniflora* implemented in a similar experimental program, which is a planned next step. The modelling of vegetation at reduced scale has not been well addressed in literature to date, and further study is needed to increase the interpretability of small-scale models of wave-vegetation interaction for the informed design of NBS for coastal protection (including hybrid solutions incorporating natural features in combination with structures). This novel study takes direct action towards addressing this research need, presenting critical knowledge to support the development of small-scale physical modelling methods for investigating wave interactions with salt marsh meadows.

# 4. Discussion

## 4.1 Limitations

This thesis presents the findings from a scale series approach to investigating wave-vegetation interactions, considering various salt marsh species native to the Canadian coastline. Both experimental programs considered the implementation of marsh plants on a gentle slope (1V:18-20H), and at low stem densities (~51 stems/$m^2$). This set-up was selected to be representative of an engineered living dyke structure rather than conditions expected for a natural marsh, which often have near flat slopes and higher stem densities than those tested herein. Furthermore, there may be deviations in live plant properties from field conditions to those reported for the laboratory-tested plants, due to the use of freshwater during testing and the lack of exposure to hydrodynamic forcing during plant establishment in the outdoor flume. Thus, it would be expected that wild plant specimens of *S. patens* and *S. alterniflora* may have different physical and biomechanical characteristics than those used for large-scale wave testing. However, no formal field surveys were conducted as a part of this thesis to consider such deviations. In general, the use of live vegetation poses challenges associated with repeatability, due to several compounding factors that may influence plant growth prior to and during experimental testing. This includes, but is not limited to, plant sourcing methods (wild or greenhouse grown), time of testing (phase of growth period) and climatic conditions (precipitation and ambient temperatures). Although these case-specific factors may pose a limitation on the quantitative reports from the large-scale study presented herein, these factors are not expected to impact the key findings of the study, such as the prominent morphological, physical, and biomechanical differences between the two target species and the resultant species-specific wave deformation responses. Furthermore, the plant parameters utilized from large-scale testing for development of the small-scale *S. alterniflora* meadow were found to be within the range of published values (Feagin et al., 2011; Chatagnier et al., 2012; Ysebaert et al., 2011; Knutson et al., 1982). Additional experimental limitations specific to each individual study were identified in Section 1.3 and Section 3.0.

## 4.2 Application

The scale series approach to modelling the living dyke structure considered herein yields practical insight for the development of experimental methods with marsh vegetation. The use of live vegetation in physical modelling of NBS is critical for the accurate capture of wave-vegetation interactions, however, it can also be costly, time intensive, and challenging, and there are few experimental facilities that can support such programs. It is not realistic to use exclusively live plant studies to develop engineering design guidance, which should consider parametric studies of structure performance with several design configurations under numerous testing scenarios. Thus, there is a necessity for surrogate vegetation studies to address such knowledge gaps. Both physical modelling approaches have a role to play in the advancement of

NBS design, and the development of robust modelling methods for both is essential. Based on experiences from the experimental programs presented herein, guidance for experimental modelling of marsh-based coastal protection structures is provided below.

## 4.2.1 Guidance on physical modelling of coastal marsh-based NBS

### 4.2.1.1 Prototype-Scale Experiments with Live Vegetation

The following should be considered when planning and implementing an experimental program with live vegetation:

- **Plant sourcing.** A choice should be made between wild (collected directly from the field) or greenhouse grown plants. The former may be restricted by environmental regulations depending on the source location. The latter may impact the plant physical and biomechanical properties relative to specimens of the same plant species found in nature.
- **Native plant zonation.** This factor will impact the experimental set-up (i.e., at which elevation the plants should be situated within the flume), as well as the watering regime. For example, *S. alterniflora* is a low-marsh species that requires frequent inundation, and thus it should be planted in low elevation zones and will need to be watered more frequently than species naturally situated in the high-marsh zone.
- **Duration of meadow establishment following transplantation.** This can depend on several factors, including time of year, plant size and health at the time of transplantation, and experimental objectives. For example, if erosion protection is to be investigated, plants may need more time to develop root systems representative of field conditions. Three weeks was found to be sufficient for plant establishment, to meet the experimental objectives of the present study.
- **Time of year.** Seasonal variations in precipitation, temperature, and hours of sunlight may impact planting success, as well as influence the plant husbandry methods following transplantation (e.g., watering regime). The plant husbandry methods presented herein were developed considering the summer climate of Quebec, Canada, with the live vegetation experimental program conducted between June-August 2021.
- **Planting method.** Several factors need to be considered including planting depth, proximity of adjacent plants, and planting pattern (staggered or uniform grid). For the present study, a staggered grid was used with 15-cm stem spacing, and the planting depth was ~10 cm. Other practical considerations include methods for digging and planting individual plants, particularly considering the size and density of the marsh. The total quantity of plants that need to be installed may require specialized equipment or additional personnel in order to improve planting efficiency. Ideally, this process should be completed in few days to prevent plant mortality.
- **Growing medium.** Plants may be planted directly into the slope, depending on the substrate. If the slope substrate cannot provide optimal conditions for plant growth, potting soil should be used. In the present study, the slope was comprised primarily of sand ($D_{50}$ = 285.9 $\mu$m) which could directly support plant growth; however, potting soil

was used to ensure planting success and accelerate establishment. Upon harvesting, *S. patens* roots were observed to remain within the potting soil mass and not extend into surrounding sand, indicating that potting soil has the potential to restrict root growth.

- **Growth supplements.** Fertilizer was used in the present study to expedite plant growth and establishment. As a result, water quality was significantly impacted, likely exacerbated by the summer climate, leading to a reduction in underwater visibility. This caused significant challenges for the present study, as a primary experimental objective was to observe plant motion using submerged cameras. No specimens were planted without fertilizer, and thus planting success in the absence of such treatments is unknown. If fertilizer is used in future studies, it is recommended to minimize the quantity applied, and consider if underwater visibility is essential for the study objectives.
- **Wave program.** The order of the wave program was found to be critical for avoiding premature plant damage. Plants were observed to experience the most significant deformation/damage when situated near the wave breaking zone, and particularly at shallow water depths. Thus, it is recommended that tests be run in the order of highest to lowest water depths, and in order of increasing wave orbital excursion.

Results from experimentation with live vegetation are highly dependent on plant properties, which may be variable between individual plants. Thus, it is essential that vegetation properties be well documented, considering several plants of each species. Collection of the following plant data is recommended; however, this may change if experimental objectives differ significantly than those of the present thesis:

- **Before wave testing.** The following stem properties should be recorded: length, diameter/tapering (diameter at increments along the stem), bending modulus (for multiple locations if significant stem tapering). The same properties should be measured for the leaves if present, as plant macrofeatures have been found to contribute significantly to vegetation drag forces (e.g., *S. alterniflora,* Zhang & Nepf, 2022). Plant frontal area may also be estimated using the image analysis methods of Neumeier et al. (2005).
- **After wave testing**. The same properties should be collected as above, as well as in-situ observations of root structure, and measurements of root growth following harvesting. If plant growth between the time of transplant and harvest is not of interest, plant parameters may be recorded only before or after wave testing.
- **Plant damage.** Plants should be regularly checked for stem damage between wave tests. Stem damage may be in the form of uprooting, stem breakage (full separation), or irreversible deformation (folding). Such observations can inform species-specific thresholds for damage, which is critical for the identification of limits on wave attenuation by salt marsh plants under extreme wave forcing.

#### 4.2.1.2 Small-Scale Modelling with Surrogate Elements

The following should be considered when developing and implementing an experimental program with surrogate vegetation, and at reduced-scale:

- **Target species.** If the model aims to target a specific plant, characteristics such as plant morphology, stem bending modulus, stem diameter and length should be researched to inform surrogate development.
- **Surrogate elements.** Complexity of the surrogate elements should be selected in consideration of the experimental objectives and scale of testing. This can include flexibility considerations (rigid vs. flexible element materials), inclusion/exclusion of plant macrofeatures (leaves), and meadow heterogeneity (identical elements or varying elements). There are several methods that may be used to consider flexibility. A simplified approach is the use of an effective rigid length (see Luhar & Nepf, 2016) to represent flexible stems, taking into account the biomechanical properties of the target plants and the range of test conditions. This method was not supported by the results of the present study, however, would benefit from additional testing. Alternatively, flexible elements may be selected considering the scaling of $E$ (e.g., Koftis et al.., 2013) or bending similitude (as in the present study), if live vegetation bending datasets are available.
- **Target marsh parameters.** Meadow length (cross-shore direction) and stem density should be selected to be representative of either field or design conditions. Stem densities in natural marsh settings are variable between species, with the lowest stem densities for *S. alterniflora* reported around 100 stems/m$^2$ (Augustin et al., 2009), and several more densely packed species reported at >1000 stems/m$^2$ (e.g., *Scirpus mariqueter,* Ysebaert et al., 2011; *Schoenoplectus pungens,* Wu & Cox, 2016; *Elymus athericus*, Rupprecht et al, 2017).
- **Target hydrodynamic conditions & facility capabilities.** Once the target hydrodynamic conditions are identified, an appropriate scale can be selected based upon the wave generation capabilities of the facility. For the present study, a 1:4 scale was considered to test prototype-scale wave heights up to $H_{m0}$ = 0.23 m (at $T_p$ = 2.77 s).
- **Downscaling method.** The selected method will determine surrogate element dimensions and stem density. Surrogate diameter should not alter stem Reynolds conditions too far from prototype-scale conditions. Potential methods for downscaling include by solid volume fraction, standing biomass, or frontal area, which can all avoid significant stem diameter reductions. However, the comparative validity of each downscaling method has not yet been well researched. The results of the present study indicate that downscaling by solid volume fraction is highly sensitive to the selection of stem diameter. The expected relationship between wave damping and vegetation volume (or standing biomass) may also have been impacted due to the amplification of stem sheltering effects at significantly reduced stem densities relative to natural marsh conditions. This supports that reasonable stem densities should also be maintained.
- **Surrogate element construction.** In the present study, surrogate elements were installed in a perforated panel (drilled plywood sheets). This seems to be the most common method for constructing surrogate meadows (Ozeren et al., 2014; Manca et al., 2012; Baker et al., 2022).
- **Scale effects.** Sensitivities to downscaling should be incorporated into the experimental design, to attempt to quantify scale effects. In this study, variations in stem diameter,

length and flexibility were considered. Another way to quantify scale effects would be to have some comparison tests with live vegetation in a similar configuration at full-scale, however this is time and resource intensive.

#### 4.2.1.3 Comparison of Modelling Methods

Live vegetation and surrogate studies are both essential for supporting the development of design guideline for nature-based coastal protection strategies. Considering the findings of the present study, the advantages and limitations associated with both methods are identified in **Table 4-1**.

**Table 4-1.** Comparison of experimental methods for evaluating coastal marsh-based NBS.

| | **Large-scale, Live vegetation** | **Small-scale, Surrogate vegetation** |
|---|---|---|
| **Advantages** | • Accurate capture of vegetation properties, flexibility, and motion – avoids inaccuracies associated with the use of plant surrogates.<br>• Avoids significant scale effects.<br>• Allows testing of large waves, and long wave orbital excursions - expected to be the most critical limitations on wave attenuation by flexible vegetation.<br>• Critical thresholds for stem damage can be directly observed and quantified.<br>• Erosion protection by marsh vegetation can be quantified considering both aboveground (reduced bed shear stresses within vegetation canopies) and belowground (root stabilization) plant contributions. | • Accessible, does not require a facility that can support full-scale wave testing, or unique conditions for maintaining live vegetation.<br>• Repeatable, not dependent on varying plant properties.<br>• No time constraints introduced by live plant care, or in avoidance of plant mortality.<br>• No restrictions on wave conditions (order of wave protocol, or magnitude of waves) as stem damage does not have to be considered.<br>• Easily reconfigurable, can test many design scenarios in a short period of time.<br>• Less costly due to smaller facility requirements, as well as lower material costs. |
| **Limitations** | • Sourcing of plants may be challenging and costly. Environmental regulations may restrict direct sourcing from the field, and there are limited suppliers for greenhouse-grown salt marsh plants.<br>• Plant health and mortality can critically impact success of the experimental program. Plant husbandry methods must be well developed, and stem damage must be considered when designing the wave protocol.<br>• Repeatability of wave testing with live vegetation is limited due to dependencies on plant properties, which can vary significantly between experimental programs.<br>• Time limitations – significant time requirements for the planning and implementation of live vegetation, as well as constraints on the testing duration. In a Canadian context, experiments with live vegetation may only be tested during certain seasons.<br>• Live vegetation studies necessitate testing at 1:1 scale, which either limits the wave heights/periods that can be tested or requires a very large testing facility.<br>• Reconfiguration of the vegetation meadow is very challenging with live vegetation, and often only one design scenario can be tested per program. Parametric studies of NBS performance are not well-suited for live vegetation testing.<br>• Actions that support plant growth in the laboratory may conflict with experimental objectives – for example, the use of fertilizer can compromise water quality and underwater visibility, and potting soil may restrict root growth. Trade-offs between planting success and experimental objectives may have to be considered. | • Difficult to capture heterogeneity in plant properties, which would occur within a natural marsh meadow, using plant surrogates.<br>• Restrictions on the coastal protection services that can be investigated - erosion protection provided by belowground plant structures cannot be captured.<br>• Stem breakage is not considered, and thus testing under high energy wave scenarios may overestimate coastal protection services associated with marsh vegetation.<br>• There is error associated with the use of plant surrogates, which often exhibit simplified morphology and flexibility in comparison to live vegetation.<br>• Scale effects are still largely unknown, and robust downscaling methods are still under development. Thus, small-scale studies may not accurately capture the coastal protection services of live marsh vegetation.<br>• Significant reduction in stem density, as a result of meadow downscaling, might amplify stem sheltering effects that are not present in full-density marshes. This might alter wave damping relationships with scaling parameters such as frontal area, solid volume fraction, or standing biomass, and invalidate the applied downscaling method. |

Experimental programs should be developed considering these advantages and limitations, selecting an appropriate modelling method for the project objectives. Studies with live salt marsh vegetation can accurately capture individual plant and meadow properties, minimizing scale effects. However, the use of live vegetation is often costly and time intensive and may not be feasible in most experimental facilities. Consequently, wave testing with live vegetation may be best for fundamental studies, to establish baseline knowledge of plant physical and biomechanical properties, plant morphology, deformation response to wave forcing, and thresholds for plant damage. Results from live plant studies can then be used to inform surrogate studies (performed at either full- or small-scale), or numerical models. Small-scale surrogate studies can better facilitate parametric studies of coastal marsh performance, due to improved experimental repeatability, and the ease at which many design scenarios may be tested. However, the use of surrogate vegetation, particularly in small-scale experimental program, has several limitations. Methods for downscaling marsh meadows are still in development, and scale effects are largely unknown. Furthermore, surrogate vegetation is often oversimplified in comparison to its live counter part, and thus may not realistically capture vegetated structure performance. This is particularly significant for hydrodynamic settings where extreme stem deformation or damage would be expected for live plants. Consequently, live vegetation studies are still essential for validating small-scale, surrogate studies and for testing coastal protection services that cannot be replicated with plant mimics (e.g., erosion protection).

# 5. Conclusions and Recommendations for Future Work

## 5.1 Conclusions

This thesis presents findings from two experimental programs that investigate the wave attenuation capacity of salt marsh plants native to the Canadian coastline. The two species investigated were *S. alterniflora* and *S. patens*. Both species were considered in full-scale wave tests with live plant specimens, and *S. alterniflora* was additionally investigated in a small-scale flume study, where a meadow of plant surrogates was developed based upon live plant observations from the former study. The two programs support the development of experimental methods concerning coastal marsh-based NBS and ultimately provide practical insight for the incorporation of *S. patens* and *S. alterniflora* into coastal protection strategies in Canada. Considering the distinct objectives associated with each experimental program, key conclusions from each study are provided separately below.

**Large-scale:**

- Three weeks was found to be a sufficient period for transplanted marsh vegetation to establish in the outdoor wave flume before testing. New growth was observed as quickly as 19 days, and significant root development was observed at the end of the six weeks that the plants spent in the flume. Minimal plant loss occurred during the growth and testing period, supporting the use of the plant husbandry methods reported herein for future studies with live vegetation.
- Differences in species morphology and plant biomechanical parameters between *S. patens* and *S. alterniflora* yielded distinctly different bending under irregular wave forcing. *S. patens* plants (thinner, flexible stems) consistently exhibited greater stem bending than *S. alterniflora* (thicker, rigid stems) under comparable incident wave conditions.
- Stem bending was sensitive to wave height and wave period, with the most significant stem deformation occurring at longer wave periods for both *S. patens* and *S. alterniflora*. Consequently, wave orbital excursion appears to be the most important parameter for stem deformation, and a reduction in wave attenuation associated with stem motion and/or bending damage can be expected for wave climates with long orbital excursions.
- No wave-induced damage to *S. alterniflora* or *S. patens* was observed. This indicates that the species are resilient under hydrodynamic forces up to, at minimum, $U_c =$ 0.37 m/s for *S. patens* and $U_c =$ 0.28 m/s for *S. alterniflora*.
- Results support the combined use of *S. alterniflora* and *S. patens* in nature-based coastal protection strategies. *S. alterniflora* appears to adopt a “resistance” strategy when faced with hydrodynamic stress, versus the “avoidance” strategy of *S. patens.* Thus, when

paired together, coastal infrastructure can derive benefits from the combined attenuative capacity of *S. alterniflora* and the resilience of *S. patens*.

**Small-scale:**

- Downscaled meadows of *S. alterniflora* surrogates yielded inconsistent wave attenuation results when stem diameter was varied but the vegetation solid volume fraction was preserved. This indicates that the downscaling of salt marsh meadows is highly sensitive to stem diameter (and stem Reynolds). Alternatively, downscaling of salt marsh meadows by frontal area may be more suitable, although this likely depends on stem density, and ultimately requires further study.
- An array of rigid cylinders can provide suitable surrogates for *S. alterniflora* meadows in downscaled physical models, eliminating the necessity for flexible surrogate selection and ultimately simplifying model development. The results of the small-scale study (1:4) support this, where moderate- to high-energy wave conditions (in the context of natural marsh environments) were considered and stem bending was observed. The extension of this finding to other scales, plant species, and hydrodynamic settings requires further testing.
- Overall, for the hydrodynamic setting and beach slope investigated, maximum wave damping effects from the simulated *S. alterniflora* meadow were observed to be around 7%, occurring at an incident wave height of $H_{s,o}$ = 0.11 m. Wave shoaling and breaking effects were found to dominate significant wave height evolution.
- Vegetation-induced damping effects were significantly reduced (if not negligible) for $H_{s,o}$ > 0.15 m. An increase in stem density is likely the best way to improve wave damping effects for the tested design, as results from the present study indicate that extreme meadow submergence would render a lengthening of the field ineffective.

## 5.2 Recommendations for Future Work

The studies presented within this thesis examine the performance of marsh vegetation in coastal protection applications and lay the groundwork for future studies of coastal marsh-based NBS in laboratory settings. Considering the knowledge gaps identified in Section 2.4, and the findings and limitations of this thesis, the following future work is recommended:

- The results of this study support the use of *S. alterniflora* and *S. patens* in combination in coastal protection strategies. Classification of the two species (avoidance vs. resistance) would have *S. patens* as the foreshore species, however, this does not align with natural species zonation. It is recommended that future studies focus on testing various configurations of *S. alterniflora* and *S. patens* to optimize coastal protection function while considering unique plant structure, function, and species zonation.

- More large-scale testing with live vegetation should be conducted to address the limitations of the present study. More specifically, the following is recommended:
    - Testing of a full-scale living dyke structure with live vegetation, for 1) comparison with the small-scale meadow configuration presented herein to quantify scale effects, and 2) to support the present predictions regarding the relative wave attenuation capacity for *S. patens* and *S. alterniflora,* made based upon stem bending and physical characteristics.
    - Consider seasonal variation in marsh properties.
    - Conduct testing with higher energy wave conditions to elucidate species-specific thresholds for damage.
    - Collect direct measurements of erosion protection, as the present study supports that root stabilization may be captured in a large-scale flume study.
    - Measure biomechanical properties for different locations along the plant stem.
    - Measure leaf properties, such as bending modulus and total area.
    - Conduct field surveys to compare characteristics between laboratory plants and plants in a natural coastal marsh setting.
- Only two species were considered herein, *S. alterniflora* and *S. patens.* These species are most relevant for coastal protection strategies on the Atlantic coast of Canada. It is recommended that other coastal marsh species be investigated, particularly additional species that are native to the Pacific coast of Canada (e.g., *Salicornia* sp., or "Pickleweed").
- Methods for downscaling surrogate vegetation still require significant investigation. This thesis investigated downscaling via the solid volume fraction of vegetation and found the results to be sensitive to stem diameter. To further guide the development of downscaling methods, it is recommended that the following be considered:
    - Downscaling of vegetation by frontal area per unit volume,
    - Downscaling by standing biomass per unit volume, and
    - A sensitivity analysis of the above methods to stem diameter (stem Reynolds), stem density (stem sheltering effects), scale, and inclusion/exclusion of plant macrofeatures.
- Further investigation of vegetation flexibility effects in downscaled vegetation meadows is recommended to better identify under which experimental conditions vegetation flexibility needs to be considered (e.g., scale, incident wave conditions, degree of live plant flexibility).
- An extensive small-scale physical modelling program was conducted, considering the wave damping effects of a downscaled surrogate *S. alterniflora* meadow. Model sensitivities to several parameters were investigated, however due to time constraints there were limitations on the number of variables considered. An expansion of the experimental program may include the following:
    - Vary beach slope.

    - Vary vegetation density.
    - Vary vegetation field length.
    - Consider heterogeneity in meadow composition (i.e., multiple species, reflected with different surrogate elements).
    - Consider progressively smaller model scales to improve understanding of scale effects.
- Overall, the feasibility and efficacy of coastal marsh-based NBS still requires significant investigation, particularly considering the practical construction of the such structures and their dynamic evolution. There is still limited knowledge of how engineered marshes will perform relative to natural marshes, and if they will show the same sensitivity/resilience to external stressors. Limitations on implementation conditions must also be identified to address thresholds for marsh establishment (e.g., initial planting density, beach slope, and hydrodynamic setting). Ultimately, these studies cannot be done in a laboratory setting as they will require long-term observations of structure evolution and performance. To acquire such knowledge, the implementation of design case studies or pilot-scale projects is recommended.

# References


Anderson, M., & Smith, J. (2014). Wave attenuation by flexible, idealized salt marsh vegetation. *Coastal Engineering, 83*, 82-92.

Atwood, T., Connolly, R., Almahasheer, H., Carnell, P., Duarte, C., Ewers Lewis, C., . . . Lovelock, C. (2017). Global patterns in mangrove soil carbon stocks and losses. *Nature Climate Change, 7*, 523-529.

Augustin, L., Irish, J., & Lynett, P. (2009). Laboratory and numerical studies of wave damping by emergent and near-emergent wetland vegetation. *Coastal Engineering, 56*, 332-340.

Baker, S., Murphy, E., Cornett, A., & Knox, P. (2022). Experimental Study of Wave Attenuation Across an Artificial Salt Marsh. *Frontiers in Built Environment*.

Barbier, E., Hacker, S., Kennedy, C., Koch, E., Stier, A., & Silliman, B. (2011). The value of estuarine and coastal ecosystem services. *Ecological Monographs, 81*(2), 169-193.

Bertness, M. (1991). Zonation of Spartina Patens and Spartina Alterniflora in a New England Salt Marsh. *Ecology*, 138-148.

Bilkovic, D., & Mitchell, M. (2017). Chapter 15: Designing Living Shoreline Salt Marsh Ecosystems to Promote Coastal Resilience. In D. Bilkovic, M. Mitchell, M. La Peyre, & J. Toft, *Living Shorelines* (pp. 293-316). New York: CRC Press.

Bilkovic, D., Mitchell, M., La Peyre, M., & Toft, J. (2017). *Living shorelines: the science and management of nature-based coastal protection.* CRC Press.

Bilkovic, D., Mitchell, M., Mason, P., & Duhring, K. (2016). The Role of Living Shorelines as Estuarine Habitata Conservation Strategies. *Coastal Management, 44*(3), 161-174.

Blackmar, P., Cox, D., & Wu, W. (2014). Laboratory Observations and Numerical Simulations of Wave Height Attenuation in Heterogeneous Vegetation. *Journal of Waterway, Port, Coastal, and Ocean Engineering*, 56-65.

Bonakdur, L., Oumeraci, H., & Etemad-Shahidi, A. (2015). Wave load formulae for prediction of wave-induced forces ona slender pile within pile groups. *Coastal Engineering*.

Bouma, T., De Vries, M., & Herman, P. (2010). Comparing ecosystem engineering efficiency of two plant species with contrasting growth strategies. *Ecology*, 2696-2704.

Bouma, T., De Vries, M., Low, E., Peralta, G., Tanczos, I., van de Koppel, J., & Herman, P. (2005). Trade-offs Related to Ecosystem Engineering: A Case Study on Stiffness of Emerging Macrophytes. *Ecology, 86*(8), 2187-2199.

Bradley, K., & Houser, C. (2009). Relative velocity of seagrass blades: Implications for wave attenuation in low-energy environments. *Journal of Geophysical Research*.

Brooks, H., Moller, I., Carr, S., Chirol, C., Christie, E., Evans, B., . . . Royse, K. (2021). Resistance of salt marsh substrates to near-instantaneous hydrodynamic forcing. *Earth Surface Processes and Landforms*, 67-88.

Cao, H., Feng, W., Hu, Z., Suzuki, T., & Stive, M. (2015). Numerical modeling of vegetation-induced dissipation using an extended mild-slope equation. *Ocean Engineering, 110*, 258-269.

Chatagnier, J. (2012). The biomechanics of salt marsh vegetation applied to wave and surge attenuation. *LSU Master's Theses.*, 1351.

Chen, H., & Zou, Q.-P. (2019). Eulerian-Lagrangian flow-vegetation interaction model using immersed boundary method and OpenFOAM. *Advances in Water Resources*, 176-192.

Chen, Q., & Zhao, H. (2012). Theoretical Models for Wave Energy Dissipation Caused by Vegetation. *Journal of Engineering Mechanics, 138*(2), 221-229.

Church, J., Clark, P., Cazenave, A., Gregory, J., Jevrejeva, S., Levermann, A., . . . et al. (2013). Sea Level Change. In *Climate Change 2013: The Physical Science Basis Contribution of Working Group I to the Fifth Assessment Report of the Intergovernmental Panel on Climate Change* (pp. 1137-1216). New York, NY: Cambridge University Press.

Coastal Zone Canada Association. (n.d.). *Cold Regions Living Shorelines Community of Practice*. Retrieved from Climate Change Adaptation Commumity of Practice: https://www.ccadaptation.ca/en/crlscop

Cuellar-Martinez, T., Ruiz-Fernandez, A., Sanchez-Cabeza, J., Perez-Bernal, L., & Sandoval-Gil, J. (2019). Relevance of carbon burial and storage in two contrasting blue carbon ecosystems of a north-east Pacific coastal lagoon. *Science of the Total Environment, 675*, 581-593.

Dalrymple, R., Kirby, J., & Hwang, P. (1984). Wave Diffraction Due to Areas of Energy Dissipation. *Journal of Waterway, Port, Coastal and Ocean Engineering, 110*, 67-79.

Davis, J., Currin, C., O'Brien, C., Raffenburg, C., & Davis, A. (2015). Living Shorelines: Coastal Resilience with a Blue Carbon Benefit. *PLoS ONE, 10*(11).

Davis, J., Takacs, R., & Schnabel, R. (2006). Evaluating Ecological Impacts of Living Shorelines and Shoreline Habitat Elements: An Example From the Upper Western Chesapeake Bay. *Management, Policy, Science and Engineering of Nonstructural Erosion Control in the Chespeake Bay: Proceedings of the 2006 Living Shorelines Summit*, (pp. 55-61). Williamsburg, Virginia.

de Oude, R. (2010). *Modelling wave attenuation by vegetation with SWAN-VEG.* University of Twente.

Ecology Action Centre. (2020). *Living Shorelines Intact Project Site Criteria.* Retrieved from https://ecologyaction.ca/livingshorelines

Falkenrich, P. (2020). *Experimental Investigations of Wave Interaction with Simulated Large Woody Debris (LWD) on a Gravel Beach and Comparison with Seawalls.* Technische Universitat Braunschweig.

Feagin, R., Irish, J., Moller, I., Williams, A., Colon-Rivera, R., & Mousavi, M. (2011). Short communication: Engineering properties of wetland plants with application to wave attenuation. *Coastal Engineering, 58*, 251-255.

Federal, Provincial and Territorial Governments of Canada. (2010). *Canadian Biodiversity: Ecosystem Status and Trends 2010.* Ottawa, ON: Canadian Councils of Resource Ministers.

Fonseca, M., & Cahalan, J. (1992). A Preliminary Evaluation of Wave Attenuation by Four Species of Seagrass. *Estuarine, Coastal and Shelf Science, 35*, 565-576.

Ghisalberti, M., & Nepf, H. (2002). Mizing layers and coherent structures in vegetated aquatic flows. *Journal of Geophysical Research, 107*(C1), 3-1-3-11.

Gittman, R., Peterson, C., Currin, C., Fodrie, F., Piehler, M., & Bruno, J. (2016). Living shorelines can enhance the nursery role of threatened estuarine habitats. *Ecological Applications, 26*(1), 249-263.

Gordon, D., Cranford, P., & Desplanque, C. (1985). Observations on the Ecological Importance of Salt Marshes in the Cumberland Basin, a Macrotidal Estuary in the Bay of Fundy. *Estuarine, Coastal and Shelf Science, 20*, 205-227.

Gosselin, F. (2019). Mechanics of a Plant in Fluid Flow. *Journal of Experimental Botany*, 3533-3548.

Government of Canada. (2021). *Daily Data Report for July 2021*. Retrieved from Historical Climate Data: https://climate.weather.gc.ca/climate_data/daily_data_e.html?hlyRange=1996-07-17%7C2021-09-06&dlyRange=1997-11-13%7C2021-09-06&mlyRange=%7C&StationID=27377&Prov=QC&urlExtension=_e.html&searchType=stnProx&optLimit=yearRange&Month=7&Day=6&StartYear=2021&End

Gracia, A., Rangel-Buitrago, N., Oakley, J., & Williams, A. (2018). Use of ecosystems in coastal erosion management. *Ocean and Coastal Management, 156*, 277-289.

Hallegatte, S., Green, C., Nicholls, R., & Corfee-Morlot, J. (2013). Future flood losses in major coastal cities. *nature climate change, 3*, 802-806.

Hardaway, C., Milligan, D., Wilcox, C., & Duhring, K. (2017). *Living Shoreline Design Guidelines for Shore Protection in Virginia's Estuarine Enviornments.* Gloucester Point, VA: Virginia Institute of Marine Science.

Henry, P.-Y., Myrhuag, D., & Aberle, J. (2015). Drag forces on aquatic plants in nonlinear random waves plus current. *Estuarine, Coastal and Shelf Science, 165*, 10-24.

Hinkel, J., Lincke, D., Vafeidis, A., Perrette, M., Nicholls, R., Tol, R., . . . Levermann, A. (2014). Coastal flood damage and adaptation costs under 21st century sea-level rise. *PNAS, 111*(9), 3292-3297.

Holthuijsen, L. H. (2007). *Waves in Oceanic and Coastal Waters.* New York, USA: Cambridge University Press.

Hoque, A., Husrin, S., & Oumeraci, H. (2018). Laboratory studies of wave attenuation by coastal forest under storm surge. *Coastal Engineering Journal, 60*(2), 225-238.

Horizon Advisors. (2019). *Benefits of Adopting Natural Infrastructure A Compariosn of Natural and Grey Infrastructure Solutions.*

IPCC. (2022). *Summary for Policymakers. In: Climate Change 2022: Impacts, Adaptation, and Vulnerability. Contribution of.* Cambridge University Press. In Press.

Johnson, M., Thomas, R., Dijkstra, J., Paul, M., Penning, W., & Rice, S. (2014). Chapter 3: Using surrogates, including scaling issues, in laboratory flumes and basins. In L. Frostick, R. Thmas, M. Johnson, S. Rice, & S. McLelland, *USers Guide to Ecohydraulic Modelling and Experimentation* (pp. 23-41). Leiden, The Netherlands: CRC Press.

Kartasalo, K., Polonen, R.-P., Ojala, M., Rasku, J., Lekkala, J., Aalto-Setala, K., & Kallio, P. (2015). CytoSpectre: a tool for spectral analysis of oriented structures on cellular and subcellular levels. *BMC Bioinformatics, 16*(344).

Keimer, K., Schurenkamp, D., Miescke, F., Kosmalla, V., Lojek, O., & Goseberg, N. (2021). Ecohydraulics of Surrogate Salt Marshes for Coastal Protection: Wave-Vegetation Interaction and Related Hydrodynamics on Vegetated Foreshores at Sea Dikes. *Journal of Waterway, Port, Coastal and Ocean Engineering*.

Knutson, P., Brochu, R., Seelig, W., & Inskeep, M. (1982). Wave Damping in Spartina alterniflora Marshes. *Wetlands*, 87-104.

Kobayashi, N., Raichle, A., & Asano, T. (1993). Wave attenuation by vegetation. *Journal of Waterway, Port, Coastal and Ocean Engineering, 119*, 30-48.

Koch, E., Sanford, L., & Chen, S. (2006). *Waves in Seagrass Systems: Review and Technical Recommendations.* Washington, DC: US Army Corps of Engineers.

Koftis, T., Prinos, P., & Stratigaki, V. (2013). Wave damping over artificial Posidinia oceanica meadow: A large-scale experimental study. *Coastal Engineering, 73*, 71-83.

Komar, P. D. (2007). The design of stable beach fills: Learning from Nature. *Coastal Sediments*.

Lara, J., Maza, M., Ondiviela, B., Trinogga, J., Losada, I., Bouma, T., & Gordejuela, N. (2016). Large-scale 3-D experiments of wave and current in interaction with real vegetation. Part 1: Guidelines for physical modeling. *Coastal Engineering, 107*, 70-83.

Lei, J., & Nepf, H. (2019). Wave damping by flexible vegetation: Connecting individual blade dynamics to the meadow scale. *Coastal Engineering, 147*, 138-148.

Lima, S., Neves, C., & Rosauro, N. (2006). Damping of gravity waves by fields of flexible vegetation. *Coastal Engineering*, 491-503.

Lin, C.-Y., & Huang, C.-J. (2004). Decomposition of incident and reflected higher harmonic waves using four wave gauges. *Coastal Engineering*, 395-406.

Losada, I., Maza, M., & Lara, J. (2016). A new formulation for vegetation-induced damping under combined waves and currents. *Coastal Engineering*, 1-13.

Lovas, S., & Torum, A. (2000). Effect of Submerged Vegetation Upon Wave Damping and Run-up on Beaches. *Coastal Engineering*, 851-864.

Lovelock, C., Atwood, T., Balfock, J., Duarte, C., Hickey, S., Lavery, P., . . . Steven, A. (2017). Assessing the risk of carbon dioxide emissions from blue carbon ecosystems. *Frontiers in Ecology and the Environment, 15*(5), 257-265.

Luhar, M., & Nepf, H. (2016). Wave-induced dynamics of flexible blades. *Journal of Fluids and Structures*, 20-41.

Macreadie, P., Nielsen, D., Kelleway, J., Atwood, T., Seymour, J., Petrou, K., . . . Ralph, P. (2017). Can we manage coastal ecosystems to sequester more blue carbon? *Frontiers in Ecology and the Environment, 15*(4), 206-213.

Manca, E., Caceres, I., Alsina, J., Stratigaki, V., Townend, I., & Amos, C. (2012). Wave energy and wave-induced flow reduction by full-scale model Posidinia oceanica seagrass. *Continental Shelf Research*, 100-116.

Mansard, E., & Funke, E. (1980). The Measurement of Incident and Reflected Spectra Using a Least Squares Method. *Proceedings 17th International Conference on Coastal Engineering*, (pp. 154-172). Sydney, Australia.

Markov, A., Stolle, J., Henteleff, R., Nistor, I., Pham Van Bang, D., Murphy, E., & Cornett, A. (2022). Deformation of Spartina patens and Spartina alterniflora stems under wave action. *Manuscript submitted for publication*.

MATLAB. (2021). Version 9.10.0 (R2020a). Natick, Massachusetts: The MathWorks Inc. .

Maza, M., Adler, K., Ramos, D., Garcia, A., & Nepf, H. (2017). Velocity and Drag Evolution From the Leading Edge of a Model Mangrove Forest. *Journal of Geophysical Research: Oceans*, 9144-9159.

Maza, M., Lara, J. L., & Losada, I. J. (2022). A paradigm shift in the quantification of wave energy due to saltmarshes based on their standing biomass. *Scientific Reports*.

Maza, M., Lara, J., & Losada, I. (2013). A coupled model of submerged vegetation under oscillatory flow using Navier-Stokes equations. *Coastal Engineering, 80*, 16-34.

Maza, M., Lara, J., & Losada, I. (2019). Experimental analysis of wave attenuation and drag forces in a realistic fringe Rhizophora mangrove forest. *Advances in Water Resources, 131*.

McClenachan, G., Donnelly, M., Shaffer, M., Sacks, P., & Walters, L. (2020). Does size matter? Quantifying the cumulative impact of small-scale living shoreline and oyster reef restoration projects on shoreline erosion. *Restoration Ecology*.

Mei, C., Chan, I., Liu, P.-F., Huang, Z., & Zhang, W. (2011). Long waves through emergent coastal vegetation. *Journal of Fluid Mechanics, 687*, 461-491.

Mendez, F., & Losada, I. (2004). An empirical model to estimate the propogation of random breaking and nonbreaking waves over vegetation fields. *Coastal Engineering, 51*, 103-118.

Mendez, F., Losada, I., & Losada, M. (1999). Hydrodynamics induced by wind waves in a vegetation field. *Journal of Geophysical Research: Oceans*, 18383-18396.

Miller, J., Rella, A., Williams, A., & Sproule, E. (2016). *Living Shorelines Engineering Guidelines.* Stevens Institute of Technology.

Moller, I., Kudella, M., Rupprecht, F., Spencer, T., Paul, M., van Wesenbeeck, B., . . . Schimmels, S. (2014). Wave attenuation over coastal salt marshes under storm surge conditions. *Nature Geoscience, 7*, 727-731.

Morison, J., Johnson, J., & O'Brien, M. (1953). Experimental Studies of Forces on Piles. *1*(4), 25.

Morris, R., Konlechner, T., Ghisalberti, M., & Swearer, S. (2018). From grey to green: Efficacy of eco-engineering solutions for nature-based coastal defence. *Global Change Biology, 24*(5), 1827-1842.

Muis, S., Apecechea, M., Dullaart, J., de Lima Rego, J., Madsen, K., Su, J., . . . Verlaan, M. (2020). A High-Resolution Global Dataset of Extreme Sea Levels, Tides, and Storm Surges, Including Future Projections. *Frontiers in Marine Science*, 263.

Mullarney, J., & Henderson, S. (2010). Wave-forced motion of submerged single-stem vegetation. *Journal of Geophysical Research*.

Natural Resources Conservation Service. (2021). Plants Database. United States Department of Agriculture.

Neumeier, U. (2005). Quantification of vertical density variations of salt-marsh vegetation. *Estuarine, Coastal and Shelf Science, 63*, 489-496.

Niedowski, N. (2000). *New York State Salt Marsh Restoration and Monitoring Guidelines.* Albany, NY.

NOAA. (2015). *Guidance for Considering the Use of Living Shorelines.*

NYSDEC. (2017). *Tidal Wetlands Guidance Document: Living Shoreline Techniques in the Marine District of New York State.* New York Department of Environmental Conservation.

Ozeren, Y., Wren, D., & Wu, W. (2014). Experimental Investigation of Wave Attenuation through Model and Live Vegetation. *Journal of Waterway, Port, Coastal, and Ocean Engineering, 140*(5).

Paul, M., & Kerpen, N. (2021). Erosion protection by winter state of salt marsh vegetation. *Journal of Ecohydraulics*.

Paul, M., Bouma, T., & Amos, C. (2012). Wave attenuation by submerged vegetation: combining the effect of organism traits and tidal current. *Marine Ecology Progress Series*, 31-41.

Paul, M., Rupprecht, F., Moller, I., Bouma, T., Spencer, T., Kudella, M., . . . Schimmels, S. (2016). Plant stiffness and biomass as drivers for drag forces under extreme wave loading: A flume study on mimics. *Coastal Engineering, 117*, 70-78.

Phan, K., Stive, M., Zijlema, M., Truong, H., & Aarninkhof, S. (2019). The effects of wave non-linearity on wave attenuation by vegetation. *Coastal Engineering*, 63-74.

Piercy, C., Simm, J., Bridges, T., Hettiarachchi, M., & Lodder, Q. (2021). *Chapter 5: NNBF Performance. International Guidelines on Natural and Nature-Based Features for Flood Risk Management.* Edited by T. S. Bridges, J. K. King, J. D. Simm, M. W. Beck, G. Collins, Q. Lodder, and R. K. Mohan. Vicksburg, MS: U.S. Army Engineer Research and Development Center.

Pontee, N., Narayan, S., Beck, M., & Hosking, A. (2016). Building with nature: lessons from around the world. *Maritime Engineering Journal, 169*, 29-36.

Poppema, D., Willemsen, P., de Vries, M., Zhu, Z., Borsje, B., & Hulscher, S. J. (2019). Experiment-supported modelling of salt marsh establishment. *Ocean and Coastal Management, 168*, 238-250.

Puijalon, S., Bouma, T., Douady, C., van Groenendael, J., Anten, N., Martel, E., & Bornette, G. (2011). Plant resistance to mechanical stress: evidence of an avoidance-tolerance trade-off. *New Phytologist*, 1141-1149.

Rahman, H., Sherren, K., & van Proosdij, D. (2019). Institutional Innovation for Nature-Based Coastal Adaptation: Lessons from Salt Marsh Restoration in Novia Scotia, Canada. *Sustainability, 11*.

Rasmeemasmuang, T., & Sasaki, J. (2015). Wave Reduction in Mangrove Forests: General Information and Case Study in Thailand. In M. Esteban, H. Tagaki, & T. Shibayama, *Handbook of Coastal Disaster Mitigation for Engineers and Planners* (pp. 511-534). Elsevier.

Reis, R., Pires-Silva, A., Fortes, C., & Suzuki, T. (2020). Experiences with SWASH on modelling wave propogation over vegetation: comparisons with lab and field data. *Journal of Integrated Coastal Zone Management, 20*(2), 145-150.

Roland, R. M., & Douglass, S. L. (2005). Estimating wave tolerance of Spartina alterniflora in Coastal Alabama. *Journal of Coastal Research*, 453-463.

Rupprecht, F., Moller, I., Paul, M., Kudella, M., Spencer, T., van Wasenbeeck, B., . . . Schimmels, S. (2017). Vegetation-wave interactions in salt marshes under storm surge conditions. *Ecological Engineering, 100*, 301-315.

Sanchez-Gonzalez, J., Sanchez-Rojas, V., & Memos, C. (2011). Wave attenuation due to Posidinia Oceanica meadows. *Journal of Hydraulic Research, 49*(4), 503-514.

Schoneboom, T., Aberle, J., & Dittrich, A. (2011). Spatial variability, mean drag forces, and drag coeffcicents in an array of rigid cylinders. In P. Rowinski, *Experimental Methods in Hydraulic Research Vol. 1* (pp. 255-265). Berlin, Heidelberg: Springer Berlin Heidelberg.

Schoutens, K., Heuner, M., Fuchs, E., Minden, V., Shulte-Ostermann, T., Belliard, J., . . . Temmerman, S. (2020). Nature-based shoreline protection by tidal marsh plants depends on trade-offs between avoidance and attenuation of hydrodynamic forces. *Estuarine, Coastal and Shelf Science, 236*.

Schulze, D., Rupprecht, F., Nolte, S., & Jensen, K. (2019). Seasonal and spatial within-marsh differences of biophysical plant properties: implications for wave attenuation capacity of salt marshes. *Aquatic Sciences, 81*(65).

Shepard, C., Crain, C., & Beck, M. (2011). The protective role of coastal marshes: A systemic review and meta-analysis. *PLoS ONE, 6*(11).

Silinski, A., Heuner, M., Schoelynck, J., Puijalon, S., Schroder, U., Fuchs, E., . . . Temmerman, S. (2021). Effects of wind waves versus ship waves on tidal marsh plants: a flume study on different life stages of Scirpus maritimus. *PLoS ONE, 10*(3).

Small, C., & Nicholls, R. (2003). A Global Analysis of Human Settlement in Coastal Zones. *Coastal Zones, 19*, 584-599.

Smith, C. S., Rudd, M. E., Gittman, R., Melvin, E., Patterson, V., Renzi, J., & Wellman, E. S. (2020). Coming to Terms ith Living Shorelines: A scoping Review of Novel Restoration Strategies for Shoreline Protection. *Frontiers in Marine Science, 7*.

Spalding, M., McIvor, A., Beck, M., Koch, E., Moller, I., Reed, D., . . . Van Wesenbeeck, B. (2014). Coastal ecosystems: a critical element of risk reduction. *Conservation Letters*, 293-301.

Sparboom, U., Hildebrandt, A., & Oumeraci, H. (2006). Group interaction effects of slender cylindrs under wave attack. *Proceedings 30th International Conference on Coastal Engineering (ICCE)*, (pp. 4430-4442). San Diego, USA.

Sumer, B., & Fredsoe, J. (2006). *Hydrodynamics around cylindrical structures. Rev ed. Vol 26,.* Singapore, Hackensack, NJ: World Scientific.

Suzuki, T., Hu, Z., Kumuda, K., Phan, L., & Zijlema, M. (2019). Non-hydrostatic modeling of drag, inertia and porous effects in wave propogation over dense vegetation fields. *Coastal Engineering, 149*, 49-64.

Suzuki, T., Zijlema, M., Burger, B., Meijer, M., & Narayan, S. (2011). Wave dissipation by vegetation with layer schematization SWAN. *Coastal Engineering, 59*, 64-71.

Temmerman, S., Meire, P., Bouma, T., Herman, P., Ysebaert, T., & De Vriend, H. (2013). Ecosystem-based coastal defence in the face of global change. *Nature, 504*(7478), 79-83.

Tempest, J., Moller, I., & Spencer, T. (2015). A review of plant-flow interactions on salt marshes: the importance of vegetation structure and plant mechanical characteristics. *WIREs Water, 2*, 669-681.

Tschirky, P., Hall, K., & Turcke, D. (2000). Wave Attenuation By Emergent Wetland Vegetation. *Coastal Engineering*, 865-877.

USACE. (2002). *Coastal Engineering Manual - Part VI.* USACE.

Van Gent, M. (2010). Dynamic cobble beaches as sea defence. *Proceedings on the Third International Conference on the Application of Physical Modelling to Port and Coastal Protection*.

van Veelen, T., Fairchild, T., Reeve, D., & Karunarathna, H. (2020). Experimental study on vegetation flexibility as control parameter for wave damping nd velocity structure. *Coastal Engineering, 157*.

Verified Carbon Standard. (2014). *Methodology for coastal wetland creation, v1.0.*

Vettori, D., & Nikora, V. (2020). Hydrodynamic performance of vegetation surrogates in hydraulic studies: a comparitive analysis of seaweed blades and their physical models. *Journal of Hydraulic Research, 58*(2), 248-261.

Vitousek, S., Barnard, P., Fletcher, C., Frazer, C., Frazer, N., Erikson, L., & Storlazzi, C. (2017). Doubling of coastal flood frequency within decades due to sea-level rise. *Sci Rep., 7*, 1-9.

Vuik, V., Suh Heo, H. Y., Zhu, Z., Borsje, B., & Jonkman, S. (2018). Stem breakage of salt marsh vegetation under wave forcing: A field and model study. *Estuarine, Coastal and Shelf Science, 200*, 41-58.

Wang, H., Yin, Z., Luan, Y., Wang, Y., & Liu, D. (2022). Hydrodynamic Characteristics of Idealized Flexible Vegetation under Regular Waves: Experimental Investigations and Analysis. *Journal of Coastal Research*, 673-680.

Wollenberg, J., Biswas, A., & Chmura, G. (2018). Greenhouse gas flux with reflooding of a drained salt marsh soil. *PeerJ*.

Woods Hole Group. (2017). *Living Shorelines in NEw England: State of the Practice.* East Falmouth, MA.

Wu, W., & Cox, D. (2016). Effects of Vertical Variation in Vegetation Density on Wave Attenuation. *Journal of Waterway, Port, Coastal, and Ocean Engineering, 142*(2).

Wu, W., Ozeren, Y., Wren, D., Chen, Q., Zhang, G., Holland, M., . . . Gordji, L. (2011). *SERRI Project: Investigation of Surge and Wave Reduction by Vegetation. Final Report of Phase I.*

Yang, Z., Tang, J., & Shen, Y. (2018). Numerical study for vegetation effects on coastal wave propogation by using nonlinear Boussinesq model. *Applied Ocean Research, 70*, 32-40.

Yin, Z., Wang, Y., & Yang, X. (2019). Regular Wave Run-up Attenuation on a Slope by Emergent Rigid Vegetation. *Journal of Coastal Research*, 711-718.

Ysebaert, T., Yang, S., Zhang, L., He, Q., Bouma, T., & Herman, P. (2011). Wave Attenuation by Two Contrasting Ecosystem Engineering Salt Marsh Macrophytes in the Intertidal Pioner Zone. *Eco-Healthy Estuarine Wetlands*.

Zeller, R., Weitzman, J., Abbett, M., Zarama, F., Fringer, O., & Koseff, J. (2014). Improved parameterization of seagrass blade dynamics and wave attenuation based on numerical and laboratory experiments. *Limnology and Oceanography, 59*(1), 251-266.

Zhang, X., & Nepf, H. (2021). Wave-induced reconfiguration of an drag on marsh plants. *Journal of Fluids and Structures*.

Zhang, X., & Nepf, H. (2022). Reconfiguration of and drag on marsh plants in combined waves and current. *Journal of Fluids and Structures*.

Zhou, Y., Feng, S., Mahbub Alam, M., & Bai, H. (2009). Reynolds number effect on the wake of two staggered cylinders. *Physics of Fluids*.

Zhu, Z., Yang, Z., & Bouma, T. (2020). Biomechanical properties of marsh vegetation in space and time: effects of salinity, inundation and seasonality. *Annals of Botany*, 277-289.

Zou, X., Zhu, L., & Zhao, J. (2019). Numerical Simulations of Non-Breaking, Breaking and Broken Wave Interaction with Emerged Vegetation Using Navier -Stokes Equations. *Water, 11*.